



UvA-DARE (Digital Academic Repository)

Brain washing

Transport of cerebral extracellular fluids and solutes

Bedussi, B.

Publication date

2017

Document Version

Final published version

License

Other

[Link to publication](#)

Citation for published version (APA):

Bedussi, B. (2017). *Brain washing: Transport of cerebral extracellular fluids and solutes*. [Thesis, fully internal, Universiteit van Amsterdam].

General rights

It is not permitted to download or to forward/distribute the text or part of it without the consent of the author(s) and/or copyright holder(s), other than for strictly personal, individual use, unless the work is under an open content license (like Creative Commons).

Disclaimer/Complaints regulations

If you believe that digital publication of certain material infringes any of your rights or (privacy) interests, please let the Library know, stating your reasons. In case of a legitimate complaint, the Library will make the material inaccessible and/or remove it from the website. Please Ask the Library: <https://uba.uva.nl/en/contact>, or a letter to: Library of the University of Amsterdam, Secretariat, Singel 425, 1012 WP Amsterdam, The Netherlands. You will be contacted as soon as possible.



BRAIN WASHING

Transport of
Cerebral Extracellular
Fluids and Solutes

Beatrice Bedussi

BRAIN WASHING

Transport of
Cerebral Extracellular Fluids and Solutes

Beatrice Bedussi

Brain washing: transport of cerebral extracellular fluids and solutes

ISBN: 978-94-92683-97-7

Author: Beatrice Bedussi

The research described in this book has received funding from the Internationale Stichting Alzheimer Onderzoek (ISAO) and from the European Union's Seventh Framework Programme for research technological development and demonstration under Grant agreement no. 606998, project SmArteR.

Copyright © 2017, Beatrice Bedussi

All rights reserved. No part of this publication may be reproduced, stored or transmitted in any part or by any means, without written permission of the author; or when appropriate, of the publishers of the publications.

Publication of this thesis was kindly supported by the Academic Medical Center.

Artwork cover: Beatrice Bedussi & Optima Grafische Communicatie.
It depicts a map of the Amsterdam canals, extracted from a 1835 city plan.

Layout and printed by: Optima Grafische Communicatie, Rotterdam, the Netherlands
(www.ogc.nl)

BRAIN WASHING

TRANSPORT OF CEREBRAL EXTRACELLULAR FLUIDS AND SOLUTES

ACADEMISCH PROEFSCHRIFT

ter verkrijging van de graad van doctor

aan de Universiteit van Amsterdam

op gezag van de Rector Magnificus

prof. dr. ir. K.I.J. Maex

ten overstaan van een door het College voor Promoties ingestelde commissie,

in het openbaar te verdedigen in de Agnietenkapel

op vrijdag 10 november 2017, te 10.00 uur

door

Beatrice Bedussi

geboren te Brescia, Italië

PROMOTIECOMMISSIE

Promotor: Prof. dr. E.T. van Bavel Universiteit van Amsterdam

Copromotor: Dr. N.T.P. Bakker Universiteit van Amsterdam

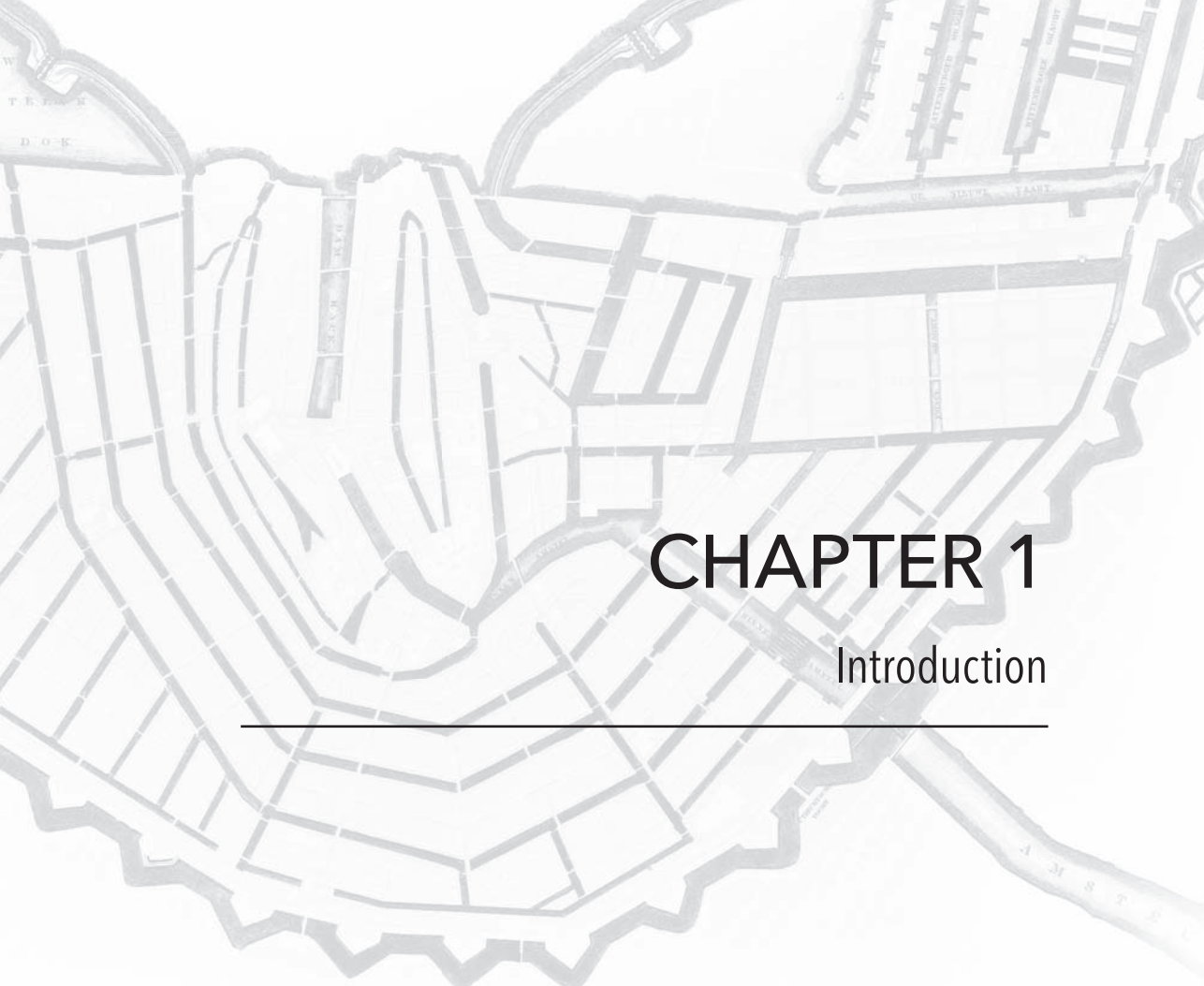
Overige leden: Prof. dr. Y.B.W.E.M. Roos AMC-UVA
Prof. dr. M.J.A.P. Daemen AMC-UVA
Prof. dr. R.O. Schlingemann AMC-UVA
Prof. dr. W.M. van der Flier VUmc
Prof. dr. M.A. van Buchem LUMC
Prof. dr. G.J. Biessels UMC Utrecht

Faculteit der Geneeskunde

TABLE OF CONTENT

Chapter 1	Introduction	7
Chapter 2	Clearance from the mouse brain by convection of interstitial fluid towards the ventricular system	21
Chapter 3	Paravascular channels, cisterns, and the subarachnoid space in the rat brain: A single compartment with preferential pathways	43
Chapter 4	Paravascular spaces at the brain surface: low resistance pathways for cerebrospinal fluid flow	63
Chapter 5	Enhanced interstitial fluid drainage in the hippocampus of spontaneously hypertensive rats: sieving as a novel mechanism to induce solute accumulation	79
Chapter 6	General Discussion	97
Chapter 7	Summary and Appendix	109
	Summary	111
	Samenvatting	113
	List of Publications	117
	Portfolio	119
	Curriculum Vitae	121
	Acknowledgements	123





CHAPTER 1

Introduction

Dementia is characterized by a progressive degradation of cognitive functions such as loss of memory, behavioral changes, impairment in daily activity and language disorders. While dementia can occur relatively early in life, the risk of developing dementia increases strongly with aging. Considering that the number of persons aged ≥ 65 is projected to increase from 6.9% to 12.0% worldwide during the period 2000-2030¹, dementia can be considered as a plague. The most frequent form of dementia is Alzheimer's disease. The formation of neurofibrillary tangles, composed of the protein tau, and the accumulation of a protein, amyloid β , into plaques, are a hallmark of this neurodegenerative disease and associated with cognitive impairment and brain atrophy^{2,3}. Despite the availability of symptomatic treatment, at present there is no cure for Alzheimer's disease. The reason for this may be its complicated etiology, that involves, among others, an impaired clearance of amyloid β associated with aging. The removal of amyloid β from the brain depends on transport into the blood across the blood-brain barrier, proteolytic degradation, and transport via interstitial fluid (ISF) and cerebrospinal fluid (CSF) towards several outflows paths⁴.

In 1854, Claude Bernard introduced the term 'Milieu Intérieur' to describe the regulation of the interstitial fluid towards a composition that maintains a viable and healthy environment for the nervous system⁵. This concept became a fundamental principle of physiology. The regulation of ISF volume and composition partly depends on the exchange of water and solutes with the two other fluids in the brain: blood and cerebrospinal fluid. These exchange processes are therefore of critical importance for the provision of nutrients, oxygen, the removal of waste products, and in general the maintenance of the Milieu Intérieur. This thesis addresses part of these exchange processes, notably between the interstitial fluid and cerebrospinal fluid compartments.

Concerning the exchange of fluid, it is relevant that the brain is enclosed in a rigid structure, the skull. Therefore, the volume occupied by brain tissue parenchyma, vasculature and extracellular fluids must remain constant. This is referred to as the Monro-Kellie dogma⁶. Together with the blood, the cerebrospinal fluid and the interstitial fluid form the extracellular fluids. The cerebrospinal fluid fills the ventricular system and subarachnoid spaces, while the interstitial fluid is present in the parenchymal extracellular spaces. The human brain contains in total 140 ml of cerebrospinal fluid, 30 ml in the ventricular system and the remaining 110 ml in the subarachnoid space. The interstitial fluid is estimated to be around 280 ml⁷. Interstitial fluid and cerebrospinal fluid have a similar composition, which suggests a relatively free communication between the two. Their composition varies significantly from that of blood plasma⁸, reflecting the prominent role of the blood-brain barrier as regulator of fluid and solute exchange between blood and interstitial fluid.

A specific feature of the brain is the apparent lack of a lymphatic system. It should be pointed out that the recently described dural lymphatics are not located in the brain

tissue but rather appear to be outlets of cerebrospinal fluid^{9,10}. In many organs, the lymphatic system helps to maintain fluid balance and participates in waste removal and immune regulation. According to Starlings' law for hydrostatic and oncotic pressures, in those organs fluid leaves the circulation at the arterial side, and is largely reabsorbed at the venous side. The remainder is removed by the lymphatic system. A long standing question has been how the brain compensates for the lack of lymphatics. Perivascular spaces have been suggested to form a channel for fluid exchange between interstitial fluid and cerebrospinal fluid that may provide such compensation. Below we discuss the interstitial and cerebrospinal fluid and compartments, and indicate how the perivascular space could be involved in fluid and solute exchange.

Interstitial Fluid

The maintenance of the microenvironment of the central nervous system depends on the interstitial fluid composition and volume that surrounds the neurons. Endothelium, pericytes and astrocytes form the capillary neurovascular unit which not only regulates local blood flow, but also affects the amount and composition of interstitial fluid¹¹. Brain capillaries differ from capillaries in the rest of the human body, as each endothelial cell is connected to the adjacent cell by tight and adherens junctions. Thus, the endothelium forms the so-called blood-brain barrier, which expresses ions channels and transporters that allow the flux of water and hydrophilic solutes such as glucose, while oxygen, carbon dioxide and other small lipophilic molecules diffuse freely¹²⁻¹⁸. As the brain endothelium is relatively impermeable for most solutes, formation of interstitial fluid in the brain is dependent on the active transport of salts, followed by osmotically driven water fluxes^{8,19}. The Na^+/K^+ pump in endothelial cells forms a critical element here. This ATPase pumps 3 Na^+ ions out of the cells, against 2 K^+ ions into the cell, against their concentration gradients. While the Na^+/K^+ pump is of critical importance for regulation of cell volume and membrane potential, it is also involved in the transport of ions and water from the capillaries to the interstitial space, as the pump is predominantly expressed at the abluminal side of endothelial cells^{8,20}. This polarized expression causes a net flux of Na^+ into the interstitium, followed by osmotically driven water flow. Since reabsorption via lymphatic vessels is absent, this generated interstitial fluid most likely drains into the cerebrospinal fluid compartment along extracellular pathways. The pressure gradient between interstitial and cerebrospinal fluid ($P_{\text{ISF}} > P_{\text{CSF}}$) may help driving the interstitial bulk flow towards the closest cerebrospinal fluid compartments²¹.

Cerebrospinal fluid

The cerebrospinal fluid is a watery and transparent medium that surrounds the brain within the skull and the spinal cord in the rachis. It has several functions, which include: shock-absorbance and cushioning of the central nervous system; buoyancy for the

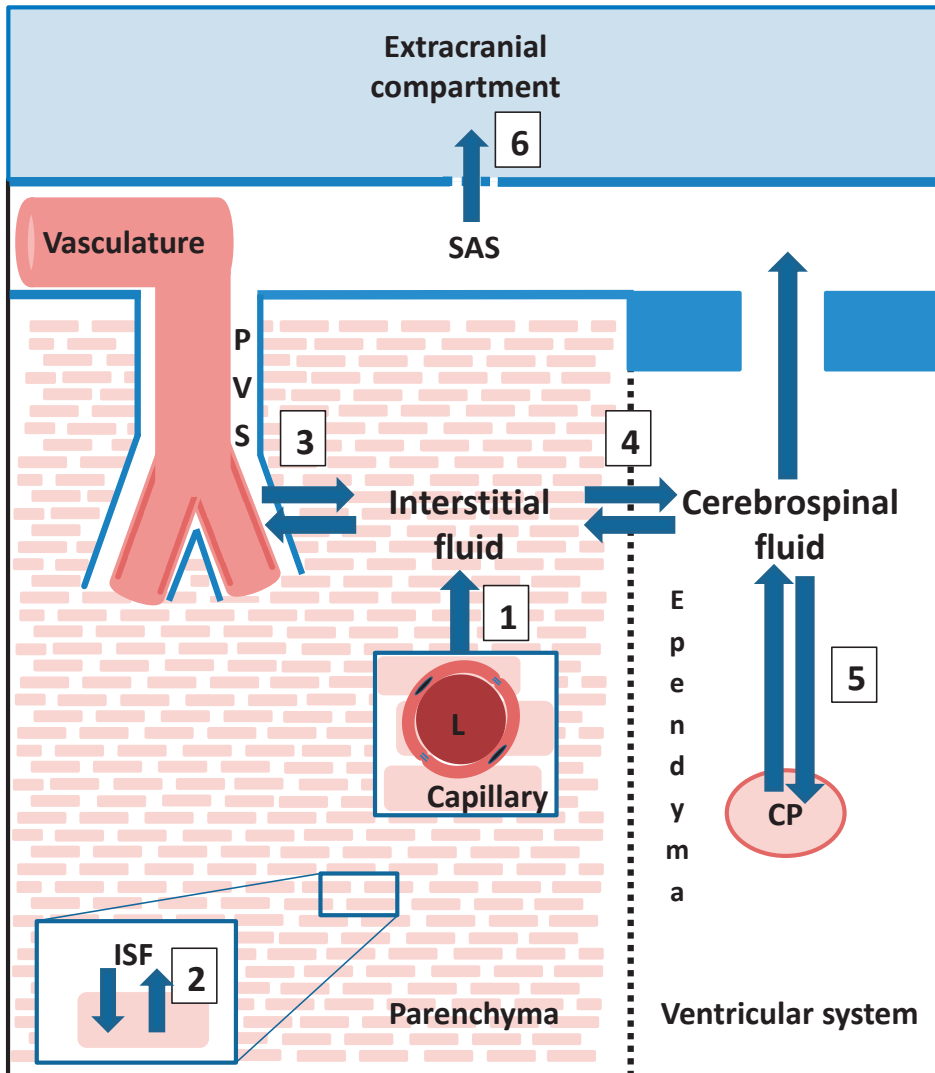


Figure 1. Schematic representation of fluid exchange and drainage in the brain. Interstitial fluid (ISF) is produced by the brain capillaries (L: lumen), via active transport of salts (Na^+/K^+ pump), followed by osmotically driven water fluxes (1). The same Na^+/K^+ pump is expressed also on parenchymal cells and it regulates exchange between intra and extracellular compartments (2). Drainage of fluid from and to the paravascular space (PVS) around brain vasculature has been hypothesized by different groups (3). The ependyma is located at the interface between the brain parenchyma and the ventricular system. Here interstitial fluid and cerebrospinal fluid communicate (4). The cerebrospinal fluid is produced in the ventricular system by specialized vascular structures, i.e. the choroid plexuses. They produce the cerebrospinal fluid but they seem to be involved in its drainage as well (5). The cerebrospinal fluid moves from the ventricular system to the subarachnoid space (SAS) and, eventually, is drained out from the brain via different outflow paths: the arachnoid granulations; the cribriform plate from which it reaches the nasal lymphatics and then the cervical lymph nodes; and the dural lymphatics (6).

brain, reducing its effective weight; delivery of neuroactive substances within the central nervous system; and removal of waste products from the central nervous system^{22,23}.

Anatomy of the Cerebrospinal fluid compartments

Cerebrospinal fluid fills the ventricular system of the brain and the subarachnoid space. The five cavities that form the ventricular system are the two lateral ventricles, the third and the fourth ventricles and the cerebral aqueduct. The lateral ventricles are paired apertures located in the depth of the two hemispheres. They both communicate with the third ventricle via the foramina of Monro (or interventricular foramina). The third ventricle is positioned between the two thalami and is connected via the aqueduct of Sylvius to the fourth ventricle, located between the cerebellum and the medulla. The fourth ventricle presents two apertures at each lateral recess, called foramina of Luschka (or lateral apertures), that are located in the pontocerebellar cisterns. The fourth ventricle presents an additional aperture, the foramen of Magendie (or median aperture), that communicates with the cisterna magna, another point of connection between the ventricular system and the subarachnoid space.

A specialized ciliated epithelium, called ependyma, lines up the cerebrospinal fluid-filled cavities, and forms the interface between the brain parenchyma and the ventricular system²⁴. The choroid plexuses, highly vascularized structures, float within the four ventricular cavities. They have a secretory epithelium with numerous microvilli on the apical surface²⁵ that overlies permeable fenestrated capillaries. The epithelial layer of the choroid plexuses forms the so-called blood-CSF barrier, which regulates influx and efflux of compounds via diffusion and active transport²⁵⁻²⁷. The anterior and the posterior choroidal arteries supply the choroid plexuses within the lateral ventricles. The plexus in the third ventricle is also supplied by the posterior choroidal artery while the fourth plexus is perfused by the anterior and posterior cerebellar arteries.

The subarachnoid space is located between two of the three meninges existing in the brain: the arachnoid on the outer face and the pia mater on the inner side. The third meninx is the dura mater, which is located beneath the skull. The subarachnoid space is thin (a few millimeters in humans) on the dorsal side of the brain, while it is wider at the base. In specific segments of the brain surface, the pia mater follows the brain parenchyma while it separates from the arachnoid to create the cerebral cisterns. The cisterna magna and the cisterna pontis are the largest of these. Within the subarachnoid space run the leptomeningeal arteries, that arise from the circle of Willis, and the leptomeningeal veins. The pia mater follows the leptomeningeal vessels up to a certain extent into the brain parenchyma. The space between the vessels and the inner meningeal sheet was firstly described by Virchow and Robin as a cavity where extracellular space and subarachnoid space communicate directly²⁸.

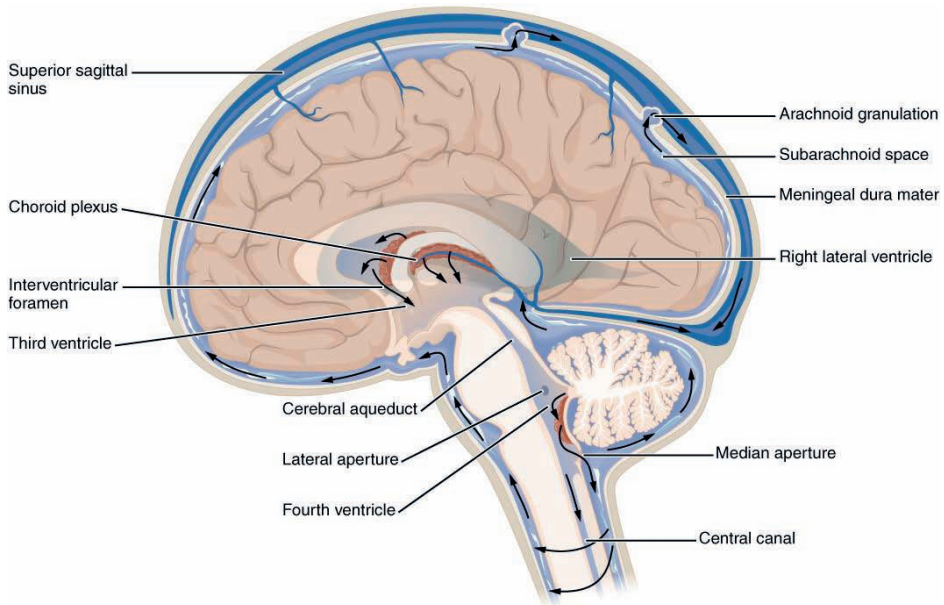


Figure 2. Cerebrospinal fluid anatomy and flow. The fluid produced by the choroid plexuses circulates within the ventricular system towards the subarachnoid space. From there it is cleared via several outflow paths. (Source: download for free at <http://cnx.org/> **Fig.2 Cerebrospinal fluid anatomy and flow.** The fluid produced by the choroid plexuses circulates within the ventricular system towards the subarachnoid space. From there it is cleared via several outflow paths. (Source: download for free at <http://cnx.org/contents/14fb4ad7-39a1-4eee-ab6e-3ef2482e3e22@8.25>.)

Cerebrospinal fluid flow

Cerebrospinal fluid is produced mainly by the four choroid plexuses, located in the ventricular system. The *vis a tergo* from the continuous production of cerebrospinal fluid from the choroid plexus propels the cerebrospinal fluid through the ventricular system. It has been suggested that this process is assisted by the pressure waves resulting from arterial pulsation and respiration, and active movement of cilia²⁵. From the lateral ventricles, cerebrospinal fluid moves to the third ventricle via the foramina of Monro. Then, through the aqueduct of Sylvius it reaches the fourth ventricle and finally leaves the ventricular system to reach the subarachnoid space via the foramina of Magendie and Luschka. A recent study described a back and forth slow bulk flow in this space that had a variable direction²⁹. From the subarachnoid space the cerebrospinal fluid is cleared by multiple outflow paths: the arachnoid granulations that empty into the venous sinus; the cribriform plate through which it reaches first the nasal lymphatics and then the cervical lymph nodes^{30,31}; and dural lymphatic vessels^{9,10,32}.

Peri or para-vascular pathways?

In 1955, Woollam et al, described “true perivascular spaces”, which communicate directly with the subarachnoid space but not with the brain parenchyma³³. However, the description of this space has been questioned and modified. Electron microscopy data on human leptomeningeal arteries showed that leptomeningeal cells coat arteries and veins in the subarachnoid space of humans, creating a separation between the cerebrospinal fluid in the subarachnoid space from the perivascular space and brain parenchyma³⁴. This has led to the concept of a drainage pathway along the basement membranes of capillaries and arteries that could drain interstitial fluid, in the opposite direction from blood flow, from the brain parenchyma into peripheral lymph nodes⁷. In 2012 however, Iliff et al. presented apparently contradictory data that suggested antegrade flow in the paravascular space of penetrating arteries, as part of a ‘glymphatic pathway’. In this view, cerebrospinal fluid recirculates from the subarachnoid space into the brain parenchyma along para-arterial spaces. CSF then mixes with interstitial fluid, and finally leaves the brain via para-venous spaces.

The term ‘glymphatic’ comes from a specific type of glial cell (i.e. the astrocytes), supposedly involved in interstitial-cerebrospinal fluid exchange in the brain. Astrocyte endfeet and ependymal cells at the boundaries between interstitial and cerebrospinal fluid express AQP4, a specific water-selective channel^{35,36}. Iliff et al. suggested that AQP4 along paravascular channels around arteries provides a low resistance pathway for cerebrospinal fluid flow into the brain parenchyma and for outflow of interstitial fluid into the para-venous space. In support of this, this group showed that deletion of AQP4 decreased the clearance of tracers from the brain³⁷. However, concerns about the role of AQP4 in the glymphatic path have been raised and need further investigation based on quantitative imaging studies³⁸.

The discrepancies regarding the anatomy of this space, and the direction of flow herein, were carefully reviewed^{8,13,36}. One possible explanation for this discrepancy could be the existence of two pathways, with flow in opposite directions, separated by meningeal sheets. An alternative explanation is that there is only one peri/paravascular space, in which the direction of flow, if any, is differently interpreted because of methodological differences. Thus, the various protocols used by these groups may explain the diversity in their results. Tracers injected into the parenchyma mostly moved retrograde along arteries, with respect to arterial blood flow (i.e. Carare), while after interstitial injection tracers moved antegrade along arteries (i.e. Iliff).

Clinical relevance of peri and para-vascular drainage

Drainage via the peri-paravascular route could allow removal of not only fluids but also solutes from the brain. Thus, fluid flow could collect waste products and drag these along towards the final outflow pathways. Iliff *et al.* showed that amyloid β is removed

via the glymphatic pathway, suggesting the relevance of this pathway for the pathophysiology of Alzheimer's disease³⁷. However, the outflow of amyloid β along peri-venous spaces is difficult to reconcile with its aggregation around arteries in Alzheimer's disease and in cerebral amyloid angiopathy^{39,40} in particular. In this respect, the model proposed by Carare⁷ more easily fits pathological findings. Yet, impaired glymphatic function preceded amyloid β aggregation in a mouse model of Alzheimer's disease control⁴¹. Thus, so far, evidence for a prominent role of extracellular fluid transport in the removal of amyloid β has been presented, albeit the direction of flow and anatomical pathways remain unclear.

Aim of the thesis

Recent findings have shed new light on the interrelationship between ISF and CSF, their flow patterns, penetration into the brain along blood vessels, and relevance for waste removal. However, the exact anatomical base for ISF – CSF exchange, the presence of peri- and/or paravascular spaces, the direction and pattern of fluid flow in these spaces, their driving forces, and the changes in vascular pathology remain unclear. Specific questions that arise from the diverging data and controversial views in the field of brain fluids include: - Is there bulk flow in the parenchyma? – If there is, what is the direction of fluid flow and how does this relate to fluid exchange between the three compartments? - What is the structure of the paravascular spaces? – In which direction, if any, does fluid convection occur here? – what are the driving forces for such convection in the paravascular spaces? - How does vascular pathology, such as hypertension, modify fluid transport and homeostasis? These are very fundamental questions in brain physiology, which are of strong relevance for normal brain function and changes in aging and hypertension, and which may also be relevant for the development of dementia. Thus, the aim of the thesis was to investigate transport processes in the brain and their possible roles in the removal of solutes.

Outline of the thesis

To investigate the direction of fluid and the presence of bulk flow in the brain, in **Chapter 2**, we investigate the clearance of tracers from cerebrospinal fluid and interstitial fluid in the mouse brain. In particular, we infuse fluorescent tracers into the brain parenchyma and into the cisterna magna and we image their distribution with confocal microscopy and three-dimensional cryomicrotome imaging.

We then study the structure of paravascular spaces. The goal of **Chapter 3** is to identify the anatomical relationships between the cerebrospinal fluid compartment and paravascular spaces. We combine different imaging techniques to get anatomical information from whole brain to nanometer scale.

The above two chapters provide clues for the involvement of pulsatility in solute transport, based on mixing in the CSF compartments, including the PVS. Therefore, in **Chapter 4** we measure the pattern and velocity profile of CSF flow in the PVS space of mouse leptomeningeal vessels, using fluorescent microspheres.

In **Chapter 5**, we investigate the impact of hypertension on interstitial fluid flow in the hippocampus using normotensive Wistar Kyoto rats (WKY) and spontaneously hypertensive rats (SHR).

Finally, the major findings of this thesis and the proposed directions for future research on brain fluids dynamics and their role in pathophysiology are discussed in **Chapter 6**.

REFERENCES

1. Public health and aging: Trends in aging—united states and worldwide. *JAMA* 289, 1371-1373, doi:10.1001/jama.289.11.1371 (2003).
2. van der Flier, W. M. & Scheltens, P. Epidemiology and risk factors of dementia. *J Neurol Neurosurg Psychiatry* 76 Suppl 5, v2-7, doi:10.1136/jnnp.2005.082867 (2005).
3. Qiu, C., Kivipelto, M. & von Strauss, E. Epidemiology of Alzheimer's disease: occurrence, determinants, and strategies toward intervention. *Dialogues Clin Neurosci* 11, 111-128 (2009).
4. Zlokovic, B. V. Neurovascular pathways to neurodegeneration in Alzheimer's disease and other disorders. *Nat Rev Neurosci* 12, 723-738, doi:10.1038/nrn3114 (2011).
5. Gross, C. G. Claude Bernard and the Constancy of the Internal Environment. *The Neuroscientist* 4, 380-385, doi:doi:10.1177/107385849800400520 (1998).
6. Mokri, B. The Monro-Kellie hypothesis: applications in CSF volume depletion. *Neurology* 56, 1746-1748 (2001).
7. Carare, R. O. et al. Solutes, but not cells, drain from the brain parenchyma along basement membranes of capillaries and arteries: significance for cerebral amyloid angiopathy and neuroimmunology. *Neuropathol Appl Neurobiol* 34, 131-144, doi:10.1111/j.1365-2990.2007.00926.x (2008).
8. Hladky, S. B. & Barrand, M. A. Mechanisms of fluid movement into, through and out of the brain: evaluation of the evidence. *Fluids Barriers CNS* 11, 26, doi:10.1186/2045-8118-11-26 (2014).
9. Aspelund, A. et al. A dural lymphatic vascular system that drains brain interstitial fluid and macromolecules. *J Exp Med* 212, 991-999, doi:10.1084/jem.20142290 (2015).
10. Louveau, A. et al. Structural and functional features of central nervous system lymphatic vessels. *Nature* 523, 337-341, doi:10.1038/nature14432 (2015).
11. Zlokovic, B. V. Neurovascular mechanisms of Alzheimer's neurodegeneration. *Trends Neurosci* 28, 202-208, doi:10.1016/j.tins.2005.02.001 (2005).
12. Abbott, N. J. Evidence for bulk flow of brain interstitial fluid: significance for physiology and pathology. *Neurochem Int* 45, 545-552, doi:10.1016/j.neuint.2003.11.006 (2004).
13. Brinker, T., Stopa, E., Morrison, J. & Klinge, P. A new look at cerebrospinal fluid circulation. *Fluids Barriers CNS* 11, 10, doi:10.1186/2045-8118-11-10 (2014).
14. Zlokovic, B. V. The blood-brain barrier in health and chronic neurodegenerative disorders. *Neuron* 57, 178-201, doi:10.1016/j.neuron.2008.01.003 (2008).
15. Sykova, E. & Nicholson, C. Diffusion in brain extracellular space. *Physiol Rev* 88, 1277-1340, doi:10.1152/physrev.00027.2007 (2008).
16. Thorne, R. G., Pronk, G. J., Padmanabhan, V. & Frey, W. H., 2nd. Delivery of insulin-like growth factor-I to the rat brain and spinal cord along olfactory and trigeminal pathways following intranasal administration. *Neuroscience* 127, 481-496, doi:10.1016/j.neuroscience.2004.05.029 (2004).
17. Thorne, R. G. & Nicholson, C. In vivo diffusion analysis with quantum dots and dextrans predicts the width of brain extracellular space. *Proc Natl Acad Sci U S A* 103, 5567-5572, doi:10.1073/pnas.0509425103 (2006).
18. Ross, T. M. et al. Intranasal administration of interferon β bypasses the blood-brain barrier to target the central nervous system and cervical lymph nodes: a non-invasive treatment strategy for multiple sclerosis. *J Neuroimmunol* 151, 66-77, doi:10.1016/j.jneuroim.2004.02.011 (2004).
19. Kimelberg, H. K. Water homeostasis in the brain: basic concepts. *Neuroscience* 129, 851-860, doi:10.1016/j.neuroscience.2004.07.033 (2004).
20. Harik, S. I. Blood-brain barrier sodium/potassium pump: modulation by central noradrenergic innervation. *Proc Natl Acad Sci U S A* 83, 4067-4070 (1986).

21. Cserr, H. F. Role of secretion and bulk flow of brain interstitial fluid in brain volume regulation. *Ann N Y Acad Sci* 529, 9-20 (1988).
22. Brinker, T., Ludemann, W., Berens von Rautenfeld, D. & Samii, M. Dynamic properties of lymphatic pathways for the absorption of cerebrospinal fluid. *Acta Neuropathol* 94, 493-498 (1997).
23. Segal, M. B. Extracellular and cerebrospinal fluids. *J Inher Metab Dis* 16, 617-638 (1993).
24. Jimenez, A. J., Dominguez-Pinos, M. D., Guerra, M. M., Fernandez-Llebarez, P. & Perez-Figares, J. M. Structure and function of the ependymal barrier and diseases associated with ependyma disruption. *Tissue Barriers* 2, e28426, doi:10.4161/tisb.28426 (2014).
25. Damkier, H. H., Brown, P. D. & Praetorius, J. Cerebrospinal fluid secretion by the choroid plexus. *Physiol Rev* 93, 1847-1892, doi:10.1152/physrev.00004.2013 (2013).
26. Redzic, Z. B. & Segal, M. B. The structure of the choroid plexus and the physiology of the choroid plexus epithelium. *Adv Drug Deliv Rev* 56, 1695-1716, doi:10.1016/j.addr.2004.07.005 (2004).
27. de Lange, E. C. Potential role of ABC transporters as a detoxification system at the blood-CSF barrier. *Adv Drug Deliv Rev* 56, 1793-1809, doi:10.1016/j.addr.2004.07.009 (2004).
28. Weed, L. H. Studies on Cerebro-Spinal Fluid. No. III : The pathways of escape from the Subarachnoid Spaces with particular reference to the Arachnoid Villi. *J Med Res* 31, 51-91 (1914).
29. Ichimura, T., Fraser, P. A. & Cserr, H. F. Distribution of extracellular tracers in perivascular spaces of the rat brain. *Brain Res* 545, 103-113 (1991).
30. Johnston, M., Zakharov, A., Papaiconomou, C., Salmasi, G. & Armstrong, D. Evidence of connections between cerebrospinal fluid and nasal lymphatic vessels in humans, non-human primates and other mammalian species. *Cerebrospinal Fluid Res* 1, 2, doi:10.1186/1743-8454-1-2 (2004).
31. Bedussi, B. et al. Clearance from the mouse brain by convection of interstitial fluid towards the ventricular system. *Fluids Barriers CNS* 12, 23, doi:10.1186/s12987-015-0019-5 (2015).
32. Andres, K. H., von Düring, M., Muszynski, K. & Schmidt, R. F. Nerve fibres and their terminals of the dura mater encephali of the rat. *Anat Embryol (Berl)* 175, 289-301 (1987).
33. Woollam, D. H. & Millen, J. W. The perivascular spaces of the mammalian central nervous system and their relation to the perineuronal and subarachnoid spaces. *J Anat* 89, 193-200 (1955).
34. Weller, R. O. Microscopic morphology and histology of the human meninges. *Morphologie* 89, 22-34 (2005).
35. Papadopoulos, M. C. & Verkman, A. S. Aquaporin water channels in the nervous system. *Nat Rev Neurosci* 14, 265-277, doi:10.1038/nrn3468 (2013).
36. Bakker, E. N. et al. Lymphatic Clearance of the Brain: Perivascular, Paravascular and Significance for Neurodegenerative Diseases. *Cell Mol Neurobiol* 36, 181-194, doi:10.1007/s10571-015-0273-8 (2016).
37. Iliff, J. J. et al. A paravascular pathway facilitates CSF flow through the brain parenchyma and the clearance of interstitial solutes, including amyloid β . *Sci Transl Med* 4, 147ra111, doi:10.1126/scitranslmed.3003748 (2012).
38. Smith, A. J., Jin, B. J. & Verkman, A. S. Muddying the water in brain edema? *Trends Neurosci* 38, 331-332, doi:10.1016/j.tins.2015.04.006 (2015).
39. Weller, R. O. et al. Cerebral amyloid angiopathy: amyloid β accumulates in putative interstitial fluid drainage pathways in Alzheimer's disease. *Am J Pathol* 153, 725-733 (1998).
40. Hawkes, C. A., Jayakody, N., Johnston, D. A., Bechmann, I. & Carare, R. O. Failure of perivascular drainage of β -amyloid in cerebral amyloid angiopathy. *Brain Pathol* 24, 396-403, doi:10.1111/bpa.12159 (2014).
41. Peng, W. G. et al. Suppression of glymphatic fluid transport in a mouse model of Alzheimer's disease. *Neurobiol Dis* 93, 215-225, doi:10.1016/j.nbd.2016.05.015 (2016).





CHAPTER 2

Clearance from the mouse brain by convection of interstitial fluid towards the ventricular system

Beatrice Bedussi¹, Monique G.J.T.B. van Lier¹, Jonas W. Bartstra¹, Judith de Vos¹, Maria Siebes¹, Ed VanBavel¹ and Erik N.T.P. Bakker¹

¹Department of Biomedical Engineering and Physics, Academic Medical Center, Amsterdam, The Netherlands

Published in Fluids Barriers CNS (2015)

doi: 10.1186/s12987-015-0019-5

Authors' contribution: BB, EvB and EB designed the study and wrote the manuscript. MS critically reviewed the manuscript. BB, EB, JdeV, JB and MvL performed the experiments. All authors read and approved the final manuscript.

ABSTRACT

Background

In the absence of a true lymphatic system in the brain parenchyma, alternative clearance pathways for excess fluid and waste products have been proposed. These mechanisms implicate a role for interstitial and cerebrospinal fluid. However, the proposed direction of flow, the anatomical structures involved, and the driving forces are controversial.

Methods

To trace the distribution of interstitial and cerebrospinal fluid in the brain, and to identify the anatomical structures involved, we infused a mix of fluorescent tracers with different sizes into the cisterna magna or striatum of mouse brains. We subsequently performed confocal fluorescence imaging of horizontal brain sections and made 3D reconstructions of the mouse brain and vasculature.

Results

We observed a distribution pattern of tracers from the parenchyma to the ventricular system, from where tracers mixed with the cerebrospinal fluid, reached the subarachnoid space, and left the brain via the cribriform plate and the nose. Tracers also entered paravascular spaces around arteries both after injection in the cisterna magna and striatum, but this appeared to be of minor importance.

Conclusion

These data suggest a bulk flow of interstitial fluid from the striatum towards the adjacent lateral ventricle. Tracers may enter arterial paravascular spaces from two sides, both through bulk flow from the parenchyma and mixing of CSF in the subarachnoid space. Disturbances in this transport pathway could influence the drainage of amyloid β and other waste products, which may be relevant for the pathophysiology of Alzheimer's disease.

Key words

interstitial fluid, cerebrospinal fluid, ventricular system, paravascular space, glymphatic pathway

BACKGROUND

Brain function is critically dependent on the extracellular fluids that surround the neurons. Interstitial fluid (ISF) is in direct contact with neuronal cells and delivers nutrients and oxygen, while at the same time it removes waste products. Brain ISF is derived from water and solutes that pass the blood-brain barrier. This process allows specific ion transporters and channels to regulate its composition¹. Next to ISF and blood plasma, cerebrospinal fluid (CSF) forms the third extracellular fluid compartment of the brain. The composition of CSF differs minimally from ISF, which suggests a relatively free communication between CSF and ISF. Although recent work identified lymphatic vessels in the dura mater^{2,3}, the brain parenchyma lacks a true lymphatic system. CSF may take over this role in fluid balance and waste removal, by drainage of excess fluid from arachnoid granulations, the aforementioned dural lymphatics, and other pathways. The classical view is that CSF is mainly secreted by specialized vascular structures, the choroid plexuses⁴. The CSF subsequently flows into the ventricular system of the brain, which consists of the two lateral ventricles, the third ventricle, and the fourth ventricle, which finally connects to the subarachnoid space. However, recent insights suggest that CSF and ISF physiology is much more complex than previously believed^{5,6}. Thus, CSF and ISF may exchange over the ependymal epithelium that covers the ventricular system^{7,8}, and CSF may also reenter the parenchyma along paravascular pathways^{4,6,9}. In addition, ISF may drain along basement membranes of capillaries and arteries, retrograde to the direction of blood flow¹⁰. Understanding the drainage pathways of the brain is required for unraveling the removal mechanisms of toxic waste products such as amyloid β , as well as for developing targeted delivery of treatment modalities. Therefore, the current study set out to investigate clearance of the brain. In particular, we focused on paravascular pathways as a clearance mechanism of the brain. To this extent we infused tracers in the ISF (striatum) and CSF compartment (cisterna magna, CM) and studied their distribution by confocal imaging of brain sections and 3D reconstruction of the whole mouse head using an imaging cryomicrotome.

METHODS

Animals

For this study, 20 animals were included, 10 for injection in the striatum (7 for confocal microscopy, 3 for 3D cryomicrotome imaging) and 10 for injection of tracers in the cisterna magna (5 for confocal microscopy, 5 for 3D cryomicrotome imaging). Male C57BL/6J0laHsd mice were obtained from Harlan (The Netherlands). Animals were fed ad libitum with standard laboratory food and free access to water. They were allowed

to acclimatize at least one week before being enrolled in experimental protocols. All experimental protocols were approved by the Committee for Animal Experiments of the Academic Medical Center Amsterdam, according to the EU guidelines.

Anesthesia

In all experiments mice were anesthetized with a mixture of ketamine (126 mg/kg, Nimatek, Eurovet, Bladel, The Netherlands) medetomidine (0.2 mg/kg, Dormitor, Orion Pharma, Mechelen, Belgium) and atropine (0.5 mg/kg, Atropinesulfaat, Eurovet) in PBS (Phosphate Buffered Saline, Lonza, Basel, Switzerland) by intraperitoneal injection (75µl/10gr body weight). To prevent swelling of the brain, 0.2 mg/ml dexamethason (Sigma-Aldrich, Zwijndrecht Nederland) in 20% ethanol (10µl/10gr body weight) was added to the anesthetic mixture. Experiments were carried during daytime hours, i.e. in the sleeping phase of the mouse diurnal rhythm.

Reagents

Dextran, Texas Red-labeled (3 kD, Ex. 595 nm / Em. 615 nm) and dextran, Fluorescein-labeled (500 kD, Ex. 494 nm/ Em. 521), both lysine-fixable, were purchased from Molecular Probes-Life Technologies (Eugene, OR, USA). For immunofluorescence, brains were embedded in Tissue-Tek (Sakura, Leiden, The Netherlands) before freezing and sectioning. Cell nuclei were stained with VECTASHIELD Mounting Medium with DAPI (4, 6-diamidino-2-phenylindole, Burlingame, CA, USA) according to the manufacturer's protocol. Anti-Laminin antibody (Sigma-Aldrich) was used to visualize the vasculature.

Experimental Procedure

When the animals were completely anesthetized, their heads were shaved. Next, the animals were fixed in a stereotactic frame (lab standard stereotaxic, Stoelting, Dublin, Ireland), while the head was kept at the same level as the body. To maintain physiological body temperature, animals were placed on a heating pad. Additional oxygen (99 %) was provided to prevent hypoxia and ocular lubricant ophthalmic (DURATEARS, Alcon, Breda, The Netherlands) was used to keep the eyes hydrated. In this study we used two different injection sites: the cisterna magna and the striatum. For cisterna magna injections, after separating the subcutaneous tissues and the midline of the neck muscle, a 29-gauge needle was placed into the cistern and connected to a polyethylene catheter. A total volume of 5µl of a mixture (1:1) of both dextrans, 3 kD Texas Red (10g/l), and 500 kD dextran, Fluorescein (10g/l), was infused at a controlled flow rate of 0.17µl /min using a syringe pump (Harvard Apparatus, Holliston, MA, USA) over a 30 min period. For injection into the striatum (coordinates from the Bregma 0.5mm rostral, 1.5mm lateral, and 2.5mm deep), animals were completely anesthetized, the skull was exposed and after additional local anesthesia (Xylocaine 10 %, AstraZeneca BV, Zoetermeer, The

Netherlands), a small burr hole was drilled using a dental drill. Subsequently, a custom-made 33-gauge polyethylene catheter was inserted into the brain using the stereotactic device. For this site of injection we anticipated that the maximum volume tolerated is smaller than in the cisterna magna. For this reason, 2 μ l of the dextran mixture was infused at a controlled flow rate of 0.066 μ l/min, over a 30 min period. In both protocols, animals were euthanized with an overdose of anesthetic 30 min after start of the infusion. Needles were removed after death.

Confocal microscopy

After sacrifice of the animal the brains were dissected, embedded in Tissue-Tek and frozen in liquid nitrogen prior to storage at -80°C. Samples were cut longitudinally with a microtome (5 μ m slices). We used 3.7 % paraformaldehyde to fix the slices and mounted them with Vectashield mounting medium containing DAPI nuclear stain. Images were acquired using a Confocal Laser Scanning Microscope (Leica TCS SP8, Buffalo Grove, IL, USA). A 10X oil immersion was used for the overviews and a 20X oil immersion objective was used to image the details.

3D cryomicrotome imaging

After surgery, animals were flushed with PBS to remove the blood in the vasculature prior the vascular filling with the replica material via the abdominal aorta. To fill the vasculature we used fluorescent (UV blue, excitation 375 nm, emission 505 nm, VasQtec, Zurich, Switzerland) replica material (Batson's #17, Polysciences, Eppelheim, Germany). After filling and polymerization, the specimens were frozen at -20°C for at least 24 hours and then the heads were cut with a guillotine. The frozen specimens were embedded in a black gel (carboxymethylcellulose sodium solvent 5 % - Brunshwig Chemie, Amsterdam, The Netherlands– mixed with Indian ink 5 % - Royal Talens, Apeldoorn, The Netherlands), and placed at -20°C. Each sample was cut from nose to the second cervical vertebrae using 50 μ m slice thickness for the nose until the start of the brain and 10 μ m for the remaining part of the head, using an imaging cryomicrotome (custom made, Amsterdam, The Netherlands)^{11,12}. After each slice a white light picture of the sample and episcopic fluorescent images for the Dextrans, 5 kD Texas Red (excitation 577 nm, emission 635 nm), and 500 kD Dextran, Fluorescein (excitation 480 nm, emission 535 nm) and vascular cast were recorded (excitation 365 nm, emission 505 nm) using a 4096 x 4096, 16 bit resolution digital camera (Apogee Alta U-16, Oceanside, CA, USA) equipped with a variable- focus lens (Nikon 70-180mm, Amsterdam, The Netherlands). The resulting registered stack of sequential images contained on average 2200 images per color with an in-plane resolution of 5 μ m.

Image processing

For visualizing purposes, two adjacent slices were combined using maximal intensity projection and converted to 8 bit greyscale images. The head was reconstructed in 3D using Amira (Visage Imaging GmbH, Berlin, Germany). This yielded a detailed 3D virtual representation of the mouse head vasculature with co-localized dextran deposition.

RESULTS

Tracers move from the striatum into the ventricles via ISF

To investigate clearance pathways in the brain interstitium, we infused a mixture of a low molecular weight tracer, TR-3, and a high molecular weight tracer, F-500, in the striatum of mice (n=7). We used this combination of high and low molecular weight tracers to estimate the respective contributions of diffusion and bulk flow to dispersion, as there should be a ~fourfold difference in diffusion distance of these tracers based on their diffusion coefficients in the brain¹³. We analyzed the distribution of the tracers by confocal fluorescence imaging of horizontal brain sections. This showed that the tracers had spread from the infusion site through the parenchyma towards the closest lateral ventricle (Fig. 1). The co-localization of the dyes, the directionality of this transport and the distance traveled indicate that this transport is dominated by convection. F-500 followed intercellular spaces from the site of injection to the wall of the ventricle. There, it crossed the ependymal layer and was detected in the ventricular cavity. TR-3 followed the same route, but was also taken up by parenchymal cells along the way towards the ventricle. Both tracers were detected further along the ventricular system, reaching the 3rd and 4th ventricle. In some experiments the tracers had reached the downstream subarachnoid space. Detailed images show the presence of both tracers in the lateral ventricle (B), cisterns (C), and the subarachnoid space (SAS; D). Figure 1E shows that TR-3 entered parenchymal cells, while F-500 appeared to remain confined to the extracellular spaces.

The low molecular weight tracer penetrates the choroid plexus

After infusion in the striatum, we observed that both tracers crossed the ependymal cells into the ventricle. However, particularly F-500 accumulated in the parenchyma close to the ependyma, suggesting it acts as a partial barrier for this tracer (Fig. 2A-D). Such accumulation, in the course from the injection site to the ventricle, is a strong additional indication for bulk flow from the parenchyma of the striatum. We also observed a bright signal for TR-3 in the choroid plexuses. TR-3 clearly penetrated the epithelial cells of the choroid plexus while F-500 was confined to extracellular side of the same cells (Fig. 2E-H).

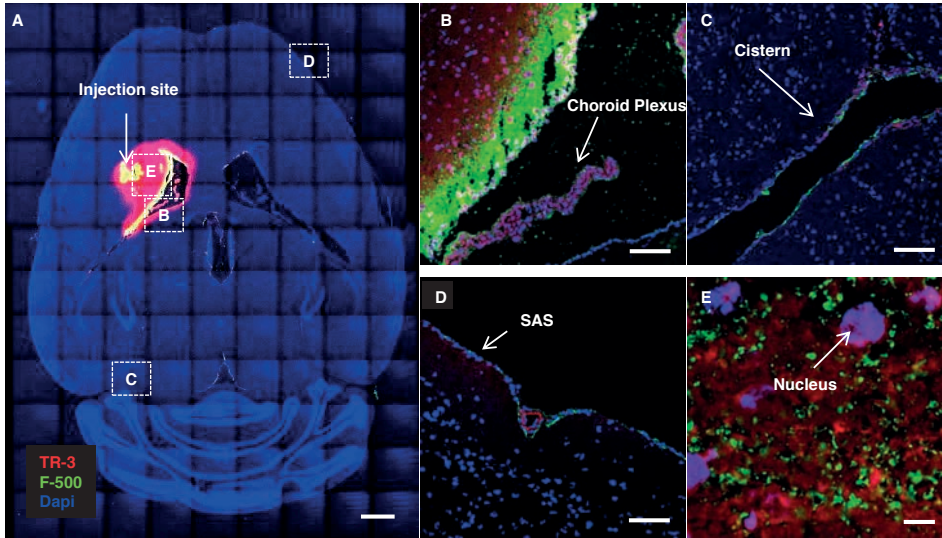


Figure 1. Distribution of the tracers (TR-3 and F-500) 30 min after injection in the striatum. (A) Tile scan of a horizontal brain section at -2 mm from the bregma. A distinct distribution of the tracers towards the lateral ventricle was observed. Scale bar: 1 mm. Anatomical details are shown in panels B-E. (B) Ventricle and choroid plexus. Tracers coming from the parenchyma reached the ventricle, crossing the ependymal layer. TR-3 is taken up by the choroid plexus while F-500 stays on its outer layer. Scale bar: 100 μ m. (C) The ambient cistern showed both tracers. Scale bar: 100 μ m. (D) The subarachnoid space showed both F-500 and TR-3, although the signal of TR-3 is weaker compared to F-500. Note the autofluorescence of elastin (red) in the meningeal artery. Scale bar: 100 μ m. Panel E Detail of the brain parenchyma. TR-3 is observed intra- and intercellular, while F-500 appears to remain extracellular. Scale bar: 10 μ m.

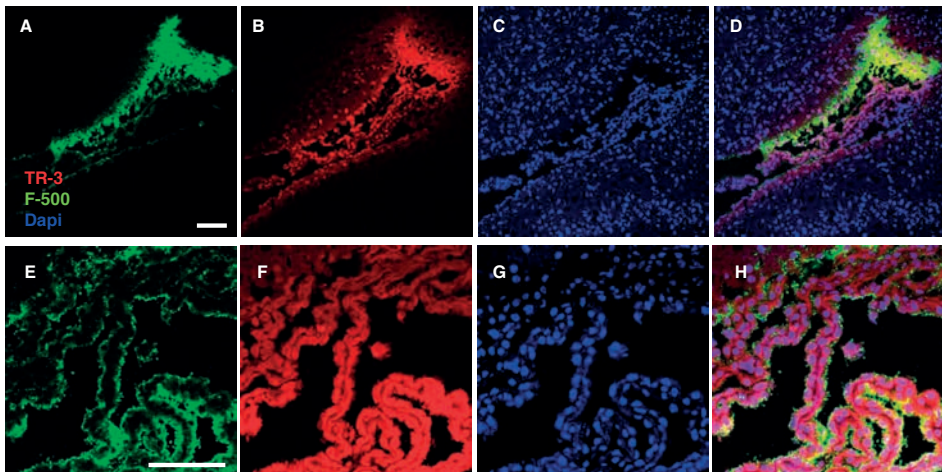


Figure 2. Penetration of TR-3 in the choroid plexus after striatum injection. Horizontal section -3 mm from the bregma. (A-D) Overview of the lateral ventricle. F-500 accumulated towards the ependymal layer (A) while TR-3 appeared to cross the ependymal more easily (B). Cell nuclei stained with DAPI (C). A merged picture is shown in panel d. (E-G) Detail of the choroid plexus. F-500 remains confined to the surface of the choroid plexus (E) while TR-3 clearly penetrated the choroid plexus (F). Cell nuclei stained with DAPI (G). Merged picture (H). Scale bar: 100 μ m.

3D reconstruction of blood vessels and tracer transport in the mouse's head after infusion in the striatum

3D images of tracer distribution after injection in the striatum were generated by an imaging cryomicrotome. After sacrifice of the animal, blood vessels were filled with fluorescent cast material via the aorta, in order to map tracer distribution against the vasculature. The whole mouse head was sectioned (approximately 2500 sections) after freezing. En face fluorescent images were taken during automated sectioning. This approach preserves dye present in fluid compartments (ISF and CSF), which could be lost during sectioning and processing. In addition, since we included the whole mouse head, it also captured the drainage pathways from the brain to peripheral structures. Figure 3 shows tracer distribution after 30 min continuous infusion in the striatum. Similar to the confocal images, in the 3D reconstruction we observed that tracers drained from the striatum to the adjacent lateral ventricle. 2D coronal views of the brain (Fig. 3.C-E) show the presence of F-500 further along the external capsule, in the ventral side of the olfactory bulb, the nasal turbinates, as well as the contralateral ventricle and third ventricle (Additional File 1). Similar to F-500, TR-3 was observed in the parenchyma close to the injection site, from where it followed the same route towards the ventricular system (not shown). Thus, these images confirmed the observations made with confocal imaging on tracer clearance from the parenchyma by bulk flow of ISF towards the ventricles.

Tracers injected into the cisterna magna disperse over the subarachnoid space

We next evaluated bulk flow using tracer infusion in the cisterna magna, using the same mix of tracers as injected into the striatum (n=5). Again we used a 30 min continuous infusion, to map the distribution of tracers from their injection site. Confocal imaging showed that after 30 min of infusion, both tracers distributed over the subarachnoid space and entered the large cisterns of the brain. As shown in the overview (Fig. 4A) and in details in panel B, the ventricles showed no signal, indicating that the tracers did not enter the ventricular system, neither along the CSF pathways nor via transport through the cortex, interstitial compartments and ventricular ependyma. Other views (Figure 4C, D) showed that F-500 remained confined to the subarachnoid space, whereas TR-3 also penetrated the parenchyma, crossing the pia mater. This is particularly evident close to the tentorium cerebelli, and around the olfactory bulb. Analysis of TR-3 penetration across the pial layer indicated that this tracer was detected up to ~200 μm into the cortex (Figure 4E). The average penetration depth was 64 μm .

Reconstruction of the mouse head in 3D after tracer infusion in the cisterna magna

We next studied 3D tracer distribution after injection of tracers in the cisterna magna. Figure 5A and B show the vasculature (in blue) and the tracers (F-500 in green and TR-3 in red); Figure 5C-E show coronal views. The 3D image confirmed the observations made

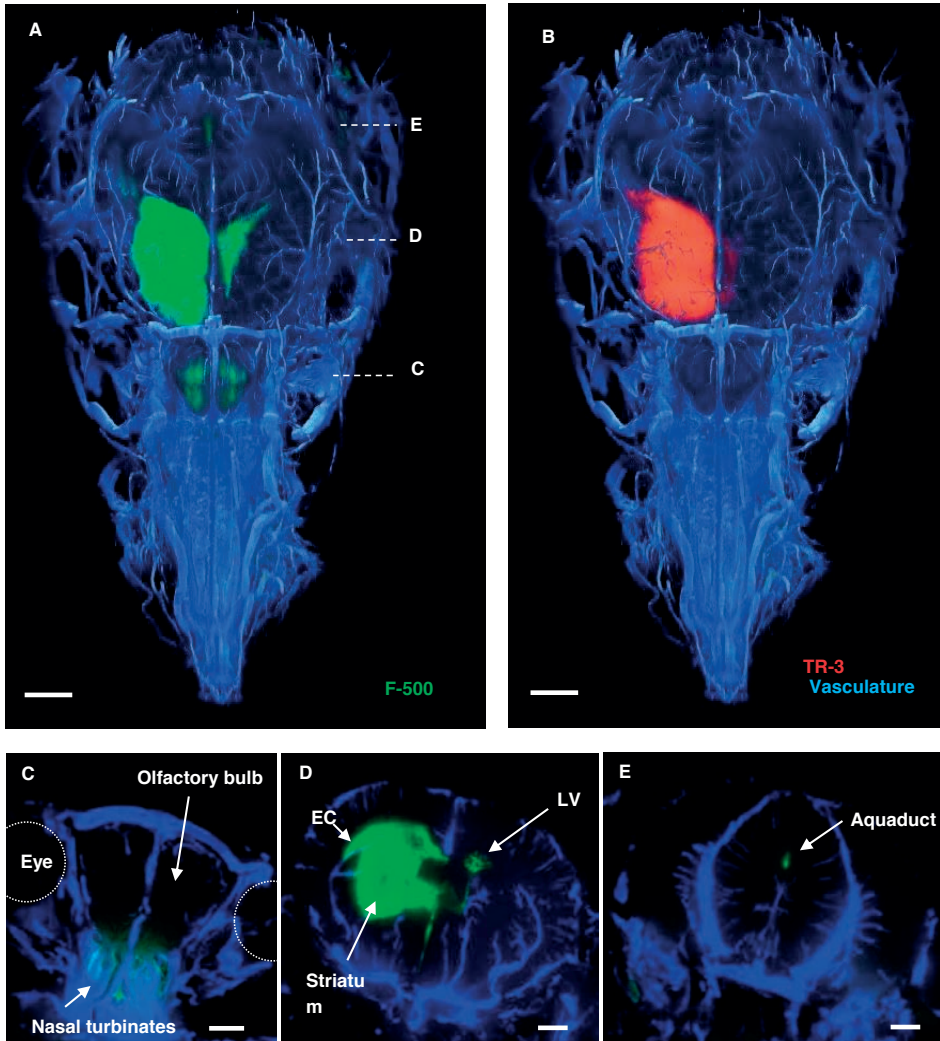


Figure 3. Three dimensional reconstruction of the vasculature and distribution of tracers in a mouse head after injection in the striatum. (A) F-500 is present at the injection site, the lateral ventricles and in the olfactory bulb. (B) TR-3 is present in the same compartments but could not be detected in the olfactory bulb. Panels c-e represent maximum intensity projections of 50 images, at the indicated levels shown in A of the vasculature and F-500. (C) F-500 reached the nasal turbinates through the cribriform plate. (D) F-500 distributed in the striatum, reached the external capsule (EC), and the contralateral ventricle (LV) via the ventricular system. (E) The aqueduct of Sylvius showed F-500. Panels A, B: dorsal view. Panels C, D, E: coronal view. Scale bar: 1 mm.

with confocal imaging (Additional file 2). Thus, most of the tracers were confined to the subarachnoid space, with a stronger signal for both tracers on the ventral side of the brain (Fig. 5E). Additionally, the dye was found in the longitudinal fissure, and around the major vessels arising from the cortex and ventral side of the brain (Fig. 5C-E). Interestingly, outside the brain the strongest signal for both was observed in the nose (Fig.

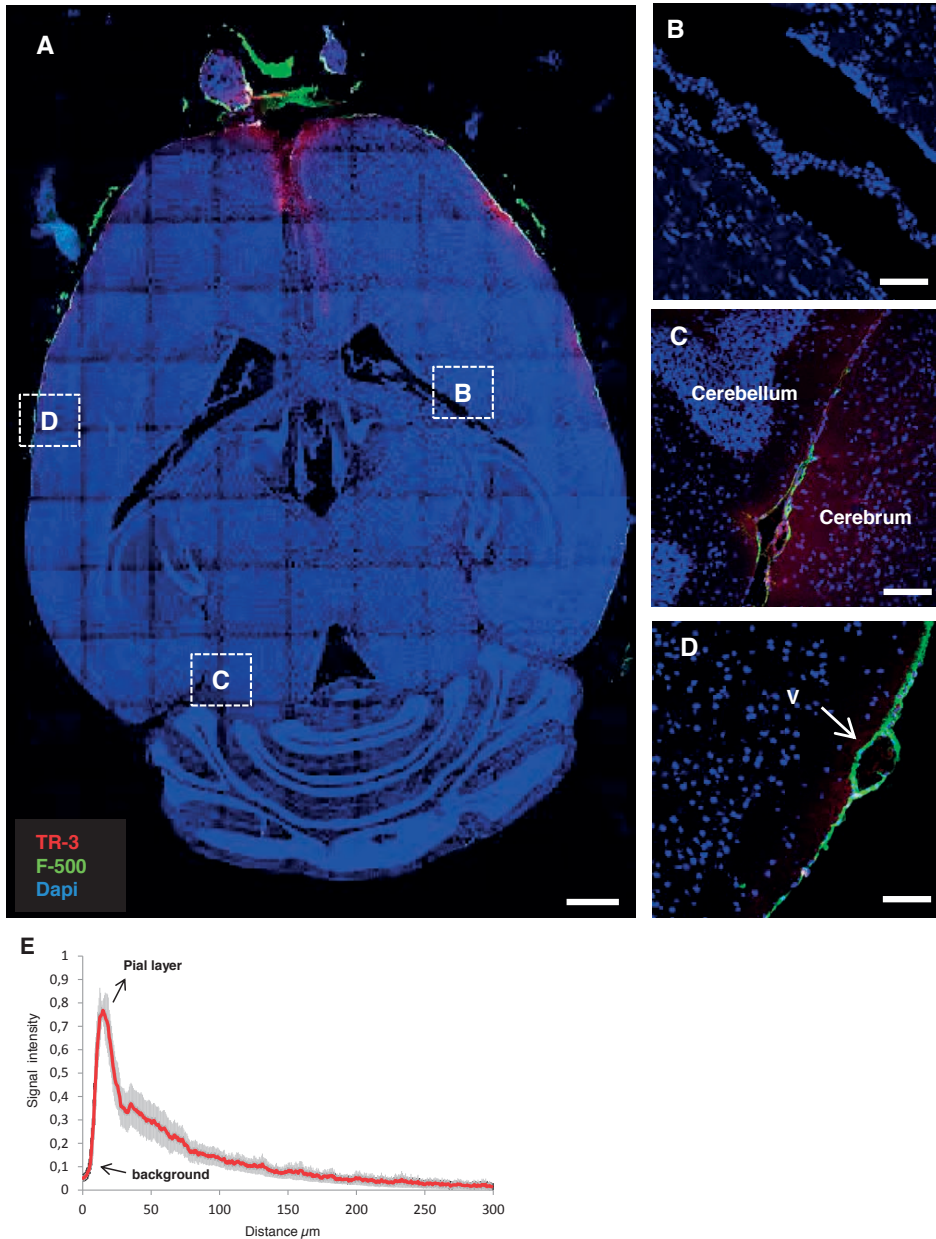


Figure 4. Distribution of the tracers 30 min after injection in the cisterna magna. (A) Tile scan of a horizontal section -2 mm from the bregma. The ventricular system showed no signal, while the olfactory bulb and the subarachnoid space showed both tracers. TR-3 and F-500 were observed in the subarachnoid space along the entire section. Scale bar: 1 mm. Anatomical details are shown in panels B-D. (B) The ventricle and choroid plexus did not show TR-3 and F-500. (C) The ambient cistern showed both tracers, with TR-3 also entering the adjacent parenchyma. (D) A leptomeningeal vein (v arrow) in the SAS showed F-500 in the paravascular space. Scale bar: 100 μm . (E) Signal intensity as a function of distance for TR-3 from the SAS to the brain parenchyma across the pial layer, 30 min after CM injection. The mean distance is $64 \pm 7 \mu\text{m}$ (N=5).

5C). The continuous presence of both dyes between the olfactory bulb and the nose suggest that these tracers leave the brain through the cribriform plate (Fig. 5C). The ventricular system was completely devoid of tracers (Fig. 5D). TR-3 showed the same distribution pattern, but more diffuse and less intense (not shown).

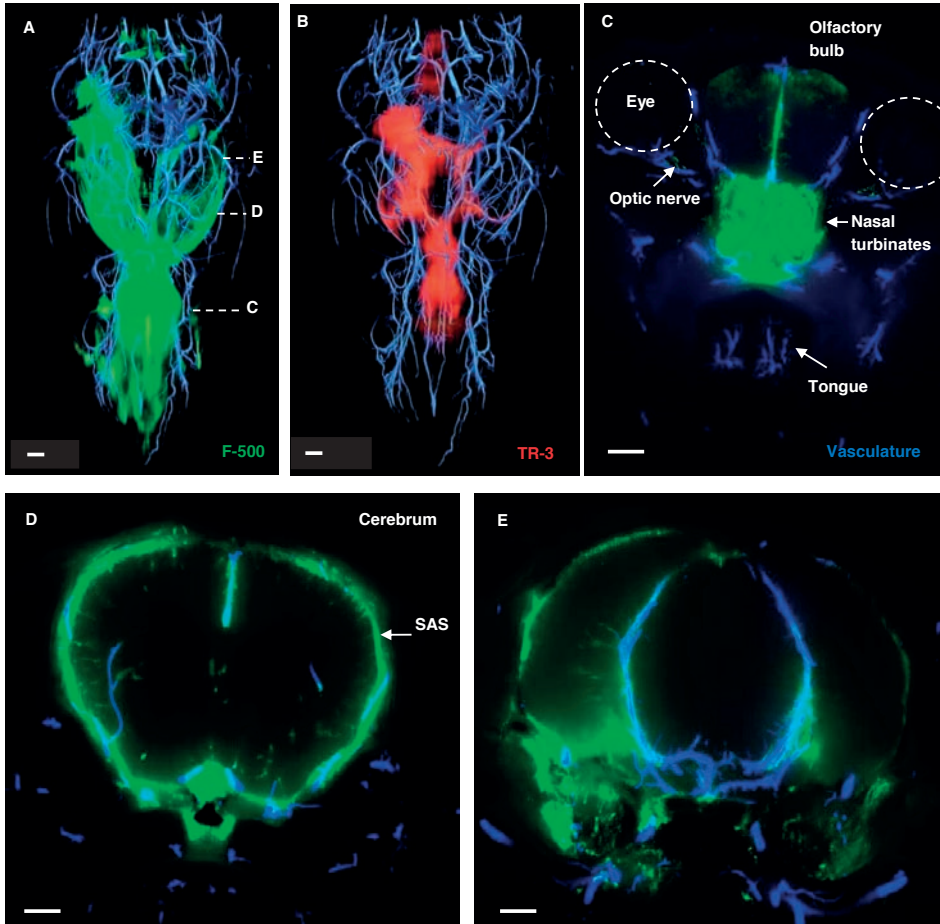


Figure 5. Three dimensional reconstruction of the vasculature with co-localized distribution of tracers in a mouse head after injection in the cisterna magna. (A) F-500 was found in the subarachnoid space and along the penetrating arteries of the brain. (B) TR-3 was observed in the same compartment, but less confined and also diffusely present in the brain parenchyma. This was particularly evident around the large arteries of the circle of Willis. (C) Outside the brain, a strong signal was found in the nasal turbinates and along the optic nerves. Maximum intensity projections of 50 images at the indicated levels of the vasculature and F-500 are shown in panels C-E. Panels A-B: dorsal view; C-E: coronal view. Scale bar: 1 mm.

Role of blood vessels in clearance

To further analyze the involvement of the vasculature and its peri- and/or paravascular spaces as potential distribution pathways, we stained sections with an anti-laminin

antibody. Laminin-positive staining was observed both within the walls of blood vessels (arteries, veins, capillaries) and the meninges. Among blood vessels, large arteries could easily be discriminated from veins, particularly in the SAS, based on the autofluorescence of elastin (Fig. 6A). Following injection into the cisterna magna (CM), tracers were seen around both arteries and veins in the SAS, with penetration of dye along the vessel walls of arteries into the parenchyma (Fig. 6A). There was no visible boundary or difference in signal intensity between the paravascular signal and the subarachnoid space, suggesting that the subarachnoidal and paravascular spaces form a continuous fluid compartment (Fig. 6A). Tracers were most clearly visible in the ambient cistern where also several large arteries enter the brain (Fig. 6B). Note that TR-3 penetrated the parenchyma of the cerebrum but not the cerebellum. Within the parenchyma of the cerebrum, F-500 was observed along vessels that penetrate the brain from the ventral side (Fig. 6C and Fig. 7). Based on wall thickness, these vessels were most likely arteries. Following injection into the striatum, neither capillaries, nor veins close to the injection

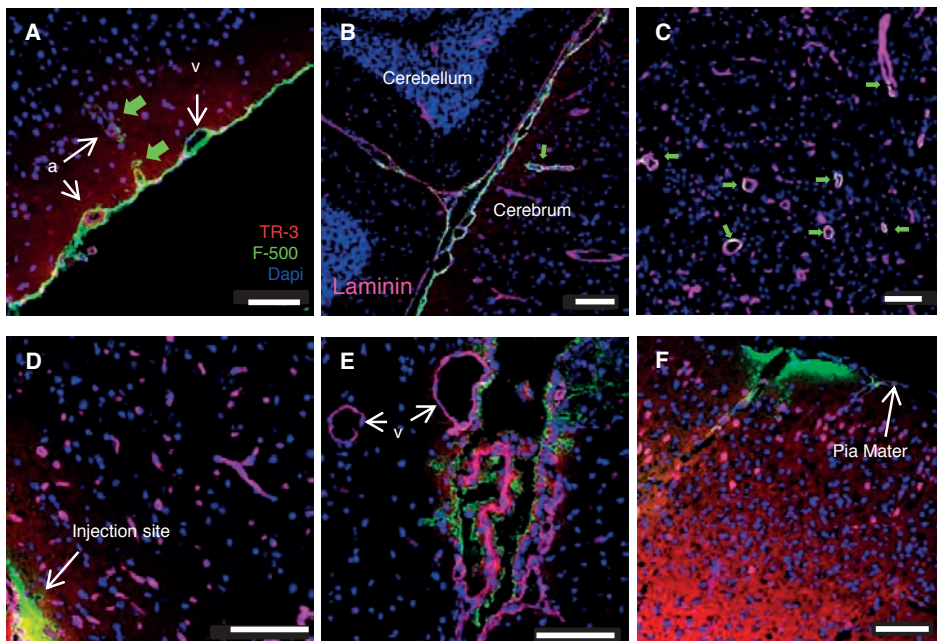


Figure 6. Role of the vasculature in bulk flow. (A-C) Cisterna magna injection, (D-F) Striatum injection. Additional laminin staining is present in panels B-F. (A) Tracers were found in the subarachnoid space, embedding arteries (a) and veins (v). Arteries showed additional red autofluorescence from elastin. Green arrows: F-500 followed paravascular spaces along arteries into the parenchyma. (B) F-500 was prominent in cisterns, where large arteries entered the brain (green arrow). (C) F-500 entered the paravascular space of vessels from the ventral side of the brain (green arrow). (D) Small vessels close to the injection site did not show tracers. (E) Choroid plexus with TR-3 and F-500, adjacent veins (v) did not show tracers. (F) Both tracers followed blood vessels towards the brain surface. F-500 accumulated at the pia mater. Scale bar: 100 μ m

site in the striatum (Fig. 6D), nor the parenchymal vessels close to the lateral ventricle (Fig. 6E) showed tracers. However, occasionally tracers were seen to accumulate towards arteries ventral to the injection site and along the vessel walls near the cortex (Fig. 6F). In this case, TR-3 was seen along the vessel walls, while F-500 accumulated towards the pia mater. These observations suggest bulk flow of ISF close to the surface of the cortex towards the SAS.

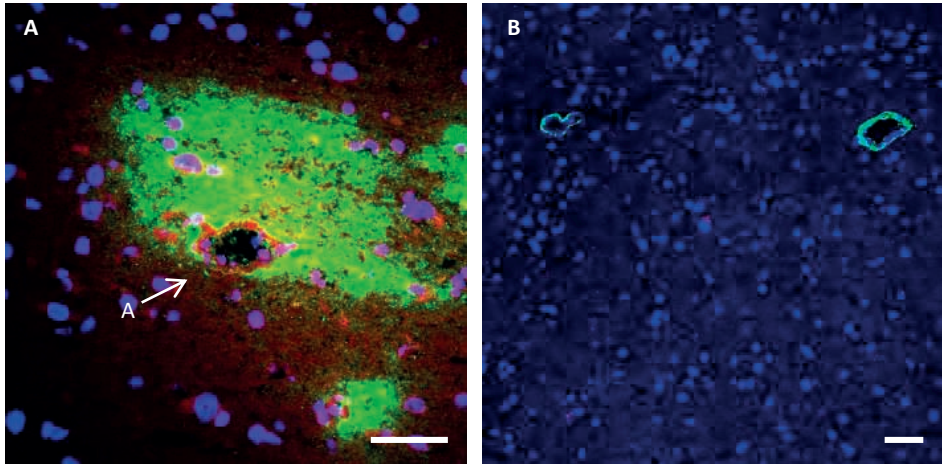


Figure 7. Different appearance of tracers around parenchymal vessels according to the injection site. (a) A case where tracers accumulated around an artery, after injection in the striatum. TR3 was taken up by smooth muscle cells and parenchymal cells, whereas F500 was not. (b) Two parenchymal vessels showing F500 after injection in the cisterna magna. In this case the tracer entered the paravascular space from the CSF, but did not enter the parenchyma. We speculate that in panel (a) tracers were carried by bulk flow towards the artery, whereas in panel (b) the tracer entered the paravascular space as a result of the continuity with the SAS and the strong mixing action caused by pulsations in the CSF. Scale bar: 50 μm .

DISCUSSION

In this study we investigated clearance of the brain and the role of peri- and paravascular pathways herein. The perivascular route is considered to be located along basement membranes within the vessel wall¹⁰. On the other hand, the paravascular space is located in between the brain parenchyma (astrocyte endfeet) and the vessel, and is filled with CSF⁹. The contribution of diffusion and bulk flow in the removal of metabolites and waste from brain extracellular fluids is a longstanding debate that recently has regained interest. Based on earlier work from Cserr¹⁴⁻¹⁶, Rennels⁴, Weller¹⁰, and others, Abbott⁶ concluded that ISF is not a static fluid, although a later review by Sykova E, Nicholson C.¹³ concludes that bulk flow is likely to be restricted to perivascular spaces and the main mechanism for exchange in the brain extracellular space is diffusion. More recent

work of the Nedergaard group^{9,17,18} suggests that paravascular pathways provide an influx route for CSF along arteries, which mixes with ISF and leaves the brain via venous outflow pathways. However, as pointed out by Hladky and Barrand¹⁹, this view is at variance with many earlier studies and awaits further confirmation.

Bulk flow from the striatum towards the ventricular system

The current study presents several arguments for the presence of bulk flow of interstitial fluid from the striatum towards the ventricles. The first evidence is the transport of the tracers after injection into the striatum, where the tracers distribute from the injection towards the nearest lateral ventricle. Both F-500 and TR-3 moved along extracellular spaces, albeit that TR-3 was also taken up by parenchymal cells, in accordance with *in vitro* data²⁰. Such transport could theoretically be caused by diffusion, convection, or both. Discrimination between these processes is possible based on the distances traveled and the directionality of such transport. F-500 would be expected to diffuse a far smaller distance than TR-3 which, in our hands, was not the case. In addition, F-500 clearly moved towards the ventricles, and accumulated strongly at the ependymal layer. The accumulation is suggestive of a sieving process, where ISF is transported to the ventricle and part of the tracer stays behind. For the small TR-3, transport distances for diffusion would still be in the order of magnitude that we found¹³, but also here the tracer preferentially moved towards the ventricles. This dye accumulated to a lesser extent, reflecting the possibility that it passes the ependymal layer more easily than F-500. Taken together, this suggests a significant contribution of tracer drainage by ISF bulk flow from the striatum into the ventricular system. In the lateral ventricle, ISF mixes with CSF once it passes the ependymal cells at the ventricle edge. Then, tracers follow CSF bulk flow along the ventricular system and get further distributed over the subarachnoid space.

The choroid plexus as a potential exit route from the CSF

Floating in the ventricles, the choroid plexus is considered as the main source of CSF. In this study, we found that TR-3 penetrates into the choroid plexus. Distances are short, so penetration could be the result of diffusion from the ventricular CSF. Alternatively, it has been shown that active transport can be bi-directional over the epithelial cells of the choroid plexus²¹. The epithelial cells of the choroid plexus constitute the blood-CSF barrier (BCSFB) that limits the movement of solutes from blood to the CSF and vice versa. However, like the blood-brain barrier, the BCSFB contains transport systems for influx and/or efflux of nutrients, metabolic products and ions, and might also be involved in detoxification processes^{21,22}. This also opens the possibility that the choroid plexus may function as an exit route for waste products from the CSF. Indeed, *ex vivo* data show the removal of amyloid β from the choroid plexus²³ and *in vivo*, there is a correlation

between choroid plexus dysfunction and amyloid β removal²⁴²⁴⁵⁴²⁴. Nevertheless, the current data did not allow us to discriminate between diffusion and active transport of this particular tracer over the BCSFB.

Lack of evidence for bulk flow from the subarachnoid space and paravascular spaces into the brain parenchyma

CSF and ISF may not only communicate at the ependymal layer of the ventricles, but also at the pial level¹⁶. In our experiments, after injection into the cisterna magna, the mixture of fluorescent tracers spread in the subarachnoid space. We observed that TR-3 entered the parenchyma close to the SAS and arteries, while F-500 was confined to the SAS and paravascular spaces. The TR-3 signal decreased steeply in deeper cortex layers, and was detected up to about 0.2 mm deep. Based on the diffusion coefficient for TR-3 in brain tissue²⁵, and an average diffusion time of 15 min in our experiments, one would estimate that this tracer may diffuse over an average distance of ~ 0.31 mm. This is more than the average distance that we observed: ~ 0.064 mm. Therefore, the penetration of tracer appears to be less than can be anticipated on the basis of diffusion. In fact, the small penetration depth suggests that diffusion is possibly hindered by bulk flow in the opposite direction. Thus, we suggest that in the current settings there was limited penetration of small solutes from the SAS into the brain by diffusion (Fig. 4), and no bulk flow from the SAS and paravascular spaces into the brain parenchyma. This is further substantiated by the distribution of the high molecular tracer along the paravascular spaces. Thus, F-500 showed a steep decrease in intensity along arteries entering the brain, while a constant or even an increased concentration of dye would be expected due to a sieving action with paravascular inflow of CSF. A more likely explanation for the distribution of tracers over the SAS and along paravascular spaces could therefore be the strong mixing movement in the subarachnoid space due to arterial pulsations²⁶.

Bulk flow of ISF: a continental divide

The current study suggests the presence of bulk flow of ISF from the striatum toward the ventricular system. We found no evidence for a contribution of recirculation or re-entrance from the subarachnoid or para-vascular spaces to this ISF flow. At this point, our interpretation differs from the glymphatic concept⁹. In particular, we did not observe outflow along parenchymal veins towards the subarachnoid space. Leptomeningeal veins may have shown tracers simply because the tracers are present in the SAS. Rather, the picture that emerges from our data is that ISF flow is generated by the transport of fluid from the capillaries to the interstitium. In other organs, such fluid transport is believed to be a very local phenomenon. According to the Starling balance of hydrostatic and oncotic pressures, fluid leaves higher pressure capillaries, close to the arterioles, and is mostly reabsorbed by venous capillaries. The remainder is removed by the lymphatic

system. In the brain, fluid transport from capillaries to interstitium depends on active transport of ions and solutes rather than Starling forces, and reabsorption is thought to be absent¹⁹. Such fluid therefore needs to find its way to the CSF compartment. This would generate a cumulating flow, small in regions far from the ventricles (like rivulets high up in the mountains), and much larger when approaching the ventricles. Occasionally (Fig. 6F) we observed that tracer present close to the cortical surface finds its way to the brain surface along blood vessels. These findings resemble the observations by Weller¹⁰. We therefore speculate that there is a ‘continental divide’, a point of highest interstitial pressure where generated ISF flows to either the ventricles or the cortex. We suggest that in the mouse this watershed is situated very close to the cortical surface. Indeed, Arbel-Ornath²⁷ found that when tracers are injected in the cortex, they quickly drain out of the brain along arteries. In this analogy, peri- and paravascular spaces could be seen as fjords, allowing fluid transport from the mountains to the sea. It should be mentioned that the concept of fluid generation from capillaries is controversial²⁸⁻³¹, and we see the above view as a working hypothesis. Many issues remain to be addressed, including the nature and regulation of water transport over the BBB, the amount of generated ISF/CSF volume as compared to production by the choroid plexus, the interstitial pressure profile, relevance for removal of toxic products, and relevance for other species and conditions, notably for humans.

Limitations

Injection of bulk fluid may be a confounding factor when studying interstitial fluid transport. The contribution of the infusion rate to tracer distribution is difficult to establish. We used an infusion rate far less than many theoretical³² and experimental studies¹⁰, but the contribution of the pumping rate still may not be completely ignored. In pilot studies we varied infusion rates both for the striatum and cisterna magna infusions, and found no clear differences in tracer distribution. Even when the infusion rate was reduced to zero, allowing only diffusion from the tip of the needle, fluorescein (0.38 kD) was found to subsequently drain from the striatum towards the lateral ventricle. Alternatively, increased perfusion rates and/or volumes applied to cisterna magna infusion did not appreciably alter the distribution of the tracers (data not shown).

Finally, the use of anesthetics in the present study might have an effect on the fluid movement. Indeed Xie L et al. showed that during anesthesia the drainage of extracellular fluid in mice is increased compared to the awake condition, but is similar to the results obtained during physiological sleep¹⁷.

Conclusion

The results of our study indicate that tracers injected in the striatum find their way to the ventricular system via ISF, dominated by bulk flow. The driving force for this flow

could originate in parenchymal capillaries that act as a source of fluid production. In the ventricular system, ISF becomes mixed with CSF. Within the ventricles, the choroid plexus could play a dual role, not only producing CSF but also taking up low molecular weight substances. Since tracers injected into the cisterna magna did not enter the ventricular system, our data are consistent with the prevailing view that CSF flows along the ventricular system, reaches the subarachnoid space via the foramen of Magendie, and subsequently enters the subarachnoid space in the cisterna magna (Fig. 8)³³. The relevance of this drainage pathway for removal of amyloid β and other waste products remains to be explored.

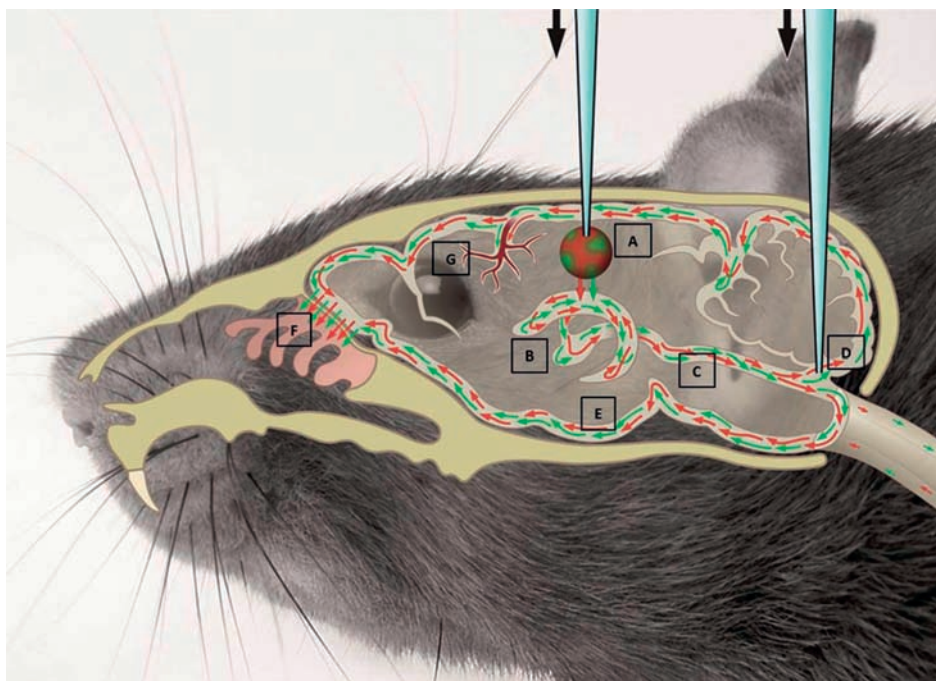


Figure 8. Overview of tracer distribution in a mouse head. Tracers injected in the striatum (A) distribute via ISF to the lateral ventricle (B) and subsequently to the ventricular system (C), where they mix with the CSF. From there, they spread along the ventricles and via the cisterna magna (D) they reach the SAS (E). Tracers leave the brain via the cribriform plate via the olfactory nerves (F). In the SAS tracers distribute along the leptomeningeal vessels, along the paravascular space (G).

Additional files

Additional file 1. Three dimensional reconstruction of the vasculature and distribution of tracers in a mouse head after injection in the striatum. Both TR-3 and F-500 entered the closest lateral ventricle. The tracers further dispersed to the contralateral ventricle, along the ventricular system, the subarachnoid space ventral of the olfactory bulb, and the nasal turbinates.

Additional file 2. Three dimensional reconstruction of the vasculature and distribution of tracers in a mouse head after injection in the cisterna magna. Both TR-3 and F-500 were observed in the subarachnoid space, particularly on the ventral side of the brain around the circle of Willis. Both tracers left the brain through the cribriform plate and nasal turbinates.

Abbreviations

ISF, Interstitial fluid; CSF: cerebrospinal fluid; SAS: subarachnoid space; CM: cisterna magna; TR-3: dextran, Texas Red, 3 kD; F-500: dextran, FITC,500 kD; BCSFB: blood-CSF barrier

Authors' contributions

BB, EvB and EB designed the study and wrote the manuscript. MS critically reviewed the manuscript. BB, EB, JdeV, JB and MvL performed the experiments. All authors have read and approved the final manuscript.

Acknowledgments

This project has received funding from the Internationale Stichting Alzheimer Onderzoek (ISAO) and from the European Union's Seventh Framework Programme for research, technological development and demonstration under grant agreement no 606998. We acknowledge the contribution of Inge E. M. Kos-Oosterling, for the medical illustration.

Compliance with ethical guidelines

Competing interests

The authors declare no competing financial interests.

REFERENCES:

1. Cserr, H. F., Harling-Berg, C. J. & Knopf, P. M. Drainage of brain extracellular fluid into blood and deep cervical lymph and its immunological significance. *Brain Pathol* 2, 269-276 (1992).
2. Louveau, A. et al. Structural and functional features of central nervous system lymphatic vessels. *Nature* 523, 337-341, doi:10.1038/nature14432 (2015).
3. Aspelund, A. et al. A dural lymphatic vascular system that drains brain interstitial fluid and macromolecules. *J Exp Med* 212, 991-999, doi:10.1084/jem.20142290 (2015).
4. Rennels, M. L., Gregory, T. F., Blaumanis, O. R., Fujimoto, K. & Grady, P. A. Evidence for a 'paravascular' fluid circulation in the mammalian central nervous system, provided by the rapid distribution of tracer protein throughout the brain from the subarachnoid space. *Brain Res* 326, 47-63 (1985).
5. Brinker, T., Stopa, E., Morrison, J. & Klinge, P. A new look at cerebrospinal fluid circulation. *Fluids Barriers CNS* 11, 10, doi:10.1186/2045-8118-11-10 (2014).
6. Abbott, N. J. Evidence for bulk flow of brain interstitial fluid: significance for physiology and pathology. *Neurochem Int* 45, 545-552, doi:10.1016/j.neuint.2003.11.006 (2004).
7. Damkier, H. H., Brown, P. D. & Praetorius, J. Cerebrospinal fluid secretion by the choroid plexus. *Physiol Rev* 93, 1847-1892, doi:10.1152/physrev.00004.2013 (2013).
8. Cserr, H. F. Relationship between cerebrospinal fluid and interstitial fluid of brain. *Fed Proc* 33, 2075-2078 (1974).
9. Iliff, J. J. et al. A paravascular pathway facilitates CSF flow through the brain parenchyma and the clearance of interstitial solutes, including amyloid beta. *Sci Transl Med* 4, 147ra111, doi:10.1126/scitranslmed.3003748 (2012).
10. Carare, R. O. et al. Solute, but not cells, drain from the brain parenchyma along basement membranes of capillaries and arteries: significance for cerebral amyloid angiopathy and neuroimmunology. *Neuropathol Appl Neurobiol* 34, 131-144, doi:10.1111/j.1365-2990.2007.00926.x (2008).
11. Spaan, J. A. et al. Visualisation of intramural coronary vasculature by an imaging cryomicrotome suggests compartmentalisation of myocardial perfusion areas. *Med Biol Eng Comput* 43, 431-435 (2005).
12. van den Wijngaard, J. P. et al. 3D Imaging of vascular networks for biophysical modeling of perfusion distribution within the heart. *J Biomech* 46, 229-239, doi:10.1016/j.jbiomech.2012.11.027 (2013).
13. Sykova, E. & Nicholson, C. Diffusion in brain extracellular space. *Physiol Rev* 88, 1277-1340, doi:10.1152/physrev.00027.2007 (2008).
14. Szentistvanyi, I., Patlak, C. S., Ellis, R. A. & Cserr, H. F. Drainage of interstitial fluid from different regions of rat brain. *Am J Physiol* 246, F835-844 (1984).
15. Cserr, H. F. Role of secretion and bulk flow of brain interstitial fluid in brain volume regulation. *Ann N Y Acad Sci* 529, 9-20 (1988).
16. Cserr, H. F., Depasquale, M., Patlak, C. S. & Pullen, R. G. Convection of cerebral interstitial fluid and its role in brain volume regulation. *Ann N Y Acad Sci* 481, 123-134 (1986).
17. Xie, L. et al. Sleep drives metabolite clearance from the adult brain. *Science* 342, 373-377, doi:10.1126/science.1241224 (2013).
18. Iliff, J. J. et al. Cerebral arterial pulsation drives paravascular CSF-interstitial fluid exchange in the murine brain. *J Neurosci* 33, 18190-18199, doi:10.1523/JNEUROSCI.1592-13.2013 (2013).
19. Hladky, S. B. & Barrand, M. A. Mechanisms of fluid movement into, through and out of the brain: evaluation of the evidence. *Fluids Barriers CNS* 11, 26, doi:10.1186/2045-8118-11-26 (2014).

20. Tansey, F. A. & Cammer, W. Differential uptake of dextran beads by astrocytes, macrophages and oligodendrocytes in mixed glial-cell cultures from brains of neonatal rats. *Neurosci Lett* 248, 159-162 (1998).
21. de Lange, E. C. Potential role of ABC transporters as a detoxification system at the blood-CSF barrier. *Adv Drug Deliv Rev* 56, 1793-1809, doi:10.1016/j.addr.2004.07.009 (2004).
22. Strazielle, N. & Ghersi-Egea, J. F. Choroid plexus in the central nervous system: biology and physiopathology. *J Neuropathol Exp Neurol* 59, 561-574 (2000).
23. Crossgrove, J. S., Li, G. J. & Zheng, W. The choroid plexus removes beta-amyloid from brain cerebrospinal fluid. *Exp Biol Med (Maywood)* 230, 771-776 (2005).
24. Gonzalez-Marrero, I. et al. Choroid plexus dysfunction impairs beta-amyloid clearance in a triple transgenic mouse model of Alzheimer's disease. *Front Cell Neurosci* 9, 17, doi:10.3389/fncel.2015.00017 (2015).
25. Thorne, R. G. & Nicholson, C. In vivo diffusion analysis with quantum dots and dextrans predicts the width of brain extracellular space. *Proc Natl Acad Sci U S A* 103, 5567-5572, doi:10.1073/pnas.0509425103 (2006).
26. Feinberg, D. A. & Mark, A. S. Human brain motion and cerebrospinal fluid circulation demonstrated with MR velocity imaging. *Radiology* 163, 793-799, doi:10.1148/radiology.163.3.3575734 (1987).
27. Arbel-Ornath, M. et al. Interstitial fluid drainage is impaired in ischemic stroke and Alzheimer's disease mouse models. *Acta Neuropathol* 126, 353-364, doi:10.1007/s00401-013-1145-2 (2013).
28. Mokgokong, R., Wang, S., Taylor, C. J., Barrand, M. A. & Hladky, S. B. Ion transporters in brain endothelial cells that contribute to formation of brain interstitial fluid. *Pflügers Arch* 466, 887-901, doi:10.1007/s00424-013-1342-9 (2014).
29. Spector, R., Keep, R. F., Robert Snodgrass, S., Smith, Q. R. & Johanson, C. E. A balanced view of choroid plexus structure and function: Focus on adult humans. *Exp Neurol* 267, 78-86, doi:10.1016/j.expneurol.2015.02.032 (2015).
30. Smith, Q. R. & Rapoport, S. I. Cerebrovascular permeability coefficients to sodium, potassium, and chloride. *J Neurochem* 46, 1732-1742 (1986).
31. Murphy, V. A. & Johanson, C. E. Acidosis, acetazolamide, and amiloride: effects on ²²Na transfer across the blood-brain and blood-CSF barriers. *J Neurochem* 52, 1058-1063 (1989).
32. Morrison, P. F., Laske, D. W., Bobo, H., Oldfield, E. H. & Dedrick, R. L. High-flow microinfusion: tissue penetration and pharmacodynamics. *Am J Physiol* 266, R292-305 (1994).
33. Mortazavi, M. M. et al. The ventricular system of the brain: a comprehensive review of its history, anatomy, histology, embryology, and surgical considerations. *Childs Nerv Syst* 30, 19-35, doi:10.1007/s00381-013-2321-3 (2014).





CHAPTER 3

Paravascular channels, cisterns, and the subarachnoid space in the rat brain: A single compartment with preferential pathway

Beatrice Bedussi¹, Nicole N. van der Wel², Judith de Vos¹, Henk van Veen², Maria Siebes¹,
Ed VanBavel¹, Erik N.T.P. Bakker¹

¹Department of Biomedical Engineering and Physics, Academic Medical Center, Amsterdam, The Netherlands

²Electron Microscopy Centre Amsterdam, Department of Cell Biology and Histology, Academic Medical Center,
University of Amsterdam, Amsterdam, The Netherlands

Published in JCBFM (2016)

doi: 10.1177/0271678X16655550

Authors' contribution: BB, EvB, and EB designed the study and wrote the manuscript. MS critically reviewed the manuscript. BB, EB, JdeV, NNvderW, and HvanV performed the experiments.

ABSTRACT

Recent evidence suggests an extensive exchange of fluid and solutes between the subarachnoid space and the brain interstitium, involving preferential pathways along blood vessels. We studied the anatomical relations between brain vasculature, cerebrospinal fluid compartments, and paravascular spaces in male Wistar Kyoto rats. A fluorescent tracer was infused into the cisterna magna, without affecting intracranial pressure. Tracer distribution was analyzed using a 3D imaging cryomicrotome, confocal microscopy, and correlative light and electron microscopy. We found a strong 3D colocalization of tracer with major arteries and veins in the subarachnoid space and large cisterns, attributed to relatively large subarachnoid space volumes around the vessels. Confocal imaging confirmed this colocalization and also revealed novel cisternal connections between the subarachnoid space and ventricles. Unlike the vessels in the subarachnoid space, penetrating arteries but not veins were surrounded by tracer. Correlative light and electron microscopy images indicated that this paravascular space was located outside of the endothelial layer in capillaries and just outside of the smooth muscle cells in arteries. In conclusion, the cerebrospinal fluid compartment, consisting of the subarachnoid space, cisterns, ventricles, and para-arteriolar spaces, forms a continuous and extensive network that surrounds and penetrates the rat brain, in which mixing may facilitate exchange between interstitial fluid and cerebrospinal fluid.

Keywords

Cerebrospinal fluid; Interstitial fluid; Subarachnoid space; Paravascular space; Intracranial pressure; Glymphatic pathway

INTRODUCTION

The cerebrospinal fluid (CSF) is mainly produced by the choroid plexuses and flows from the ventricular system into the subarachnoid space (SAS), from where it leaves the brain via multiple exit pathways. Apart from well-known structures such as the cribriform plate and arachnoid granulations, recently discovered dural lymphatic vessels^{1,2} may contribute to CSF outflow. Interestingly, work from the Nedergaard group³ suggested that part of the CSF is recirculated along paravascular routes along arteries into the brain, where it mixes with brain interstitial fluid (ISF), and leaves the brain along veins. This mechanism is referred to as the glymphatic pathway and could be important for clearance of the brain, washing out waste products and toxic substances such as amyloid β . Several features of this pathway however, are unclear, as these are described as a 'physically and functionally distinct subcompartment' at the level of the SAS. In addition, the paravascular route seems at variance with the perivascular route described earlier by Carare et al.⁴, which describes the drainage of ISF along basement membranes of small vessels and arteries out of the brain. An excellent review by Hladky and Barrand⁵ recently evaluated the evidence for both views. These authors pointed out several caveats and theoretical concerns for both views, among others related to the anatomical base for proposed transport channels and the presence or not of compartments and barriers for bulk fluid transport around blood vessels. Hladky and Barrand outline several possible routes for fluid drainage, based on the apparently conflicting experimental data indicated above.

The purpose of the current study therefore is to better identify the nature of transport routes surrounding leptomeningeal and parenchymal blood vessels. We set out to elucidate the distribution of fluorescent tracers injected into the cisterna magna (CM) of rats, focusing on the spatial relation with the brain vasculature. For this purpose, we imaged the rat brain vasculature and CSF compartments with a combination of three imaging modalities. At the whole brain level, a custom-built automated imaging cryomicrotome was used^{6,7}. This instrument, based on sequential episcopic fluorescence imaging of the tissue block rather than the individual sections, enables detailed 3D reconstruction of large structures. At the microscopic level, immunostaining and confocal microscopy were used to study paravascular structures and tracer distribution in brain sections. Lastly, correlative light electron microscopy (CLEM) was employed to gain insight into the anatomy of the PVS at the sub-micron level.

MATERIALS AND METHODS

Animals

For this study 12 Male Wistar Kyoto rats (WKY/NCrl), 4 months old, mean weight 326 gr \pm 2g, were purchased from Charles River. Rats were housed in groups under a 12 h light-dark cycle and fed ad libitum with standard laboratory food and free access to water. All experimental protocols were approved by the Committee for Animal Experiments of the Academic Medical Center Amsterdam, according to the ARRIVE and European directive 2010/63/EU.

Anaesthesia

During the experiments, rats were anaesthetized by intraperitoneal injection of a combination of ketamine (75 mg/kg, Nimetek, Eurovet, Bladen, The Netherlands), dexmedetomidine (0.5 mg/kg, Dexdor, Orion Pharma, Mechelen, Belgium), and atropine (0.05 mg/kg, atropinesulfaat, Eurovet) dissolved in phosphate-buffered saline (PBS, Lonza, Basel, Switzerland). Experiments were carried in the laboratory during the sleeping phase of the rat diurnal rhythm, i.e. during daytime hours.

Reagents

Fluorescein-labeled dextran (500 kD, Ex. 494 nm/Em. 521) tracer, lysine-fixable, was purchased from Molecular Probes-Life Technologies (Eugene, OR, USA). The tracer was dissolved in artificial cerebrospinal fluid (aCSF) at a concentration of 20 mg/ml. For immunofluorescence, before freezing and sectioning, brains were embedded in Tissue-Tek (Sakura, Leiden, The Netherlands). Cell nuclei were stained with Vectashield mounting medium with DAPI (4, 6-diamidino-2-phenylindole, Burlingame, CA, USA). Anti-laminin antibody (Sigma-Aldrich) was used for visualization of the vasculature and pial sheets. To discriminate between veins and arteries we used an anti-smooth muscle myosin heavy chain 11 antibody (Abcam).

Cisterna magna infusion

After anaesthesia, animals were placed on a heating pad to maintain body temperature at 37 °C, as monitored by a rectal thermometer. Additional oxygen was provided to prevent hypoxia. Ocular lubricant ointment (Duratears, Alcon, Breda, The Netherlands) was applied to keep the eyes hydrated. The surgery was performed according to the protocol previously described for mice⁸. For the rat, the subcutaneous tissues and the midline of the two layers of neck muscles was separated along the midline in order to reach the cisterna magna. Then, a 29-gauge needle connected to a polyethylene tube was inserted. A total volume of 10 μ l of the 500 kD fluorescein dextran (F-500) solution (20 mg/ml), was infused at a controlled flow rate of 0.34 μ l/min using a syringe pump

(Harvard Apparatus, Holliston, MA, USA) over a 30-min period. At the end of infusion, the animals were euthanized with an overdose of anaesthetic and rapidly decapitated.

Intracranial pressure measurement

Two rats were used in this group. To measure intracranial pressure (ICP) during different rates of infusion, a second 29-gauge needle was inserted into the cisterna magna. This needle was connected to a pressure transducer by stiff polyethylene tubing to prevent damping of pulsations. Data were recorded with a PowerLab acquisition system and analyzed with Chart data analysis software (AD instruments).

3D cryomicrotome imaging and image processing

In this group, three animals were included to obtain a representative picture of the vasculature and outline of tracer distribution. After infusion of tracer and just before sacrifice of the animals, 100 μ l of heparin solution was injected IP to prevent clotting of blood in the vasculature. Immediately after death, animals were flushed with PBS via the abdominal aorta to remove the blood from the vasculature before filling. The vasculature was filled with replica material (Batson's #17, Polysciences) that was fluorescently labeled (UV blue, VasQtec) at 80 mmHg to maintain physiological pressure. After polymerization (45 min), we carefully dissected the brains and stored these at -20°C . Once frozen, the brains were embedded in a black gel (carboxymethylcellulose sodium solvent 5% - Brunschwig Chemie - mixed with Indian ink 5% - Royal Talens), and placed back at -20°C . Using an imaging cryomicrotome, equipped with multispectral power LEDs and selectable filters (custom-built, AMC, Amsterdam, The Netherlands)^{6,7}, the brains were automatically cut into sequential coronal slices of 10 μ m thickness. After each cut, 4096x4096 pixel en face images of the remaining tissue block were taken at 16 bit grey scale resolution by a digital camera (Apogee Alta U-16) equipped with a variable-focus lens (Nikon 70-180mm). These images included a white light reflection image and fluorescence images for the 500 kD fluorescein dextran tracer (excitation 480 nm, emission 535 nm) and vascular cast (excitation 365 nm, emission 505 nm). This resulted in co-registered stacks of about 2200 images (per color) with an in-plane resolution of 8 μ m. For reconstruction, all images were converted into 8 bit greyscale. The brain was then reconstructed in 3D using Amira (FEI Europe B.V., Eindhoven, Netherlands) to obtain a detailed virtual representation of the brain, vasculature, and tracer distribution.

Immunofluorescence and confocal microscopy

In this set of experiments, three rats were used. After infusion of tracer and sacrifice of the animals, brains were carefully dissected and cut into three coronal blocks using an adult rat brain slicer matrix (Zinc instruments). The blocks were separately embedded in Tissue-Tek, snap frozen in liquid nitrogen and stored at -80°C . Subsequently, 5 μ m

coronal sections were cut using a cryostat (Microm HM 560) and then stored at -80 °C until use. Before imaging, sections were fixed in 3.7% paraformaldehyde (PFA) for 30 minutes and then coverslipped with fluorescent mounting medium (DAPI). To visualize vascular structures and pial sheets, some sections were stained with anti-laminin. Staining for myosin heavy chain was done to discriminate arteries and veins. A confocal laser scanning microscope (Leica TCS SP8) was used to acquire fluorescent images, with a 10x objective for overviews and a 20x objective for details.

Correlative Light Electron Microscopy (CLEM)

Four animals were used in this protocol. After infusion of tracer and immediately before sacrifice of the animals, 100 µl of heparin solution was injected IP to prevent blood clotting. Immediately after death, rats were flushed via the abdominal aorta with PBS to remove all blood from the vasculature before perfusion fixation with PFA (4%). After fixation for 10 min at 80 mmHg, the brains were carefully dissected, and cut into several coronal blocks using an adult rat brain slicer matrix (Zinc instruments). The blocks were quickly observed under fluorescent microscope to confirm the presence of the tracer in PVS, placed in PFA (4%) and fixed for two days. Then, regions of interest were selected for CLEM and incubated in 2% gelatine for 30 min. Then small blocks of 2-3 mm² were cut and embedded in increasing amounts of gelatine (2, 5, 12 %in PBS). Blocks were incubated overnight in 2 M sucrose and snap-frozen on a pin in liquid nitrogen. Semi and ultrathin sections were cut as described by van der Wel et al.⁹ and semi-thin sections (300-400 nm) were first analysed using confocal microscopy (Leica SP8), using FITC detection and DAPI for counterstaining of nuclei in the tissue. When vessels positive for FITC were detected, 70-100 nm thin sections were cut, transferred to a 150 mesh copper grid. For TEM analysis, grids with ultrathin sections were washed and stained using a Uranyl acetate/ Tylose mixture and imaged using Tecnai T12 at 120kV. Combining the Light and Electron Microscopy images was performed at numbered grids (Electron Microscopy Science, Alphabetic Finders) to be able to image the identical vessel by both microscope techniques. In addition, serial sections of blocks of maximal 0.1 x 0.1mm were imaged first in FM and the next section in TEM. The position of the nuclei stained with DAPI, which is visible in both FM and EM, was used to align and overlay the images using rigid registration.

RESULTS

Impact of infusion rate on intracranial pressure

To study the anatomy of the paravascular system and its connection to the CSF compartment, we infused fluorescently labeled dextran as a tracer molecule. We used a high

molecular weight tracer to avoid diffusion of tracer into the parenchyma, which would obscure the anatomical outline of these structures. Distribution of tracers however, may be affected by the infusion rate. To avoid artifacts due to increased ICP generated by the infusion pump, we measured ICP at different infusion rates into the CM. Before starting infusion, we recorded the baseline physiological ICP, which averaged 5.7 ± 1.3 mmHg (SEM, $n=2$). Figure 1 shows a tracing of the pressure profile in the CM. The pressure profile was found to be highly oscillatory, which was attributable to the heartbeat and respiration. Herein, respiration had the larger effect (see insert). The infusion rate used in the current manuscript ($0.34 \mu\text{L}/\text{min}$) did not increase ICP. In the example shown in figure 1, ICP slightly increased, from 4.8 to 5.1 mmHg, when the infusion rate was raised up to $3 \mu\text{L}/\text{min}$. More obvious changes in ICP were observed when the infusion rate was increased up to $10 \mu\text{L}/\text{min}$. After stopping the pump, ICP decreased gradually.

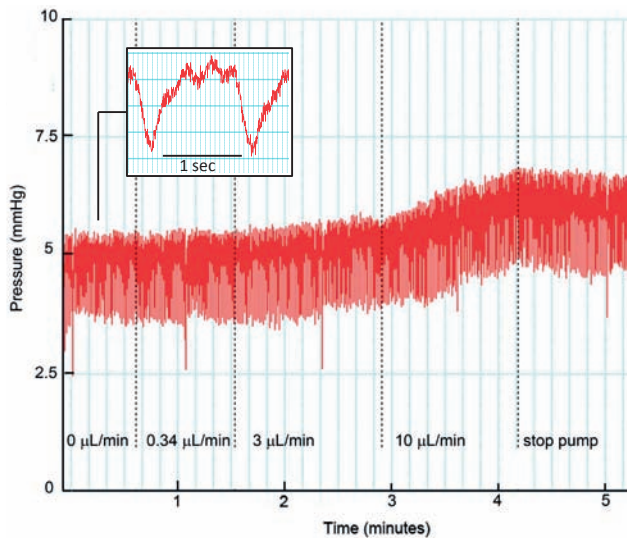


Figure 1. Changes in ICP during infusion of aCSF in the cisterna magna. Pressure (mmHg) as a function of time (min). The dotted lines indicate a stepwise increase in infusion rate ($\mu\text{L}/\text{min}$). At baseline ($0 \mu\text{L}/\text{min}$), the mean ICP was 4.8 mmHg in this example. An infusion rate of $0.34 \mu\text{L}/\text{min}$ did not change the ICP, while a further stepwise increase in infusion rate to $10 \mu\text{L}/\text{min}$ clearly raised ICP. Insert: the pressure profile was affected by the heartbeat, but more importantly, by respiration. Three heartbeats are visible between two large pressure drops induced by inspiration.

3D analysis of rat brain vasculature and tracer distribution

To obtain a combined 3D representation of the vasculature and CSF compartments of the whole brain, we first evaluated vascular and CSF tracer distribution at $8 \mu\text{m}$ resolution with an imaging cryomicrotome. Figure 2A shows the major arteries, including the circle of Willis, hippocampal arteries, dorsocerebellar arteries, anterior choroidal arteries, as well as the major veins such as the transverse sinus, superior sagittal sinus and superior

olfactory sinus. Tracer signal was strong at the base of the brain around the circle of Willis, and in several of the large cisterns (Fig. 2B-C). The tracer was particularly present in the ambient cistern, where it co-localized with the anterior choroidal arteries. Tracer was also observed along the dorsal middle cerebral artery, as well as around the azygos anterior cerebral artery, and olfactory arteries. Moreover, the tracer was found around the superior sagittal sinus, the superior olfactory sinus and to some extent around the transverse sinus. Thus, tracer spreading was evident around all major vessels supplying and draining the brain. Anatomically, these vessels are embedded in the SAS, after which some follow the major cisterns to deeper brain parts (striatum, hippocampus).

A 3D representation of the vasculature and tracer distribution is provided in the supplemental movie. This movie shows that the subarachnoid space, cisterns and spaces surrounding the major arteries and veins form a functional continuum without barriers.

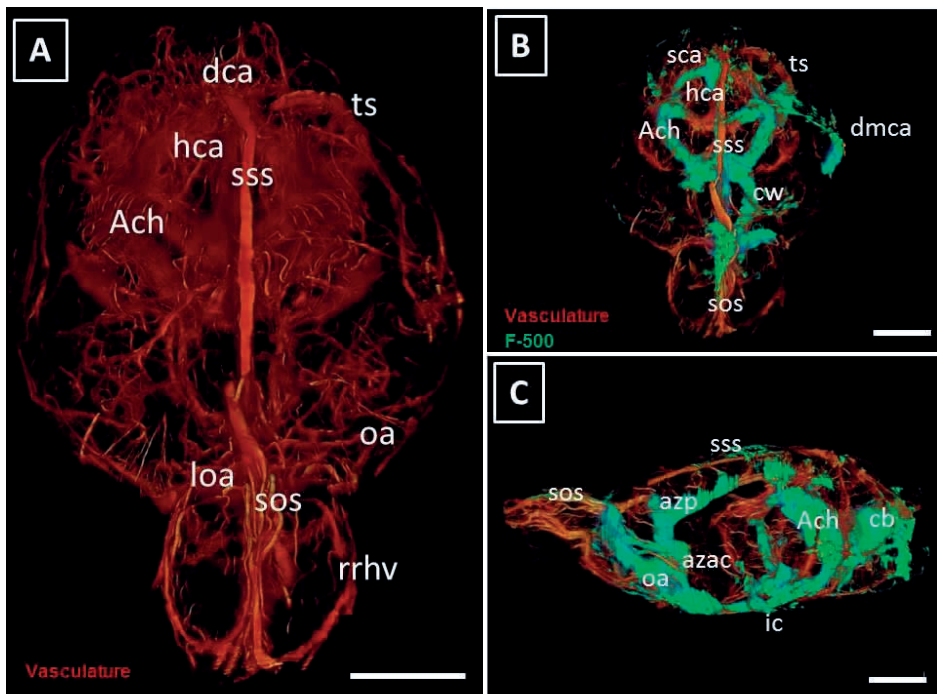


Figure 2. 3D visualization of the rat cerebral vasculature and CSF tracer distribution after infusion in the cisterna magna. Panel A: 3D reconstruction of the rat brain vasculature. Vessels were filled with fluorescent cast material (orange). Panel B: Frontal view of the rat brain. Tracer (F500, green) is visible around the circle of Willis (cw), and the anterior choroidal arteries (ach); along the dorsal portion of the middle cerebral artery (dmca), in the region of the hippocampal arteries (hca), and along the major sinuses-transverse sinus (ts) superior sagittal sinus (sss), and superior olfactory sinus (sos). Panel C: Lateral view of the rat brain. Tracer is present around the azygos anterior cerebral artery (azac) that dorsally becomes the azygos pericallosal artery (azp). Signal was present also caudally along the vasculature of the cerebellum (cb) and the around the superior sagittal sinus in the SAS. Scale bar represents 5 mm.

Continuity between the subarachnoid space, cisterns, and ventricular system

Next, we analyzed the distribution of the CSF tracer by confocal fluorescence imaging on longitudinal and coronal sections of the brain. Sections were stained with an anti-laminin antibody to visualize the arachnoid, pial membranes and basement membranes of blood vessels. Control sections were negative (data not shown).

The tracer had spread from the infusion site over the SAS. Similar to the 3D approach, tracer signal was strong on the ventral side of the brain. The tracer found its way along the deep clefts between the major brain structures that connect the cerebral cisterns (quadrigeminal, ambiens and interpeduncular cistern (Fig. 3A). Virtually all major arteries were found to be embedded in the SAS and followed these cisterns further into the brain. Thus, the SAS, cisterns and vessels were part of a continuous compartment, filled with CSF. Remarkably, we observed that tracer reached the lateral ventricles (Fig. 3B-C) via one of these cisterns in which the longitudinal hippocampal arteries run. Thus, these images show the presence of a connection between the ventricular system and the SAS via the interpeduncular cistern.

Paravascular space

After making a general outline of tracer distribution over the brain, we focused on paravascular spaces along parenchymal and leptomeningeal vessels. Figure 4A shows the posterior cerebral artery and the interpeduncular vein, located in the interpeduncular cistern at the base of the brain. Both artery and vein are embedded in the SAS and bathed by the CSF. There was no visible anatomical boundary between these vessels that would suggest different compartments. Panel B shows the paravascular localization of the tracer around the posterior cerebral artery in detail. A particularly strong signal was observed along the outside of this and other arteries, continuous with the signal along the arachnoid mater.

All vessels in the SAS were surrounded by tracer, indicating direct contact with the CSF in this compartment. Additional staining for myosin heavy chain confirmed that this was the case for both arteries and veins (Fig. 4C-D). As anticipated for this high molecular weight tracer, it did not cross the pia mater or the PVS to enter the brain tissue.

Selective tracer distribution along arteries in the brain parenchyma

While in the cisterns and SAS both arteries and veins were surrounded by tracer, a different pattern appeared within the parenchyma. While the dorsal and lateral part of the brain showed minimal presence of tracer along penetrating arteries, several vessels at the ventral side of the brain showed strong tracer signal. Here, we observed tracer around the arteries but not the veins (Fig. 5A-B). Tracer surrounding the parenchymal arteries was found to adjoin the smooth muscle cell layer (Fig. 5C-D).

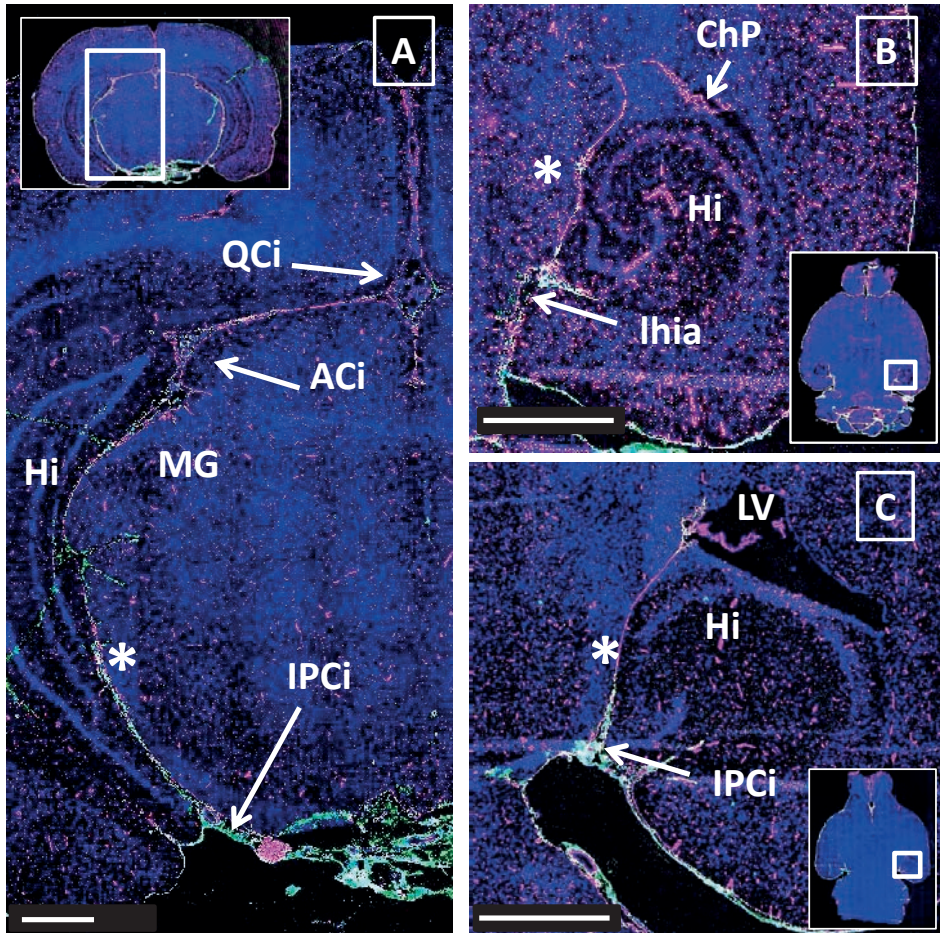


Figure 3. Tracer distribution over the SAS and cisterns of the rat brain. Sections were stained for laminin (pink) and cell nuclei (blue). Tracer is shown in green. Panel A: Coronal section of a rat brain at approximately 5.6 mm posterior to the bregma showing some of the major cerebral cisterns. In the left upper corner a miniature of the whole section. Tracer was present along the cleft (*) between the hippocampus and the medial geniculate nucleus (MG). This space connected the interpeduncular cistern (IPci) at the base of the brain, with the ambient cistern (ACi) and the quadrigeminal cistern (QCi). Arteries and veins followed the outline of these cisterns and were embedded in tracer. Panel B and C: horizontal sections of the rat brain at approximately -7 mm from the bregma. The stars show the presence of an extension of the interpeduncular cistern that connects the SAS with the lateral ventricle (LV). The tracer was observed along this tract, which followed the outline of the hippocampus (Hi) up to the lateral ventricle. Scale bar represents 1 mm.

Correlative light and electron microscopic imaging of the paravascular space.

To further study the subcellular distribution of tracer around blood vessels in more detail we used correlative light and electron microscopy (CLEM). This technique is based on merging of images from two consecutive slices of the same specimen acquired with the two techniques. Figure 6, panels A, shows a parenchymal artery with tracer signal super-

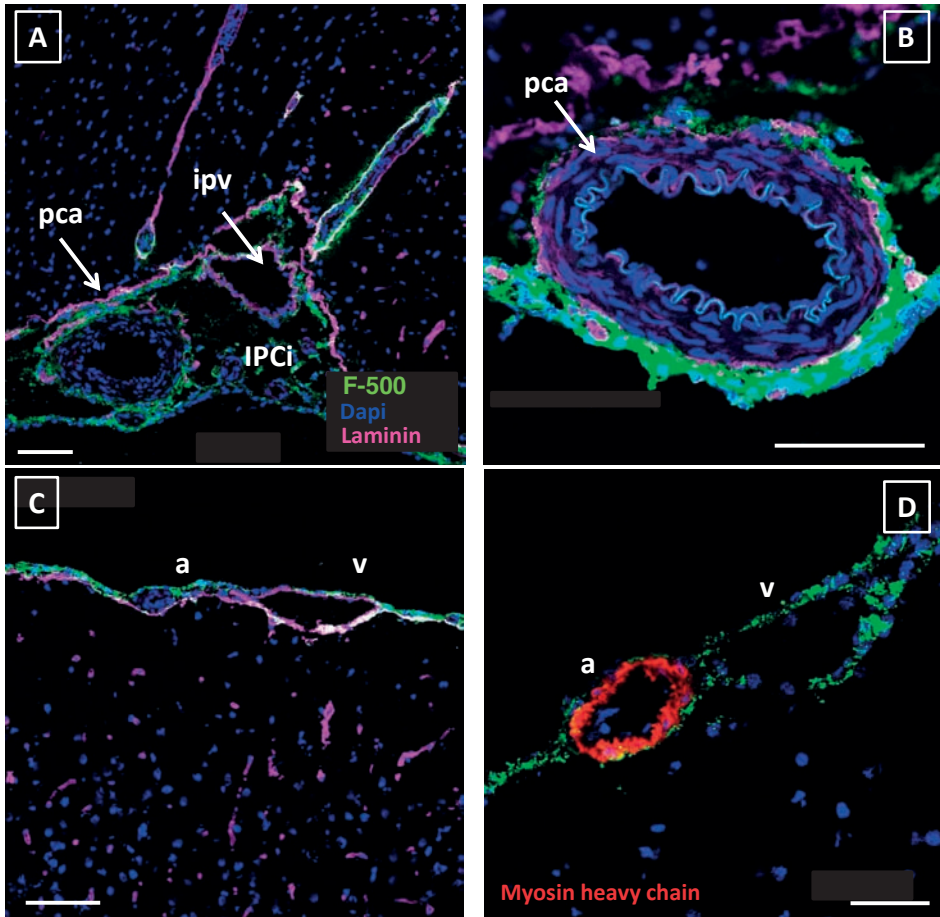


Figure 4. Anatomical details of tracer distribution around blood vessels. Sections were stained for laminin (pink) and cell nuclei (blue). Tracer is shown in green. Panel A shows the interpeduncular cistern (IPCi) filled with CSF, which embedded the posterior cerebral artery (pca) and the intrapeduncular vein (ipv) Panel B: close-up of the posterior cerebral artery. Panel C: Tracer surrounded a leptomeningeal artery (a) and vein (v) but did not penetrate along vessels into the parenchyma in this area. Panel D: Myosin heavy chain staining was used to discriminate arteries from veins. Both artery and vein in the SAS showed tracer signal. In all pictures, the tracer is present around the leptomeningeal vessels, in the SAS, and cisterns. Scale bar in panels A-C represents 100 μm , panel D 50 μm .

imposed. The tracer encircled the vessel, just outside the SMC layer. A pericyte was also surrounded by a thin layer of tracer. Panel B shows a detail of the same arteriole, in panel C the fluorescent signal is superimposed. These images show tracer between a smooth muscle cell and a pericyte. The basement membrane (BM) of the smooth muscle cells is well fixed and preserved. When using the Uranyl stained EM preparation technique, membranes will appear white and electron lucent. Indeed, the membranes surrounding the extracellular matrix of the BM are visible (Fig. 6B). The lumen of the vessel and the first layer of BM did not show tracer. Panel D depicts a parenchymal capillary surrounded by tracer.

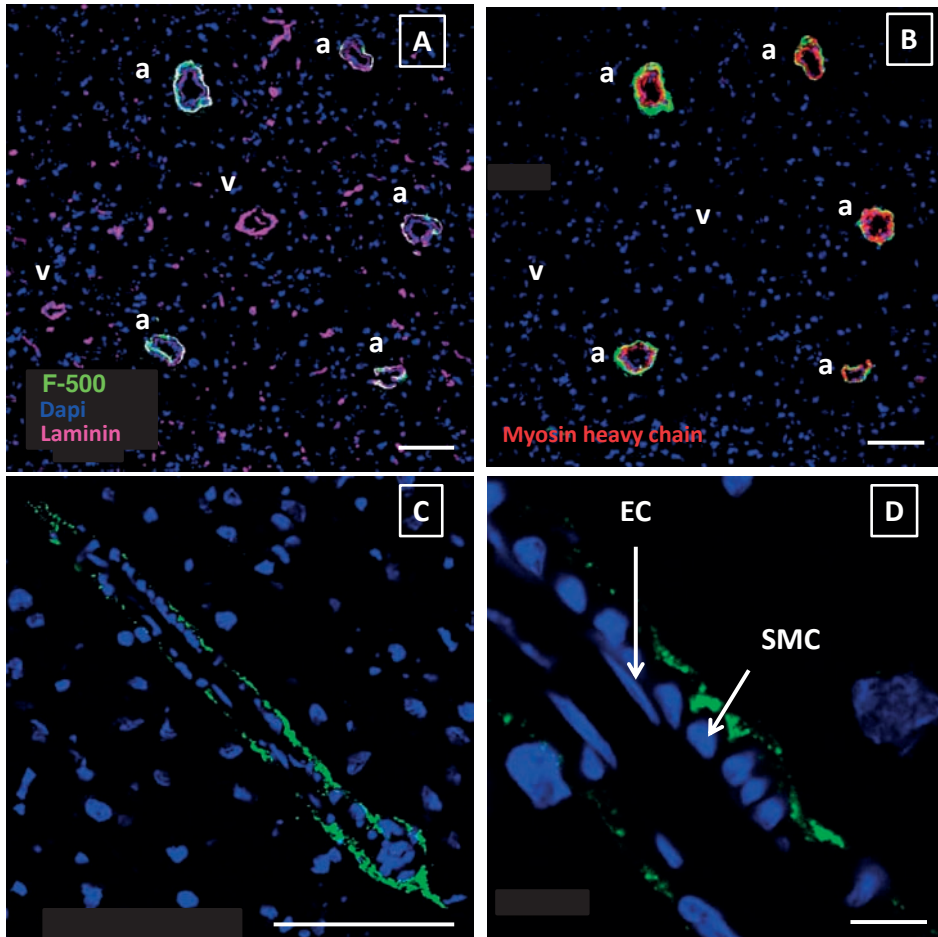


Figure 5. Paravascular distribution of CSF tracer within the brain parenchyma. In contrast to the cortex, tracer was found to penetrate into the parenchyma along vessels on the ventral side of the brain. Sections were stained for laminin (panel A; pink) or myosin heavy chain (panel B; red) and cell nuclei (blue). Tracer is shown in green. Panel A-B: adjacent slides from the same specimen. Panel A was stained for laminin, while panel B was stained for myosin heavy chain, to discriminate arteries (a) from veins (v). This revealed that tracer signal was confined to arteries only. Panels C and D show a longitudinal section of a small artery. The tracer is present around the artery and is located just outside the SMC layer. EC: endothelial cell, SMC: smooth muscle cell. Panel A-B: scale bar 100 μm; Panel C-D: scale bar 10 μm

DISCUSSION

The most important results from the present study are: 1) The vasculature of the brain has an intricate relationship with the CSF compartment. The main feeding arteries are embedded in the SAS, follow the cisterns and outlines of the major brain structures, and are surrounded by CSF throughout their course; 2) Preferential pathways for CSF trans-

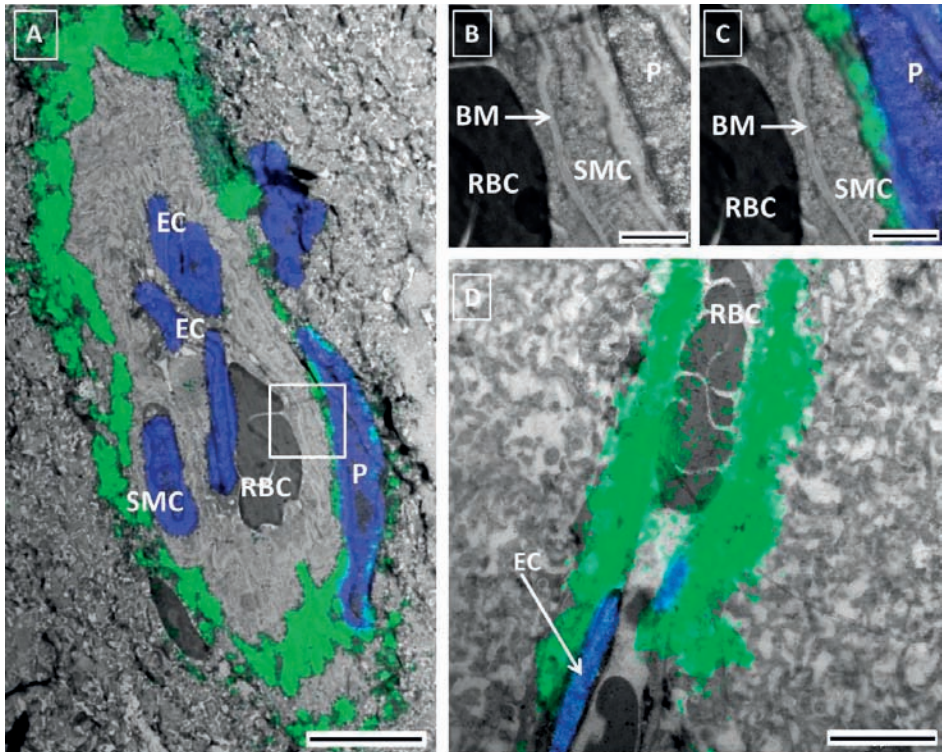


Figure 6. Correlative Light Electron Microscopy (CLEM) of the PVS. Panel A: CLEM image of a small artery obtained after merging fluorescent (green tracer, blue nuclei) and EM images of two consecutive slices of the same brain. Red blood cells (RBC) are present in the lumen. Endothelial cells (EC) and smooth muscle cells (SMC) were identified based on location and morphology. The tracer was found in the extracellular space immediately surrounding the smooth muscle layer of the artery and in between the latter and the pericyte (P). Panel B-C are higher magnifications of the vessel wall without the fluorescent (B) and with the fluorescent (C) signal superimposed. The basement membrane between the EC and the SMC did not present signal. Panel D shows a capillary with tracer immediately below the endothelium. Panel A: scale bar 5 μm Panel B-C: scale bar 1 μm ; Panel D: scale bar 5 μm

port within the SAS exist around arteries, due to a local widening of the SAS; 3) A novel functional connection between the lateral ventricle and the SAS has been identified; 4) Paravascular spaces within the parenchyma are continuous with and extensions of the CSF compartment, which under low rate tracer injection are mainly observed at the ventral part of the brain; 5) Paravascular spaces are located just outside the endothelial layer at the capillary level and immediately outside of the smooth muscle layer in arteries.

Slow infusion in the CM does not increase ICP

A high rate of tracer infusion may alter the pattern of CSF flow and leave a false impression of tracer penetration along paravascular spaces. We therefore first established that infusion at the chosen low rates did not appreciably alter pressure. Therefore, we are

confident that the results obtained in this study are not obscured by the infusion rate. Kress et al.¹⁰ observed an increase in ICP of about 2.5 mmHg, using a pump rate of 2 μ l/min in mice. These authors reported that the effect persisted during the infusion and upon stopping the pump, the ICP returned to normal values. Such an increase in pressure may seem insignificant, but given the low ICP in rat of approximately 5 mmHg, this represents an increase in pressure of about 50%. It is therefore quite conceivable that such pressures may affect the normal CSF flow and tracer distribution.

One large CSF compartment

In our experiments we observed that tracer signal was prominent along the ventral side of the rat brain up to the olfactory bulb. Arteries of the circle of Willis were clearly embedded in tracer. This probably reflects the relatively large size of the SAS at these locations. From the base of the brain, tracer spread into the cisterns. The major vessels feeding the brain followed the outline of these structures. It thus appears that these major vessels are embedded in a connected network of cisterns that separate the main anatomical structures of the brain. An initial study in mice pointed at a similar distribution of tracer⁸. Thus, also there the CSF tracer followed the outline of the major arteries and cisterns. The large tracer similarly penetrated the brain along arteries, particularly at the base of the brain, but not along veins.

Within the SAS, tracer was visible around both arteries and veins. The lack of paravascular sheets or other structures that would allow physical separation between arteries and veins suggests that CSF surrounding these vessels forms a single compartment. This view contradicts the notion of Iliff et al.³ who proposed a “physically and functionally distinct subcompartment” within the SAS that surrounds arteries. Their view is based on the observation that 5 min after the infusion, the tracer is present in the PVS only, but in the course of 30 min spread all over the cortical surface. An alternative view that we propose is that tracers appear first around arteries because the PVS is a widening of the SAS. Due to lower resistance, tracers would travel much faster in the wider PVS portion of the same compartment, as compared to the narrower SAS. Thus, based on differences in local resistance, tracer is expected to appear first in the PVS and later in the SAS, when injected in the CM.

We therefore propose that at least in rats, the SAS is one compartment, which widens around arteries because of their rigidity and round shape. This creates a functional, rather than a physically separated compartment.

Our data provide evidence for an additional connection between the ventricular system and SAS via the interpeduncular cistern. The importance of this alternative pathway is unclear, and flow along these tracts may be negligible under physiological conditions. However, some studies showed that in an animal model of hydrocephalus with obstructed fourth ventricular outlets, CSF “leaked” from the third ventricle to the

quadrigeminal cistern and from the lateral ventricle to the ambient cistern, via 'compensatory CSF pathways'^{11,12}. Also, Ghersi-Egea et al.¹³ described in rat an alternative spread of sucrose infused into the lateral ventricles to the CSF cisterns via the velum interpositum and superior medullary velum. Thus, these and our observations extent current knowledge on the ventricular system and CSF flow with pathways that may become important under conditions where normal outflow is obstructed.

Peri- and paravascular tracts, one and the same?

The exact location, namely along the basement membranes of endothelial cells and smooth muscle cells (i.e. perivascular) or outside the vessel wall (i.e. paravascular), is subject of discussion. Alternatively, two pathways might exist along arteries, carrying flow in opposite directions. Here, we investigated tracer localization after infusion in the CM. The source location of the tracer may be important for the exact pathway and perceived direction of tracer distribution (and thus flow). Thus, in most cases the paravascular compartment described by Iliff et al.³ was identified after injection of tracers in the CM. On the other hand, Weller and Carare⁴ mostly injected tracers into the parenchyma, from where they describe perivascular outflow along basement membranes of capillaries and arterial smooth muscle cells. Our data show that tracer, injected into the CM, follows the space just outside the layer of smooth muscle cells and further downstream along the basement membrane of capillaries. The basement membranes of endothelial cells and smooth muscle cells were continuous with the extracellular matrix and space surrounding the vessels, in agreement with recent work from Morris et al¹⁴. Thus, a physical separation between the paravascular space and basement membranes was not found. In a previous work, Zhang et al¹⁵ found a thin layer of pial cells around arteries in the SAS of human brain. Here, we found no evidence for pial sheets along arteries within the tissue using EM. It is therefore possible that species differences and the exact localization play a role here. Taken together, we believe that the most probable anatomical outline is therefore that one compartment is present, rather than the combination of a peri- and paravascular compartment that would facilitate bulk flow in opposite directions. Not only would two pathways running in opposite directions make little sense physiologically, but the physical separation into compartments that is needed for this scenario was not found. Whether this space should be referred to as peri- or paravascular, remains a semantic issue.

Despite the continuity between the paravascular space and the basement membrane of smooth muscle cells and endothelial cells, there was limited penetration into the vessel wall. We anticipate that this relates to the relatively large size of the tracer (500 kD). We anticipate that this relates to the relatively large size of the tracer (500 kD).

CSF flow and solute transport

According to textbook knowledge, CSF flows from the ventricles, where it is produced, via the foramen of Magendie into the SAS from where it is cleared via various outflow paths. We add to this that the spaces surrounding cortical and cisternal vessels provide preferential pathways. While net flow depends on production rate, we found strong pulsatility of ICP, suggesting that CSF velocity patterns are dynamic. Bulk oscillating movement between ventricles and the spinal lumbar space has been observed in MRI¹⁶. Yet, considering the available space, dynamic CSF velocity patterns may also exist along the cortical and cisternal vessels. Respiration was a much larger source for ICP oscillations than cardiac contraction, indicating coupling of intrathoracic pressure and ICP via veins. Additional effects may have come from arterial pulsations related to the aortic pressure. Such pulsations cause a sloshing and mixing of CSF that may help transport of solutes. This dynamic regime around cortical and cisternal vessels may extend into the paravascular space of parenchymal vessels, explaining tracer penetration here without a net forward flow. This would simultaneously allow waste removal from these paravascular spaces.

LIMITATIONS

The data provided in the current study rely on tracer distribution that is analyzed by ex-vivo methods. Thus, caution needs to be taken interpreting the data, as tissue dissection and processing may obscure analysis. Here we used a high-molecular weight, fixable tracer to minimize tracer spread after sacrifice of the animal. Brain tissue is notoriously difficult to fix for EM purposes and fixation with aldehydes can cause shrinkage of tissues. Still, since we used perfusion fixation followed by on block fixation (all using EM-grade fixatives), the vessels and the surrounding tissues appear well fixed. The basement membrane and the membranes surrounding it were intact and visible. In addition, as currently most researchers in the field agree that CSF and paravascular flow is dependent on vital functions^{17,18}, we expect that tracer spreading after sacrifice was limited. Another limitation of the study is that we only used male rats. Future studies should therefore include both genders.

CONCLUSIONS

Our results reveal a continuous and extensive CSF compartment, consisting of the SAS, cisterns and paravascular spaces, embedding the main vasculature of the brain. We found a new connection between the SAS and the ventricular system, the importance of

which remains to be established. Paravascular spaces extend from the SAS and cisterns into the parenchyma, and provide a possibility for waste removal that could be facilitated by a mixing action generated by pressure pulsations in the CSF (Fig. 7).

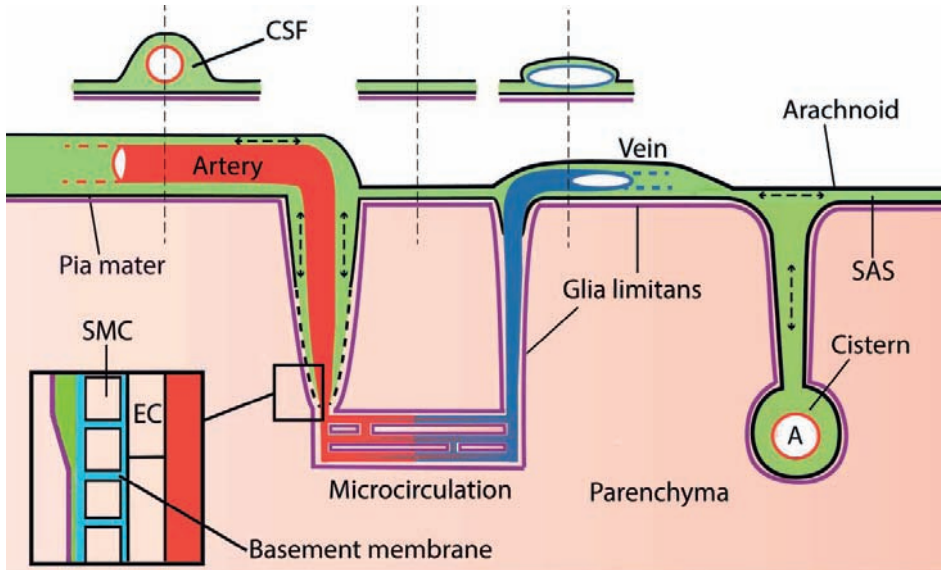


Figure 7. Schematic representation of the CSF compartment. Tracer injected in the cisterna magna distributes via the CSF and reaches the SAS and paravascular space, which extends along arteries into the parenchyma. Leptomeningeal vessels are bathed by the CSF. However, the space around artery and vein may be different due to the particular shape of these vessels: bigger around the circular arteries and smaller around the flattened veins (see sketched cross-section). Cerebral cisterns connect to the SAS and embed major branches of leptomeningeal arteries. Pressure oscillations produced respiration and heart beat cause mixing within the CSF compartment. Insert: at the level of the microcirculation, the PVS disappears and fuses with the basement membrane of smooth muscle cells, pericytes, and endothelial cells. Green: CSF; red: artery; blue: vein; purple: glia limitans; light blue: basement membrane; pink: parenchyma.

Funding

This project has received funding from the Internationale Stichting Alzheimer Onderzoek (ISAO) and from the European Union's Seventh Framework Programme for research technological development and demonstration under Grant agreement no 606998.

Acknowledgements

We thank Duy Ha Ly for his help with the cryomicrotome data.

Declaration of conflicting interests

The author(s) declared no potential conflicts of interest with respect to the research, authorship, and/or publication of this article.

Authors' contributions

BB, EvB and EB designed the study and wrote the manuscript. MS critically reviewed the manuscript. BB, EB, JdeV, NNvderW and HvanV performed the experiments.

Supplementary material

Supplementary material for this paper can be found at <http://jcbfm.sagepub.com/content/by/supplemental-data>

REFERENCES

1. Louveau, A. et al. Structural and functional features of central nervous system lymphatic vessels. *Nature* 523, 337-341, doi:10.1038/nature14432 (2015).
2. Aspelund, A. et al. A dural lymphatic vascular system that drains brain interstitial fluid and macromolecules. *J Exp Med* 212, 991-999, doi:10.1084/jem.20142290 (2015).
3. Iliff, J. J. et al. A paravascular pathway facilitates CSF flow through the brain parenchyma and the clearance of interstitial solutes, including amyloid beta. *Sci Transl Med* 4, 147ra111, doi:10.1126/scitranslmed.3003748 (2012).
4. Carare, R. O. et al. Solutes, but not cells, drain from the brain parenchyma along basement membranes of capillaries and arteries: significance for cerebral amyloid angiopathy and neuroimmunology. *Neuropathol Appl Neurobiol* 34, 131-144, doi:10.1111/j.1365-2990.2007.00926.x (2008).
5. Hladky, S. B. & Barrand, M. A. Mechanisms of fluid movement into, through and out of the brain: evaluation of the evidence. *Fluids Barriers CNS* 11, 26, doi:10.1186/2045-8118-11-26 (2014).
6. Spaan, J. A. et al. Visualisation of intramural coronary vasculature by an imaging cryomicrotome suggests compartmentalisation of myocardial perfusion areas. *Med Biol Eng Comput* 43, 431-435 (2005).
7. van den Wijngaard, J. P. et al. 3D Imaging of vascular networks for biophysical modeling of perfusion distribution within the heart. *J Biomech* 46, 229-239, doi:10.1016/j.jbiomech.2012.11.027 (2013).
8. Bedussi, B. et al. Clearance from the mouse brain by convection of interstitial fluid towards the ventricular system. *Fluids Barriers CNS* 12, 23, doi:10.1186/s12987-015-0019-5 (2015).
9. van der Wel, N. N., Fluitsma, D. M., Dascher, C. C., Brenner, M. B. & Peters, P. J. Subcellular localization of mycobacteria in tissues and detection of lipid antigens in organelles using cryo-techniques for light and electron microscopy. *Curr Opin Microbiol* 8, 323-330, doi:10.1016/j.mib.2005.04.014 (2005).
10. Kress, B. T. et al. Impairment of paravascular clearance pathways in the aging brain. *Ann Neurol* 76, 845-861, doi:10.1002/ana.24271 (2014).
11. Park, J. H. et al. Cerebrospinal fluid pathways from cisterns to ventricles in N-butyl cyanoacrylate-induced hydrocephalic rats. *J Neurosurg Pediatr* 8, 640-646, doi:10.3171/2011.8.PEDS1190 (2011).
12. Yoon, J. S., Nam, T. K., Kwon, J. T., Park, S. W. & Park, Y. S. CSF flow pathways through the ventricle-cistern interfaces in kaolin-induced hydrocephalus rats-laboratory investigation. *Childs Nerv Syst* 31, 2277-2281, doi:10.1007/s00381-015-2901-5 (2015).
13. Gherzi-Egea, J. F., Finnegan, W., Chen, J. L. & Fenstermacher, J. D. Rapid distribution of intravenicularly administered sucrose into cerebrospinal fluid cisterns via subarachnoid velae in rat. *Neuroscience* 75, 1271-1288 (1996).
14. Morris, A. W., Carare, R. O., Schreiber, S. & Hawkes, C. A. The Cerebrovascular Basement Membrane: Role in the Clearance of beta-amyloid and Cerebral Amyloid Angiopathy. *Front Aging Neurosci* 6, 251, doi:10.3389/fnagi.2014.00251 (2014).
15. Zhang, E. T., Inman, C. B. & Weller, R. O. Interrelationships of the pia mater and the perivascular (Virchow-Robin) spaces in the human cerebrum. *J Anat* 170, 111-123 (1990).
16. Hamilton, R. et al. Intracranial pressure pulse waveform correlates with aqueductal cerebrospinal fluid stroke volume. *J Appl Physiol* (1985) 113, 1560-1566, doi:10.1152/jappphysiol.00357.2012 (2012).
17. Iliff, J. J. et al. Cerebral arterial pulsation drives paravascular CSF-interstitial fluid exchange in the murine brain. *J Neurosci* 33, 18190-18199, doi:10.1523/JNEUROSCI.1592-13.2013 (2013).
18. Bakker, E. N. et al. Lymphatic Clearance of the Brain: Perivascular, Paravascular and Significance for Neurodegenerative Diseases. *Cell Mol Neurobiol* 36, 181-194, doi:10.1007/s10571-015-0273-8 (2016).





CHAPTER 4

Paravascular spaces at the brain surface: low resistance pathways for cerebrospinal fluid flow

Beatrice Bedussi¹, Judith de Vos¹, Ed vanBavel¹, and Erik N.T.P. Bakker^{1*}

¹Department of Biomedical Engineering and Physics, Academic Medical Center, Amsterdam, The Netherlands

Accepted JCBFM (2017)

Author's contribution: BB, EvB and EB designed the study and wrote the manuscript. BB, EB, and JdeV performed experiments

ABSTRACT

Clearance of waste products from the brain is of vital importance. Recent publications suggest a potential clearance mechanism via paravascular channels around blood vessels. Arterial pulsations might provide the driving force for paravascular flow, but its flow pattern remains poorly characterized. In addition, the relationship between paravascular flow around leptomeningeal vessels and penetrating vessels is unclear. In this study, we characterized the dynamics of paravascular flow along leptomeningeal vessels of mice, using fluorescent microspheres injected into the cisterna magna. We also determined blood flow and diameter pulsations through a thinned-skull cranial window. We observed that microspheres moved preferentially in the paravascular space of arteries rather than in the adjacent subarachnoid space or around veins. Paravascular flow was pulsatile, generated by the cardiac cycle, with net antegrade flow. Ex vivo confocal imaging showed microspheres distributed along leptomeningeal arteries, while their presence along penetrating arteries was limited to few vessels. These data suggest that paravascular spaces around leptomeningeal arteries form low resistance pathways on the surface of the brain that facilitate cerebrospinal fluid flow.

Keywords

Cerebrospinal fluid; Interstitial fluid; Subarachnoid space; Paravascular space; Intracranial pressure; Fluid Dynamics

INTRODUCTION

The cerebrospinal fluid (CSF) is produced mainly by the choroid plexuses, located in the ventricular system. CSF leaves the ventricles via the median and lateral apertures, where it enters the subarachnoid space (SAS). It is subsequently removed via diverse outflow pathways, including arachnoid granulations and the cribriform plate^{1,2}. Recent work from Iliff et al. suggests that part of the CSF is recirculated into the brain via paravascular spaces around arteries³, possibly providing interstitial bulk flow that aids the removal of waste products such as amyloid β . This was based on 2-photon microscopy of tracer distribution at the brain surface and confocal imaging of brain sections. In mice, transport of tracers along the vessels at the brain surface has been confirmed with MRI⁴⁻⁶. In humans, paravascular spaces within the brain parenchyma are detectable with MRI⁷⁻¹⁰ but their presence and dimensions at the brain surface are relatively unexplored.

As the brain is encapsulated within a rigid skull, pulsations derived from the cardiac cycle, but also from respiration, are transmitted to the brain parenchyma and fluids^{4,11}. Arterial pulsations are considered as the driving force for paravascular transport along vessels^{12,13}. However, even though several steps were made in understanding the anatomical structures involved in the CSF drainage^{3,14,15}, quantitative measurements of fluid flows via paravascular pathways are lacking. In particular, pulsatility in the PVS has not been established, while the direction of flow, and differences in flow patterns along arteries and veins, remains equivocal^{14,16,17}. Therefore, in this study we characterized paravascular flow along leptomeningeal vessels in mice, using fluorescent microspheres that were imaged via a thinned cranial window. As we anticipated previously¹⁵ that pulsations might facilitate ISF-CSF exchange through mixing, we imaged the PVS at the brain surface using high speed imaging of vascular diameter, blood velocity, and microsphere movement, to capture the flow pattern in the PVS in relation to blood vessel pulsatility.

MATERIAL AND METHODS

Reagents

The cerebrospinal fluid movement along the paravascular space was traced by fluorescent polystyrene microspheres (1 μm , Ex.495/ Em.515), purchased from Molecular Probes-Life Technologies. To prevent aggregation, microspheres were conjugated with albumin (15 mg/ml). Prior to infusion in the CM, 10 μl of microspheres conjugated with albumin were diluted in 90 μl of artificial cerebrospinal fluid (aCSF- 135 mM NaCl, 5.4 mM KCl, 1 mM MgCl_2 , 1.8 mM CaCl_2 , 5 mM HEPES). To visualize the vasculature in vivo, we intravenously infused FITC dextran (Sigma, 10mg/ml in PBS, 500 kD, Ex. 494 nm/ Em. 521).

Animal studies

All animal experiments complied with the ARRIVE guidelines and were carried out in accordance with the U.K. Animals (Scientific Procedures) Act, 1986 and associated guidelines, EU Directive 2010/63/EU for animal experiments. Mice were housed in groups under a 12 h light-dark cycle and fed *ad libitum* with standard laboratory food and free access to water. For this study, seven male mice (4 months old) were used. Two mice were used for the intracranial pressure measurements and five for intravital microscopy. Male C57BL/6J OlaHsd mice were obtained from Harlan (The Netherlands). Animals were fed *ad libitum* with standard laboratory food and had free access to water. They were allowed to acclimatize at least one week before being enrolled in experimental protocols. All experimental protocols were approved by the Committee for Animal Experiments of the Academic Medical Center Amsterdam, according to the ARRIVE and EU guidelines.

Anesthesia

In all experiments mice were anesthetized with a mixture of 17% ketamine (Nimatek, Eurovet) 3% medetomidine (Dormitor, Orion Pharma) and 7% atropine (Atropinesulfaat, Eurovet) in PBS (Phosphate Buffered Saline, Lonza) by intraperitoneal injection (75 µl/10gr body weight).

Intracranial pressure

To measure intracranial pressure (ICP) during different rates of microsphere infusion, a 29-gauge needle was inserted into the cisterna magna. This needle was connected to a pressure transducer by stiff polyethylene tubing to prevent damping of pulsations. Data were recorded with a PowerLab acquisition system and analyzed with Chart data analysis software (AD instruments).

Experimental design

After completely anesthesia (lack of toe pinch reflex), the heads and the necks were shaved with an electrical razor. To maintain physiological body temperature, animals were placed on a heating pad. We used an ocular lubricant (DURATEARS, Alcon) to keep the eyes hydrated. The animals were artificially ventilated (Minivent, Harvard Apparatus) at 8 mL/kg body weight stroke volume and 120 strokes/min. To visualize the cerebral vasculature, 50 µl of fluorescent dye was injected in the dorsal penile vein. During the whole experiment, the heart rate of the animals was monitored based on the ECG (PLUG-SYS Minicase Type 609, Harvard Apparatus). Subsequently, the animal was turned in the prone position and fixed to the stereotactic frame (lab standard stereotaxic, Stoelting). To obtain a thinned skull cranial window, we cut the skin on the head. The window was located over the branches of the middle cerebral artery. Before scraping the bone away, we applied a local anesthetic (1% xylocaine). The thinned skull technique we used in

the current study was based on the model described by Yang G. et al¹⁸. The selected area of the skull was thinned using a portable micromotor high-speed drill. During this step, the skull was continuously wetted with artificial CSF (aCSF) to prevent overheating of the area and to remove the bone's dust. We used a mini blade with round tip (Synga medical) to gently scrape the skull until $\sim 20 \mu\text{m}$ thickness. The cortical vasculature was clearly visible through the thinned window. At this point we prepared the animal for the injection of microspheres in the cisterna magna as described previously¹⁷. Briefly, we separated the subcutaneous tissues and the neck's muscle. Then, we placed a 29-gauge needle, connected to a polyethylene catheter and a prefilled syringe into the cisterna magna. The needle was fixated by glue. When the animal was in position for imaging we connected the syringe to the pump (Harvard Apparatus) and we started infusing the mixture of aCSF and fluorescent microspheres in the cisterna magna at $0.34 \mu\text{l} / \text{min}$.

Image acquisition

The custom made intravital fluorescence microscope was equipped with a power LED (Thorlabs M470L2, wavelength 470 nm) for excitation of FITC-dextran to visualize the blood stream and the fluorescent microspheres. The cortical vasculature was visualized through the thinned skull using a 20x magnification water immersion objective (Olympus). The space between the skull surface and the objective was filled by a transparent viscoelastic solution (2% hydroxypropyl methylcellulose solution, Ocucoat). Images were recorded with a high speed camera (Orca Flash 4.0, Hokawo). Once the videos were acquired, the animals were sacrificed and the brain was rapidly collected for ex vivo confocal microscopy.

Blood flow dynamics

Blood vessels were visualized using intravenously injected FITC-dextran. Red blood cells (RBC) appeared dark against the bright fluorescent background of plasma. The selected vessels were positioned horizontally in the field of view and 10 sec videos were acquired at a high frame rate (typically between 200 and 300 frames/s) to measure RBC speed and vessel diameter. The videos were then analyzed with a custom made software (see below).

Measurement of CSF dynamics in the paravascular space

The vessels with microspheres in the PVS were recorded for 10 sec. The videos were analyzed using ImageJ software¹⁹. Brightness was adjusted and a Gaussian Blur filter was applied prior to tracking of microspheres along the vessels. We tracked the microspheres using the manual tracking plugin. Microspheres that appeared to be stuck were excluded for analysis.

Data analysis

We developed custom made software in MatLab for the analysis of vascular diameter and blood velocity in the cranial window setup. In summary, vascular inner diameter and its pulsatility were estimated from intensity thresholding over a few hundred micrometer of vessel length. RBC velocity was determined from the axial movement of the intensity profile, as imaged by diagonal streaks of displacement-time images. The software estimates the angle of these streaks and converts this to velocity and direction.

Confocal microscopy

Confocal microscopy was performed on frozen brain sections. After sacrifice of the animals, the brains were dissected and embedded in Tissue-Tek and immediately frozen in liquid nitrogen prior to storage at -80°C . Samples were cut in two different planes (coronal and sagittal) with a cryomicrotome, and slices were collected (5 μm thickness). The slices were fixed by 3.7% paraformaldehyde and mounted with DAKO fluorescence mounting medium (Agilent). Sections were stained for laminin (Sigma-Aldrich) or Von Willebrand factor (Abcam). We acquired images using a Confocal Laser Scanning Microscope (Leica TCS SP8) with 20X oil immersion objective.

Statistics

In all figures, data are expressed as mean \pm SEM. Differences in microsphere location were evaluated by one-way ANOVA, followed by Tukey's *post hoc* test. A *p* value of <0.05 was considered significant. We used Prism software (Graphpad) to perform statistics.

RESULTS

Impact of infusion rate on intracranial pressure

To image paravascular flow dynamics, we infused fluorescently labeled microspheres into the cisterna magna of mice. As a high infusion rate may increase intracranial pressure (ICP) and obscure physiological flow patterns, we tested different infusion rates while measuring the ICP via the cisterna magna. First, we recorded the baseline ICP, which averaged 4.1 ± 0.4 mmHg (SEM, $n=2$). We then increased the infusion rate stepwise, while recording pressure. At 0.34 $\mu\text{l}/\text{min}$ the ICP rose to 4.2 mmHg, while at 1 $\mu\text{l}/\text{min}$ the mean ICP rose to 5.3 mmHg. At higher infusion rates pressure increased without reaching a steady state. The ICP decreased gradually after ending the infusion. Based on these measurements we chose to use a microsphere infusion rate of 0.34 $\mu\text{l}/\text{min}$ in the subsequent experiments, as this infusion rate minimally increased ICP.

Location of microspheres

The thinned skull cranial window was made on the edge of the dorsal part of the skull (see Fig. 1A), to image branches arising from the middle cerebral artery (MCA). This location was chosen as previous work¹⁵ showed spreading of fluorescent dextrans around the circle of Willis and the larger vessels arising from it, including the MCA, after injection into the CSF. After a delay of approximately 45 minutes, microspheres appeared around the branches of the MCA (Fig. 1B). The microspheres traveled mainly in close vicinity of the arterial wall. This was substantiated by a significant difference in microsphere counts between adjacent and more remote areas (Fig. 1C). Occasionally, we observed microspheres moving further away from vessels. Some microspheres appeared to be stuck. A video with a typical example of microspheres moving along a branch of the MCA is shown in supplement 1.

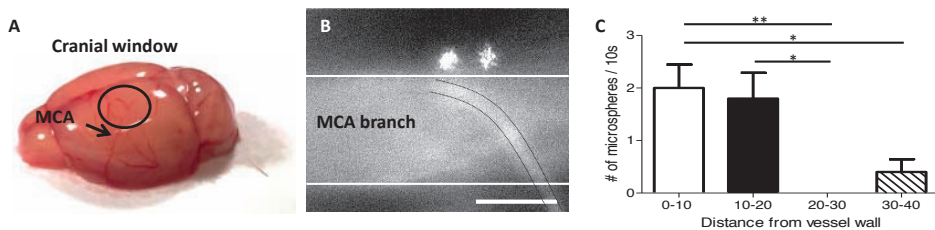


Figure 1. Microspheres move along arteries. The cranial window (black circle in panel A) was made to image branches of the MCA. Panel B shows a typical image of two microspheres moving close to the vessel wall (indicated by the white lines). A capillary crosses the MCA branch (black lines). The majority of the microspheres were found close to the vessel wall, suggesting that the paravascular space is around 20 micrometer in width at this level of the vascular tree (Panel C). Only a few microspheres were observed at larger distance, presumably in the subarachnoid space (SAS). Data are mean \pm SEM. Scale bar represents 50 μ m. * Indicates $p < 0,05$ and ** $p < 0,01$.

Pulsatility in vascular diameter, blood velocity and microsphere movement

Automated tracking of blood vessel diameter and blood velocity showed a pulsatile pattern, generated by the heartbeat. Microspheres were manually tracked offline. The ensemble average for vascular diameter, blood velocity, and microsphere position illustrates a clear pulsatile pattern for all signals (Fig. 2). The microspheres moved forward during systole and the first part of diastole, and moved backward during the second half of diastole.

Pulsatile back and forth movement along paravascular spaces

During *in vivo* imaging we observed a back and forth movement of the microspheres (see video in supplement 1). The frequency of the oscillations was attributable to the cardiac cycle. The mean amplitude of the back and forth movement of the microspheres was $20.5 \pm 2.3 \mu$ m ($n=5$) μ m per cycle. In all experiments we observed this oscillatory pattern. Figure 3 shows a typical pattern over 2 sec. The net movement of microspheres in the PVS was in the same direction as the blood flow, with an average velocity of $27 \pm 4 \mu$ m/sec (based on 3 microspheres/animal, SEM, $n=5$).

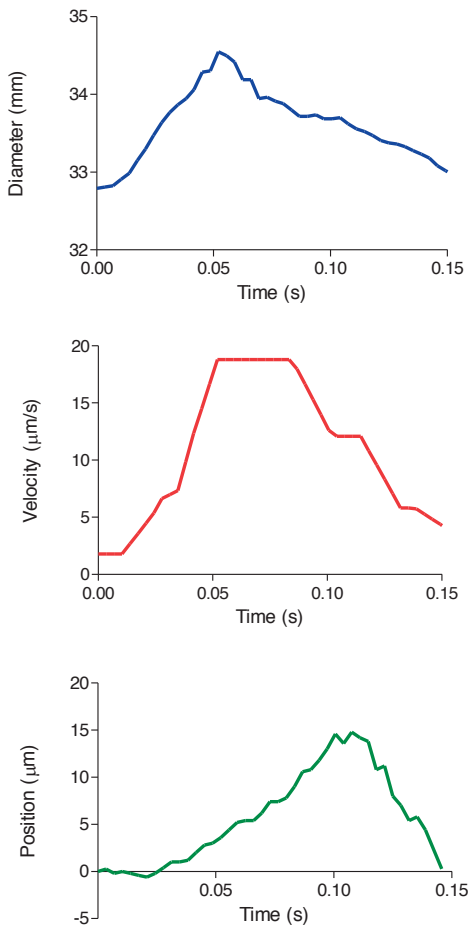


Figure 2. Ensemble average of diameter, blood velocity and microsphere position. The ensemble average was constructed from a typical recording over 2 seconds. All parameters showed a pulsatile pattern attributable to the heartbeat. The microspheres showed a to and fro movement during the cardiac cycle. Position of the microsphere indicates the deviation from the net forward trend.

Blood velocity and diameter pulsatility

Tracking of centerline blood velocity yielded values ranging from 0.9 to 5.5 $\mu\text{m/s}$. Table 2 shows velocity values for one vessel of each animal. Diameter values ranged from 21 to 39 μm . Oscillations in diameter were relatively small, or even undetectable in some vessels.

Ex vivo microsphere localization

As the cranial window observations were limited to a particular location and have a limited depth resolution, we further analyzed microsphere distribution ex vivo using confocal microscopy on brain sections. This showed the presence of microspheres around arteries, veins, and in the SAS around the whole brain. Microspheres were abundant in the big cisterns at the base of the brain. Microspheres were more frequently found

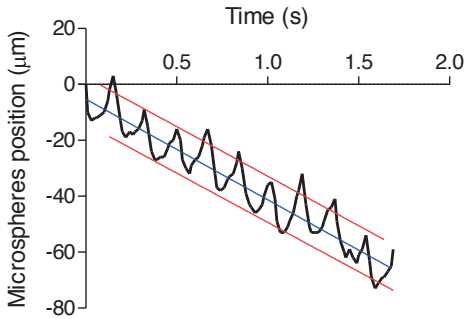


Figure 3. Microspheres oscillate in the paravascular space of leptomeningeal vessels. The microspheres moved along the vessels in an oscillatory manner. The frequency of the oscillations corresponded to the heart rate of the animal.

Table 1. Blood speed and diameter parameters.

	Mean V ($\mu\text{m/s}$)	Median V ($\mu\text{m/s}$)	Mean D (μm)	Median D (μm)	Relative change D %
N1	5.5 ± 0.9	5.6 ± 0.8	33.8 ± 0.2	33.8 ± 0.2	10.0 ± 3.0
N2	3.6 ± 1.0	3.9 ± 0.8	39.0 ± 2.3	39.0 ± 2.3	6.0 ± 2.0
N3	3.0 ± 0.3	3.1 ± 0.2	21.1 ± 0.3	21.1 ± 0.3	not pulsatile
N4	0.9 ± 0.8	0.5 ± 0.5	29.2 ± 2.8	29.1 ± 2.8	not pulsatile
N5	3.9 ± 0.5	4.0 ± 0.4	20.6 ± 7.4	20.7 ± 7.4	1.0 ± 1.0

Mean and median blood velocity (*V*) and diameter (*D*) values. Diameter oscillations are given as percentage of diameter. All values are expressed as mean \pm SEM, derived from multiple recordings of each single vessel. Two out of five vessels did not show pulsatility.

around arteries as compared to veins (Fig. 4). With few exceptions at the ventral part of the brain (Figure 4B, green arrow), there was very limited penetration of microspheres along vessels in the parenchyma.

DISCUSSION

In this study we investigated PVS flow dynamics in relation to blood flow and blood vessel diameter in mice using microspheres. Microspheres appeared in the cranial window with some delay, after injection into the CSF of the cisterna magna. The vast majority of microspheres was observed within a 20 micrometer range next to arteries. This corresponds well with data from Iliff et al³ that were obtained with in vivo 2-photon imaging. In the present study, ex vivo confocal images confirmed the abundant presence of microspheres around arteries. However, microspheres were also found more scattered throughout the much larger surface area of the SAS, and occasionally around the largest veins. In our view, the simplest explanation for this finding is that PVS around arteries and veins are continuous with the SAS, but that the PVS is larger around arteries than veins, and much wider than the SAS.

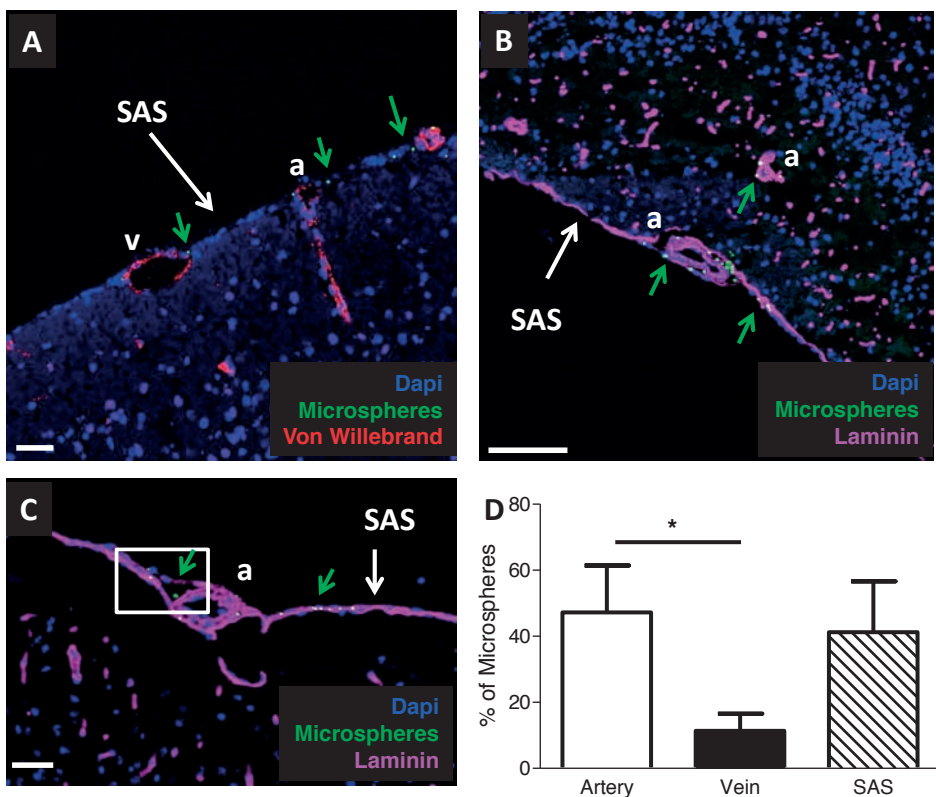


Figure 4. Microsphere distribution around arteries, veins, and the SAS. Panel A and B show the SAS with microspheres (green arrows) around arteries (a), veins (v), and in the SAS. Microspheres were present at the surface, but did not follow the PVS along penetrating vessels at the dorsal side of the brain (panel A). However, they were present in the paravascular space of some parenchymal arteries at the ventral side of the brain (Panel B). In Panel C a large paravascular space is evident next to a leptomeningeal artery (white box). Panel D: Quantification of microspheres. Microspheres were observed more frequently around arteries as compared to veins. Microsphere numbers were similar around arteries as compared to the SAS, which however occupied a much larger surface area. Blue: nuclear stain, green: microspheres, magenta: laminin and red: Von Willebrand, to identify vessels and pial membranes. Panel A: Scale bar 200 μm and panel B and C scale bar 50 μm . Data are mean \pm SEM. * Indicates $p < 0.05$.

To analyze the flow pattern in the PVS, we traced fluorescent microspheres. These showed a pulsatile to and fro movement, induced by the heartbeat. This movement along arteries correlated with an oscillatory blood velocity pattern and diameter changes. However, diameter oscillations were small and in some cases undetectable at the measurement location. This suggests that diameter oscillations either further upstream or downstream may contribute to fluid displacement in the PVS. Microspheres moved along the PVS with a net component in the same direction as blood flow. It is important to stress that we found bulk flow at the surface of the brain only. We did not observe penetration of microspheres into the brain parenchyma along paravascular spaces

at the lateral and dorsal part of the brain. One possibility is that paravascular spaces become very narrow when entering the cortex and do not allow 1 μm microspheres to pass. However, in previous work¹⁵ we found that fluorescent dextrans also poorly penetrate the brain along PVS, with exception of a few arteries at the ventral part of the brain. Therefore, we believe a more likely explanation is that CSF flows along PVS on the brain surface towards the front of the brain, and exits the skull via the cribriform plate, consistent with previous findings from our group and others^{17,20,21}. We found no evidence for bulk flow entering the tissue along PVS of penetrating arteries and removal via paravenous spaces. Furthermore, our findings suggest a direct connection between PVS around arteries and veins at the level of the SAS. This would eliminate a pressure gradient, which is necessary to sustain glymphatic flow²².

Arterial pulsations have repeatedly been suggested to drive paravascular flow. Indeed, one study showed that altered pulsatility in the cerebral vasculature affected the penetration of tracers along PVS and into the parenchyma¹². In addition, Kiviniemi et al.⁴ proposed that CSF propulsion is governed by a fast cardiovascular pulsation, together with the respiratory pulsation and slow vasomotor wave fluctuations. However, in the absence of valves, it is difficult to see how pulsations are able to create net flow. Thus, a more simple explanation for the PVS flow we observed is that it originates from the *vis a tergo* CSF production from the choroid plexus and exits from the cribriform plate and other structures. However, we do believe that pulsatile flow at the brain surface may be important for waste removal from the brain parenchyma. Thus, we speculate that arterial pulsations generate mixing in the PVS of penetrating arteries. Mixing, without bulk flow into or out of the parenchyma, may still increase ISF-CSF exchange. Through a physical connection with the paravascular spaces at the brain surface, solutes and waste products may be subsequently swept away by bulk flow of CSF around leptomeningeal arteries. Recent theoretical work supports this notion²³. Lack of pulsatility, as may be anticipated in conditions associated with vascular stiffening, such as aging and hypertension, therefore might affect brain clearance.

CONCLUSIONS

In conclusion, we showed that paravascular spaces are present around leptomeningeal vessels in mice. The PVS appears much larger around arteries, but is continuous with the SAS and spaces around veins. The large PVS around arteries creates a low resistance pathway for CSF flow. For branches of the MCA, bulk flow in the PVS is in the same direction as blood flow, and likely caused by CSF production by the choroid plexus and exit via the cribriform plate and other routes. Flow within the PVS around arteries is pulsatile, generated by the heartbeat. While we speculate that pulsatility in itself does not create

bulk flow in the PVS, this may be important to facilitate ISF-CSF exchange via PVS that extent into the parenchyma.

Acknowledgments

The ImageJ manual track plugin was developed by Fabrice Cordelieres.

Funding

This project has received funding from the Internationale Stichting Alzheimer Onderzoek (ISAO) and from the European Union's Seventh Framework Programme for research technological development and demonstration under Grant agreement no 606998.

Author contributions

BB, EvB and EB designed the study and wrote the manuscript. BB, EB, and JdeV performed experiments.

Competing financial interests

The authors declare no competing financial interests.

REFERENCES

1. Brinker, T., Stopa, E., Morrison, J. & Klinge, P. A new look at cerebrospinal fluid circulation. *Fluids Barriers CNS* 11, 10, doi:10.1186/2045-8118-11-10 (2014).
2. Hladky, S. B. & Barrand, M. A. Mechanisms of fluid movement into, through and out of the brain: evaluation of the evidence. *Fluids Barriers CNS* 11, 26, doi:10.1186/2045-8118-11-26 (2014).
3. Iliff, J. J. et al. A paravascular pathway facilitates CSF flow through the brain parenchyma and the clearance of interstitial solutes, including amyloid beta. *Sci Transl Med* 4, 147ra111, doi:10.1126/scitranslmed.3003748 (2012).
4. Kiviniemi, V. et al. Ultra-fast magnetic resonance encephalography of physiological brain activity - Glymphatic pulsation mechanisms? *J Cereb Blood Flow Metab* 36, 1033-1045, doi:10.1177/0271678X15622047 (2016).
5. Gaberel, T. et al. Impaired glymphatic perfusion after strokes revealed by contrast-enhanced MRI: a new target for fibrinolysis? *Stroke* 45, 3092-3096, doi:10.1161/STROKEAHA.114.006617 (2014).
6. Iliff, J. J. et al. Brain-wide pathway for waste clearance captured by contrast-enhanced MRI. *J Clin Invest* 123, 1299-1309, doi:10.1172/JCI67677 (2013).
7. Bouvy, W. H. et al. Visualization of perivascular spaces and perforating arteries with 7 T magnetic resonance imaging. *Invest Radiol* 49, 307-313, doi:10.1097/RLI.000000000000027 (2014).
8. Bouvy, W. H. et al. Perivascular spaces on 7 Tesla brain MRI are related to markers of small vessel disease but not to age or cardiovascular risk factors. *J Cereb Blood Flow Metab* 36, 1708-1717, doi:10.1177/0271678X16648970 (2016).
9. Kilsdonk, I. D. et al. Perivascular spaces in MS patients at 7 Tesla MRI: a marker of neurodegeneration? *Mult Scler* 21, 155-162, doi:10.1177/1352458514540358 (2015).
10. van Veluw, S. J. et al. Cerebral amyloid angiopathy severity is linked to dilation of juxtacortical perivascular spaces. *J Cereb Blood Flow Metab* 36, 576-580, doi:10.1177/0271678X15620434 (2016).
11. Wagshul, M. E., Eide, P. K. & Madsen, J. R. The pulsating brain: A review of experimental and clinical studies of intracranial pulsatility. *Fluids Barriers CNS* 8, 5, doi:10.1186/2045-8118-8-5 (2011).
12. Iliff, J. J. et al. Cerebral arterial pulsation drives paravascular CSF-interstitial fluid exchange in the murine brain. *J Neurosci* 33, 18190-18199, doi:10.1523/JNEUROSCI.1592-13.2013 (2013).
13. Sharp, M. K., Diem, A. K., Weller, R. O. & Carare, R. O. Peristalsis with Oscillating Flow Resistance: A Mechanism for Periarterial Clearance of Amyloid Beta from the Brain. *Ann Biomed Eng*, doi:10.1007/s10439-015-1457-6 (2015).
14. Carare, R. O. et al. Solutes, but not cells, drain from the brain parenchyma along basement membranes of capillaries and arteries: significance for cerebral amyloid angiopathy and neuroimmunology. *Neuropathol Appl Neurobiol* 34, 131-144, doi:10.1111/j.1365-2990.2007.00926.x (2008).
15. Bedussi, B. et al. Paravascular channels, cisterns, and the subarachnoid space in the rat brain: A single compartment with preferential pathways. *J Cereb Blood Flow Metab*, doi:10.1177/0271678X16655550 (2016).
16. Arbel-Ornath, M. et al. Interstitial fluid drainage is impaired in ischemic stroke and Alzheimer's disease mouse models. *Acta Neuropathol* 126, 353-364, doi:10.1007/s00401-013-1145-2 (2013).
17. Bedussi, B. et al. Clearance from the mouse brain by convection of interstitial fluid towards the ventricular system. *Fluids Barriers CNS* 12, 23, doi:10.1186/s12987-015-0019-5 (2015).
18. Yang, G., Pan, F., Parkhurst, C. N., Grutzendler, J. & Gan, W. B. Thinned-skull cranial window technique for long-term imaging of the cortex in live mice. *Nat Protoc* 5, 201-208, doi:10.1038/nprot.2009.222 (2010).

19. Schneider, C. A., Rasband, W. S. & Eliceiri, K. W. NIH Image to ImageJ: 25 years of image analysis. *Nat Methods* 9, 671-675 (2012).
20. Johnston, M., Zakharov, A., Papaiconomou, C., Salmasi, G. & Armstrong, D. Evidence of connections between cerebrospinal fluid and nasal lymphatic vessels in humans, non-human primates and other mammalian species. *Cerebrospinal Fluid Res* 1, 2, doi:10.1186/1743-8454-1-2 (2004).
21. Nagra, G., Koh, L., Zakharov, A., Armstrong, D. & Johnston, M. Quantification of cerebrospinal fluid transport across the cribriform plate into lymphatics in rats. *Am J Physiol Regul Integr Comp Physiol* 291, R1383-1389, doi:10.1152/ajpregu.00235.2006 (2006).
22. Jin, B. J., Smith, A. J. & Verkman, A. S. Spatial model of convective solute transport in brain extracellular space does not support a "glymphatic" mechanism. *J Gen Physiol* 148, 489-501, doi:10.1085/jgp.201611684 (2016).
23. Asgari, M., de Zelicourt, D. & Kurtcuoglu, V. Glymphatic solute transport does not require bulk flow. *Sci Rep-Uk* 6, doi:ARTN 3863510.1038/srep38635 (2016).





CHAPTER 5

Enhanced interstitial fluid drainage in the hippocampus of spontaneously hypertensive rats

Beatrice Bedussi¹, Daphne M.P. Naessens¹, Judith de Vos¹, Rik Olde Engberink²,
Micha M. M. Wilhelmus³, Edo Richard⁴, Malyssa ten Hove¹, Ed vanBavel¹,
and Erik N.T.P. Bakker^{1*}

¹Department of Biomedical Engineering and Physics, Academic Medical Center, Amsterdam, The Netherlands

²Division of Nephrology, Academic Medical Center, University of Amsterdam, Amsterdam

³Department of Anatomy and Neurosciences, Neuroscience Campus Amsterdam, VU medical center,
Amsterdam, The Netherlands

⁴Department of Neurology, Academic Medical Centre, Amsterdam, Netherlands; Department of Neurology,
Radboud University Medical Centre, Nijmegen, Netherlands.

Published in Scientific Reports (2017)

doi: 10.1038/s41598-017-00861-x

Authors' contribution: BB, EvB, and EB designed the study and wrote the manuscript. BB, EB, DN, MtenH, ROE and JdeV performed the experiments. MW, ER critically reviewed the manuscript.

ABSTRACT

Hypertension is associated with cognitive decline and various forms of dementia, including Alzheimer's disease. In animal models of hypertension, many of Alzheimer's disease characteristics are recapitulated, including brain atrophy, cognitive decline, amyloid β accumulation and blood brain barrier dysfunction. Removal of amyloid β and other waste products depends in part on clearance via the brain interstitial fluid (ISF). Here we studied the impact of hypertension on ISF drainage, using spontaneously hypertensive rats (SHR) and normotensive Wistar Kyoto rats (WKY). At 8 months, high (500 kD) and low (3 kD) fluorescent molecular weight tracers released passively into the hippocampus showed a drastically enhanced spreading in SHR. Tracer spreading was inhomogeneous, with accumulation at ISF-CSF borders, around arteries, and towards the stratum lacunosum moleculare. These locations stained positively for the astrocyte marker GFAP, and aquaporin 4. Despite enhanced dispersion, clearance of tracers was not affected in SHR. In conclusion, these data indicate enhanced bulk flow of ISF in the hippocampus of hypertensive rats. ISF drains along astrocytes towards the cerebrospinal fluid compartment, which leads to sieving of high molecular weight solutes. Sieving may lead to a local increase in the concentration of waste products and potentially promotes the aggregation of amyloid β .

INTRODUCTION

Microvascular dysfunction, including impaired neurovascular coupling and blood brain barrier (BBB) disruption, occurs in both vascular dementia and Alzheimer's Disease (AD)¹. These changes may interfere with the clearance of potentially toxic waste products such as amyloid β , which are released in the brain interstitial fluid (ISF) and accumulate in the parenchyma and vessel walls¹. Hypertension may aggravate neurodegenerative diseases². Indeed, mid-life hypertension is associated with an increased risk of dementia³, while antihypertensive drugs have been found to reduce the risk to develop AD^{4,5}. Induction of high blood pressure by transverse aortic coarctation promotes amyloid β accumulation in the brain of mice⁶. Similarly, work in mouse models of AD showed that hypertension exacerbates AD-like pathology⁷⁻¹¹. Spontaneously hypertensive rats (SHR) develop white matter damage, cognitive decline (novel object recognition) and BBB disruption, among other pathological changes¹². Stroke-prone SHR show an age-dependent deposition of amyloid β ¹³. Thus, there is a strong link between hypertension and dementia in both human and animal studies. However, the underlying mechanisms for this relation are not well understood. As the clearance of waste products, including amyloid β from the brain parenchyma depends on transport via the interstitial fluid and subsequent removal via the BBB and paravascular pathways¹⁴⁻¹⁷, we hypothesized that hypertension may alter fluid dynamics in the brain interstitium. This, in turn, could interfere with the clearance of solutes from the brain. Thus, in the present study we set out to determine the effect of hypertension on distribution and clearance of solutes via the interstitial fluid. For this purpose, we studied the fate of fluorescent tracers released into the ISF of the hippocampus of normotensive and hypertensive rats.

MATERIALS AND METHODS

Reagents

Dextran, Texas Red-labelled (3 kD, Ex. 595 nm/Em. 615 nm) and dextran, fluorescein-labelled (500 kD, Ex. 494 nm/Em. 521), both lysine-fixable, were purchased from Molecular Probes-Life Technologies (Eugene, OR, USA). These dyes were dissolved in artificial cerebrospinal fluid (aCSF). In the passive release experiments we increased the final concentration of FITC dextran to 50 mg/ml. For immunohistochemistry we used antibodies against: smooth muscle myosin heavy chain 11 antibody (Abcam), Aqp4 (Millipore) and GFAP (Dako Cytomation, Glostrup). Cell nuclei were stained with bisbenzimidazole (Sigma). Slices were mounted in fluorescent mounting medium (Dako). RIPA buffer consisted of 150 mM sodium chloride, 1.0% Triton X-100, 0.5% sodium deoxycholate, 0.1% SDS, 1 mM EDTA, in 50 mM Tris, pH 8.0.

Animals

For this study 39 animals were used. Male normotensive Wistar Kyoto rats (WKY/NCrI) (n=20) and male spontaneously hypertensive rats (SHR/NCrI) (n=19) were obtained from Charles River at the age of 11 weeks. Animals were kept until 8 months of age, housed in groups and fed *ad libitum* with standard laboratory food and free access to water. Experiments were done during daytime, which is the sleep phase for rats. One animal died during anesthesia, before the start of the experiment. All experimental protocols were approved by the Committee for Animal Experiments of the Academic Medical Center Amsterdam, and in accordance with the European Communities' Council Directive 2010/63/EU.

Blood pressure measurements

Blood pressure (BP) was measured non-invasively with a tail-cuff system (Kent Scientific, Torrington, Connecticut, USA). Rats were accustomed to handling and to the restrainer during a training period of 4 days before the BP measurements. During the measurements, the animals were placed in the restrainer on a heating pad, for at least 10 minutes to warm up the tail. In each animal, 4 to 10 BP measurements were made and averaged. In a subset of animals we also measured BP under KDA anaesthesia (see below). This revealed no difference in BP between anaesthetized and awake animals (data not shown).

Anaesthesia

In initial experiments, where tracers were infused into the brain by pumping, rats were anaesthetized by intraperitoneal injection of 2 ml/kg of KDA mix, consisting of a combination of ketamine (75 mg/kg, Nimatek, Eurovet), dexdomitor (0.5 mg/kg, Orion Pharma), and atropine (0.05 mg/kg, atropine sulphate, Eurovet) dissolved in PBS (Phosphate Buffered Saline, Lonza). Additional oxygen (99%) was administered via a nose cap to prevent hypoxia. As we experienced a more stable and adjustable level of anaesthesia with isoflurane, the remainder of the study was carried out with animals under anaesthesia with isoflurane (3% in O₂) applied via an inhalation mask.

General surgical procedure

The animals were anaesthetized and the scalp was shaved. Subsequently, heads were immobilized in a stereotactic frame (Stoelting) and the core body temperature was maintained using a heating pad. Ocular lubricant ointment (Duratears[®], Alcon) was applied to keep the eyes hydrated. The temperature was monitored with a rectal thermometer (Greisinger Electronics) during the procedure. A small longitudinal skin incision was made on the skull and 10% xylocaine (AstraZeneca B.V.) was provided as additional local anaesthesia. The periosteum was scratched off using a scalpel. Subsequently, according to the Paxinos and Watson Rat Brain atlas (6th edition, 2007), we defined the stereotactic

coordinates for the CA1 region of the hippocampus as -4.0 mm caudal, 2.0 mm lateral, and 4.0 mm deep, from the bregma point. The depth was calculated taking into account the thickness of the skull. A small burr hole was drilled with a dental drill (W&H). Subsequently, a 33-gauge needle (Hamilton) connected to a polyethylene catheter was inserted into the hippocampus using the stereotactic device. The catheter was connected to a syringe filled with a mixture of green (500 kD) and red (3 kD) fluorescent dextran. Both tracers were used at a final concentration of 10 mg/ml.

Infusion of tracers into the hippocampus

In this set of experiments, rats were anaesthetized with KDA mix. We infused 2 μ l of the dextran mixture at a controlled flow rate of 0.066 μ l/min using a syringe pump (Harvard Apparatus, Holliston, MA, USA), over a 30 minute period. After infusion, the syringe pump was stopped and the needle was removed 1 minute after the end of the infusion period. Subsequently, the animals were euthanized with an overdose of the anaesthetic and rapidly decapitated, after which the brains were carefully dissected. The brains were weighed and cut into three coronal blocks using an adult rat brain slicer matrix (Zinc instruments). The blocks were separately embedded in Tissue-Tek (Sakura), snap frozen in liquid nitrogen, and stored at -80 °C. The brains were then cut in coronal sections, 5 μ m thick, using a cryostat (Microm HM 560) and collected on SuperFrost slides (Menzel-Gläzer). After sectioning, sections were stored at -80 °C until they were used for immunohistochemistry.

Passive tracer release in the hippocampus

In the remainder of the study, animals were anaesthetized with isoflurane. For this set of experiments we inserted the needle via the burr hole and we let the tracers diffuse from the tip of the needle into the rat hippocampus for 30 minutes. At the end of the diffusion period the animals were euthanized and the brain processed as described for the infusion set of experiments.

Confocal imaging

Prior to imaging, brain slices were fixated in 3.7% paraformaldehyde (PFA) for 30 minutes. Then, cell nuclei were stained with bisbenzimidazole (Sigma). Selected slices were additionally stained to identify specific cell types and proteins. To discriminate between arteries and veins we stained for myosin heavy chain. Antibodies against GFAP and aquaporin 4 (Aqp4) were used to stain astrocytes and water channels. Fluorescent images were acquired using a confocal laser-scanning microscope (Leica TCS SP8), with a 20x objective for details and 10x objective for overviews. ImageJ software was used to quantify the distribution area of the tracers. Care was taken to prevent pixel saturation and to apply the same confocal settings to sections within each group of experiments.

Clearance of tracer from the hippocampus

To quantify the clearance we first infused a known volume (2 μ l) of the dextran mixture at 0.066 μ l/min for 30 min. Then, we allowed a subsequent 30 min period for spreading and clearance of the tracers. We used active infusion of tracer in this set of experiments, because measuring clearance requires a similar and known quantity of tracer to start with in WKY and SHR. Animals were then euthanized rapidly and brains were carefully dissected and weighed. Brains were subsequently homogenized in 7 ml of RIPA buffer, using a manual potter and an automated blender to obtain a homogenous suspension. Fluorescence spectrometry was then performed and the total amount of both dyes in the brain homogenate was determined from integration of the spectra over the appropriate wavelengths. In order to normalize for possible differences in turbidity in the different samples, the spectrometry was repeated after addition of a known quantity of the tracers to the samples.

Brain ashing procedure

We used snap frozen brain samples to analyze water, potassium, and sodium content. To determine brain water content, we compared brain sample weights before and after desiccation at 90 °C for 48 hours. Next, samples were dry ashed for 40 hours at 450 °C. After ashing, all samples were dissolved in 5% HNO₃. Sodium and potassium concentrations were determined by flame photometry.

Statistics

Data are expressed as mean \pm SEM. Data were analysed using Students' t-test or two-way ANOVA. A *p* value of <0.05 was considered statistically significant.

RESULTS***Hypertension is associated with a different ionic composition of the brain***

Spontaneously hypertensive rats were lighter than normotensive WKY rats (Table 1). Also brain weight was lower in SHR as compared to WKY. As expected, both systolic and diastolic blood pressure were higher in SHR, while also heart rate was significantly increased in SHR as compared to WKY. SHR brains showed a tendency for increased water content, as based on the wet and dry brain weights (Table 1). As edema and altered fluid homeostasis may be more sensitively detected by altered ion concentrations, we measured the concentration of both sodium and potassium. This revealed a significant decrease in potassium content in the SHR brain. As the sodium content showed a small, non-significant increase, a highly significant increase in Na⁺/K⁺ ratio was present in SHR brain.

Table 1. Animal characteristics and brain composition.

	WKY	SHR	t-test
Weight			
Body (gr)	(n=20) 404 ± 5	(n=19) 372 ± 5	p<0.001
Brain (gr)	(n=20) 2.26 ± 0.01	(n=19) 2.12 ± 0.03	p<0.001
Blood Pressure			
Systolic	(n=20) 163 ± 4	(n=19) 189 ± 4	p<0.001
Diastolic	(n=20) 118 ± 5	(n=19) 146 ± 4	p<0.001
BPM	(n=20) 378 ± 8	(n=19) 460 ± 5	p<0.001
Water content			
%	(n=6) 77.155 ± 0.021	(n=6) 77.612 ± 0.1	0.052
Ions			
Na⁺ (mmol/ml Water)	(n=6) 0.060 ± 0.001	(n=6) 0.062 ± 0.001	0.117
K⁺ (mmol/ml Water)	(n=6) 0.111 ± 0.002	(n=6) 0.106 ± 0.001	0.004
Na⁺ to K⁺ ratio	(n=6) 0.539 ± 0.012	(n=6) 0.592 ± 0.011	0.008

SHR body weight and brain weight were lower as compared to WKY. Systolic and diastolic blood pressure, and heart rate were elevated in SHR. Water content in SHR brain tended to be higher as compared to WKY. Whole brain sodium concentration was not different, but the potassium concentration was significantly lower in SHR brain as compared to WKY. Data are mean ± SEM.

Infusion of tracers into the hippocampus

To study the impact of hypertension on the spreading and removal of solutes from the brain extracellular space, we infused a small quantity of fluorescently labelled dextrans into the hippocampus. We infused 2 µl of a mixture of a high and low molecular weight dextran. The combination of a large and a small dextran was used as an indication for diffusion or bulk flow. A large difference in distribution would suggest diffusion, whereas a comparable distribution would suggest bulk flow. For neither tracer did we observe any difference between SHR and WKY (Fig. 1). After using this approach however, we speculated that tracer spreading may have been affected by the infusion itself. We therefore decided to investigate the fate of tracers in the absence of pumping any volume of fluid into the tissue.

Passive release of tracer in the hippocampus

In the second set of experiments we changed our approach and studied tracer spreading after passive release from the needle tip. After stereotactic placement of the needle in the hippocampus, both tracers were allowed to enter the brain from the needle tip by diffusion only, followed by further spreading through the interstitium. Under these conditions, we observed a significant difference in the distribution area between SHR and WKY rats. Thus, both tracers distributed over a 5–6 fold larger area in SHR as compared to WKY (Fig. 2). Remarkably, the distribution area of the small and large tracer was comparable in size for both SHR and WKY. This finding suggests that after release from the needle tip, tracers spread by bulk flow of ISF rather than by diffusion.

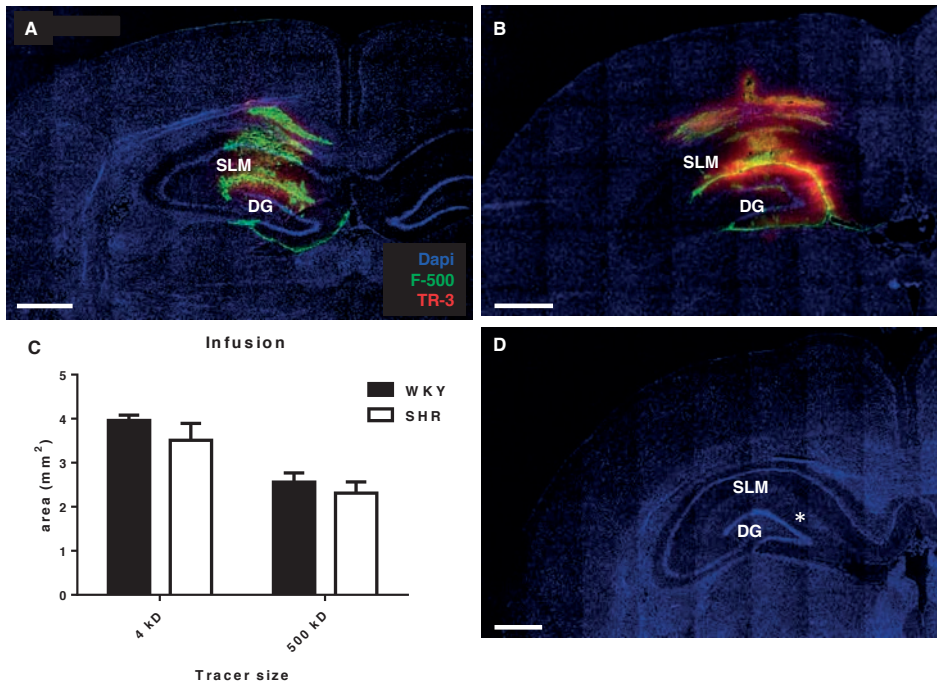


Figure 1. Distribution of fluorescent tracers after infusion into the hippocampus. Panel A and B show coronal slices of WKY (left) and SHR (right) hippocampus at the infusion level. We did not observe a difference in the distribution area of either the low or high molecular weight tracer between WKY (N=6) and SHR (n=7). Mean data \pm SEM are shown in panel C. In panel D the expected infusion site (*) is shown, based on the stereotactic coordinates for the rat brain. Scale bar 1 mm.

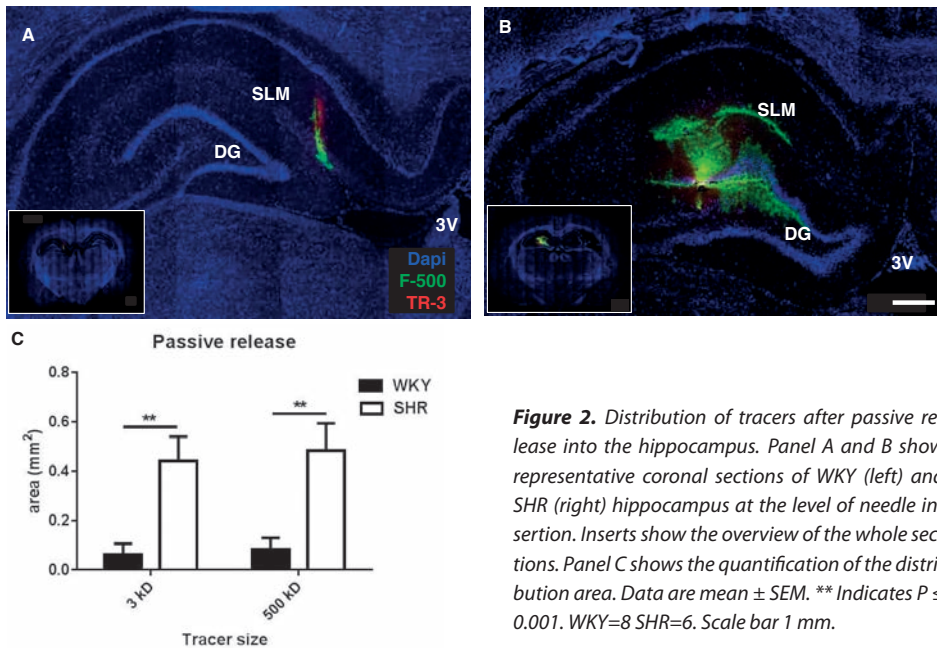


Figure 2. Distribution of tracers after passive release into the hippocampus. Panel A and B show representative coronal sections of WKY (left) and SHR (right) hippocampus at the level of needle insertion. Inserts show the overview of the whole sections. Panel C shows the quantification of the distribution area. Data are mean \pm SEM. ** Indicates $P \leq 0.001$. WKY=8 SHR=6. Scale bar 1 mm.

Clearance of tracers from the hippocampus

The large difference in distribution area between SHR and WKY after passive release of tracers may influence the clearance of these tracers from the brain. Therefore, in the next set of experiments we quantified the removal of tracers from the brain. We first infused equal amounts of tracers into the hippocampus of SHR and WKY, and then allowed a 30 min period of spreading and clearance. Brain homogenates were then analysed for remaining fluorescence by spectrophotometry. Clearance was much higher for the low versus high molecular weight tracer. However, clearance of either tracer was not significantly different between SHR and WKY rats (Fig. 3).

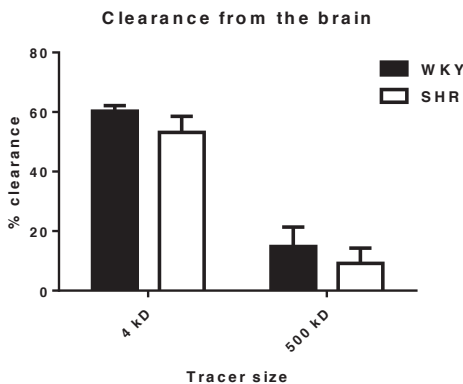


Figure 3. Clearance of tracers from the hippocampus. Clearance was calculated as the amount of tracer removed from the brain as percentage of the initially injected quantity. There was no difference in clearance for both the low and high molecular weight tracer in WKY as compared to SHR. Clearance was larger for the small tracer (3 kD) as compared to the large tracer (500 kD; $P < 0.00001$). WKY=6 SHR=6. Data are mean \pm SEM.

Pattern of tracer distribution

Tracer spreading was highly inhomogeneous. Figure 4 shows an example of tracer spreading after passive release in the hippocampus. The high molecular weight tracer spread along the stratum lacunosum moleculare (SLM) and further in the caudal direction following blood vessels, suggesting a highly preferential route for fluid movement. Based on myosin staining, these vessels were identified as arteries. Whether the tracers followed the arteries upstream or downstream could not be determined.

Colocalization of tracers with aquaporin 4 and GFAP

The spreading of tracers via the SLM region and around arteries was also seen after infusion of the tracers, suggesting a low resistance pathway of ISF flow. However, in the case of infusion, tracers spread further and also accumulated at ISF-CSF borders. As these areas are known to be rich in astrocytes and their endfeet, we investigated the possible colocalization of tracer with astrocytes and aquaporin 4 (Aqp4). Indeed, we observed clear staining for the astrocyte marker GFAP and Aqp4 in areas of tracer accumulation (Fig. 5).

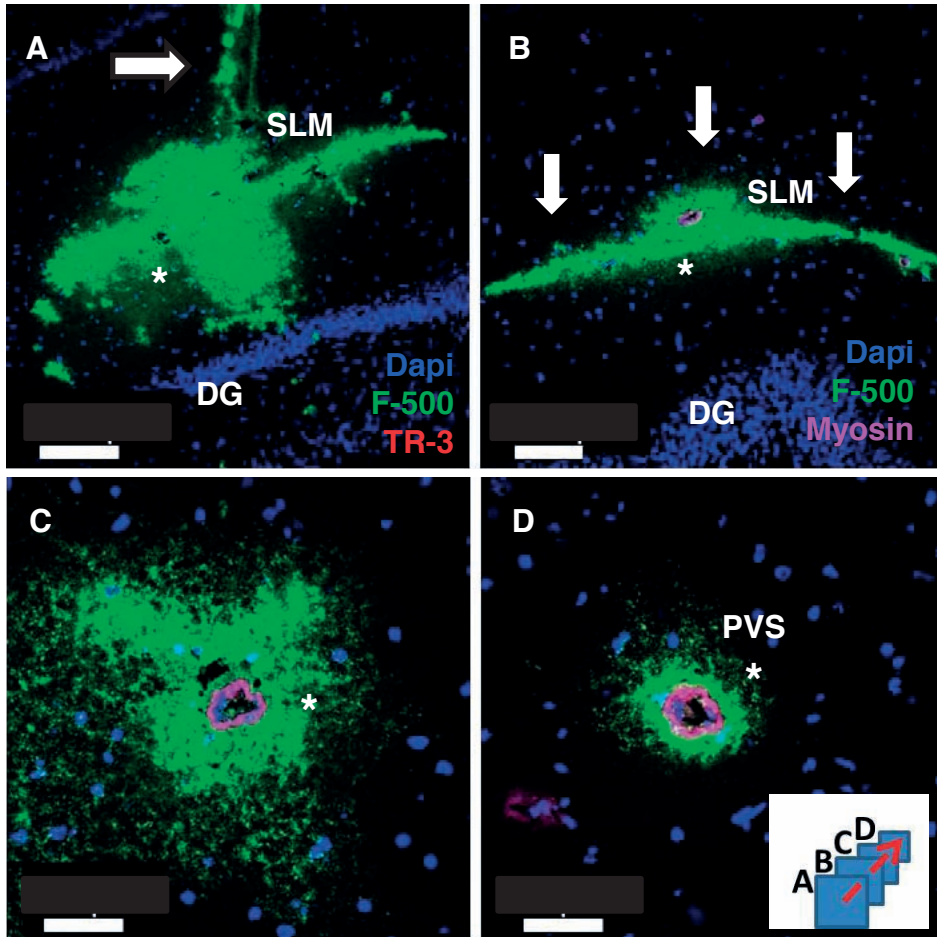


Figure 4. Tracer spreading within the hippocampus. Sequential sections of a SHR from the injection site (panel A; arrow indicates needle track) moving towards the caudal side of the brain (panels B-D). Tracer (500 kD) is shown in green. Panel B: 0.75 mm caudal from infusion area. Tracer spread along the SLM (arrows) and embedded arteries. Panel C: 1 mm from the infusion area, tracer co-localized with an artery. Panel D: 1.25 mm from the infusion area, stronger co-localization with the same artery. Dentate gyrus (DG); Stratum Lacunosum Moleculare (SLM); Paravascular Space (PVS). Stars indicate the same artery in the different panels. Blue: nuclear stain, magenta: smooth muscle myosin heavy chain, identifying the arterial nature of these vessels. Scale bar in A: 200 μm , B: 100 μm , C-D: 50 μm .

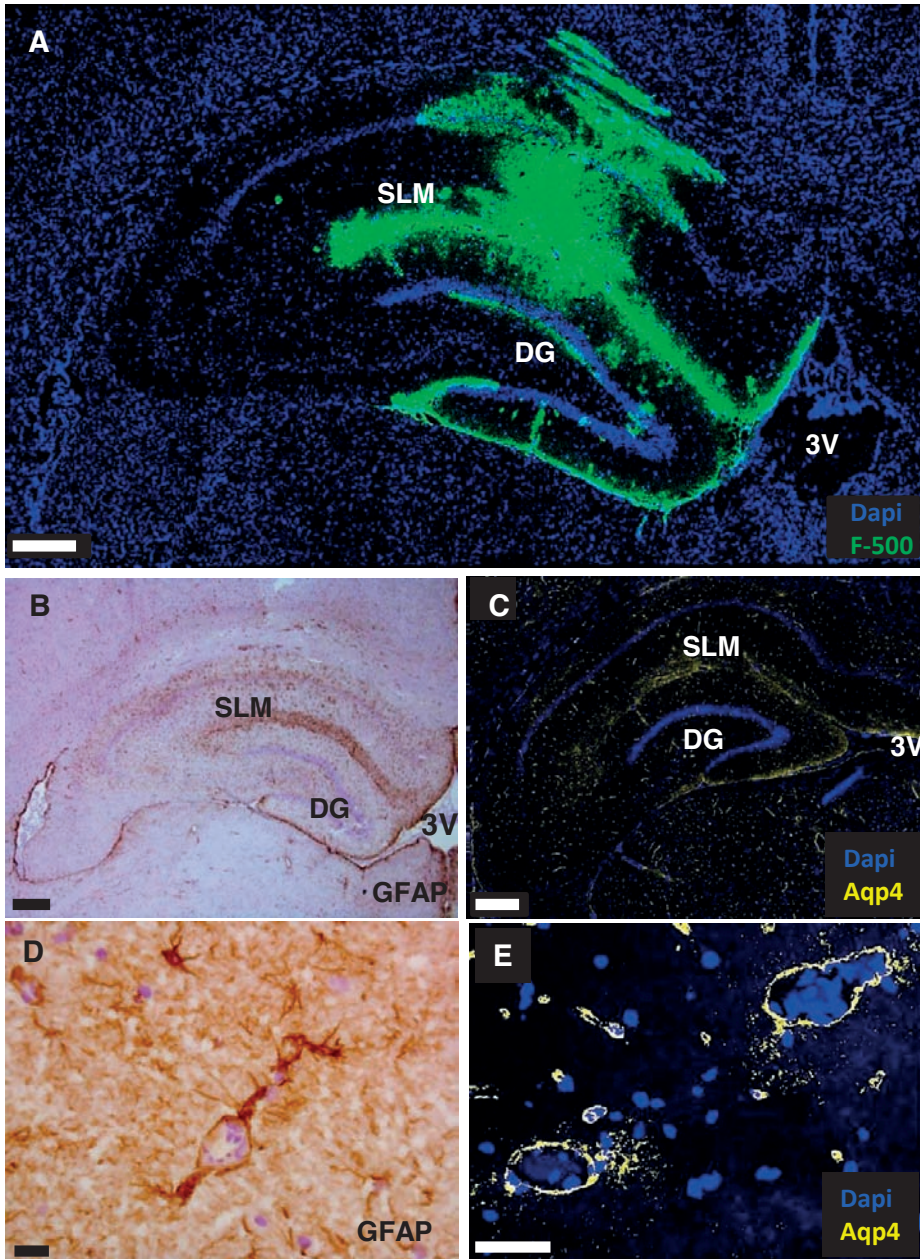


Figure 5. Co-localization of tracer accumulation with GFAP and aquaporin 4 staining. Panel A: High molecular weight tracer (green) distribution after infusion in the hippocampus of a WKY. Tracer accumulates along the stratum lacunosum moleculare (SLM) and at the boundaries of the hippocampus. Panel B: Expression of the astrocyte marker GFAP. Panel C: Expression of aquaporin 4. Tracer, GFAP and Aqp4 co-localize at the suprapyramidal and infrapyramidal blades of the dentate gyrus and the ependyma layer at the third ventricle. DG: dentate gyrus. 3V: third ventricle. Scale bar in A–C 400 μm . Panels D and E show a close up of the vessels present at the SLM region. Both GFAP and Aqp4 are expressed around vessels. Scale bar in D=15 μm , E=50 μm .

DISCUSSION

In this study we investigated the impact of hypertension on the distribution and clearance of tracers from the brains of rats. In the first set of experiments we infused tracers into the hippocampus, using a small volume and low infusion speed to reduce the impact of the infusion itself. This resulted in a non-homogeneous distribution of tracers, but no difference in the distribution area between WKY and SHR. We then followed a still more subtle approach, and allowed tracers to spread passively from the needle tip. To the best of our knowledge, this approach has not been reported before. Although the distribution area was much smaller in this case, this uncovered a large difference in distribution area in SHR as compared to WKY. We believe that the impact of infusion is an issue that has been underestimated in many studies. Infusion of 1 microliter into the brain introduces a volume of 1 mm³. With the extracellular space being roughly 20% of the total volume, this 1 microliter replaces the ISF of 5 mm³ of brain tissue (total volume of a mouse hippocampus ≈25 mm³, rat hippocampus ≈100 mm³). The endogenous production rate of ISF is unknown and difficult to determine¹⁸, but the results of the current study indicates that even for very limited infusion rates, endogenous transport mechanisms are easily overwhelmed.

The presence of bulk flow of ISF is debated¹⁹. In the current study, the low and high molecular weight tracers distributed over similar areas, which was the case in both rat strains after passive release. In SHR, there was also a strong accumulation of particularly the high molecular weight tracer in specific areas. These two features are a clear indication that solutes are dispersed via bulk flow of ISF rather than by diffusion in SHR. The larger distribution area in SHR as compared to WKY after passive release of tracers also suggests that ISF flow is markedly enhanced in the hippocampus of SHR. It should however be noted that other factors could also play a role in the difference in distribution area, such as differences in extracellular matrix composition, which could lead to sticking or retention of tracers, and differences in tortuosity of the extracellular space. A further limitation is that a direct quantitative comparison of distribution areas between the two tracers is not straightforward. First of all, the fluorophores have different optical properties. Second, the distribution area is determined not only by spreading but also by simultaneous clearance.

While the distribution area was different in size between infusion and passive release, the pattern was similar. In both cases, tracers spread and accumulated at the stratum lacunosum moleculare (SLM), around arteries, into the corpus callosum, and at the edges of the hippocampus including the border with the third ventricle. This was the case for both WKY and SHR, albeit this became only apparent after infusion in the WKY, since there was limited tracer spreading after passive release in this group. Immunostaining showed that these areas are rich in astrocytes, and strongly express aquaporin 4. Thus, it

appears that ISF, containing tracers, travels from the parenchyma towards these border zones where ISF mixes with CSF. While in general the ISF-CSF border is considered less tight than the BBB, barrier properties are apparently still significant and lead to accumulation of the tracers.

The presence of aquaporin 4 also suggests that facilitated water transport is necessary in these regions. This capacity may be provided by astrocytes, which are known to mediate water transport, particularly via aquaporin 4 in their endfeet²⁰. It is interesting to note that arteries, but not veins, accumulated tracers. Arteries are invested with at least one, and perhaps two peri- or paravascular transport pathways^{15-17,21}. Our data indicate that in the present study, part of the tracers exited the hippocampus along arteries. This finding is consistent with data from Carare et al¹⁶, and at variance with the view proposed by Iliff et al¹⁷. We previously showed that these pathways around arteries connect to the CSF compartment, either at the subarachnoid space or via one of the cisterns that penetrate the brain²². Also in this study a similar anatomy was found, with most of the feeding arteries entering the parenchyma from the cisterns around the hippocampus. Thus, ISF appears to drain from the hippocampus into the CSF either directly via the 3rd ventricle, or indirectly via cisterns and paravascular spaces around arteries. The apparent increase in bulk flow in the SHR hippocampus raises the question what the origin of this fluid is. An obvious source for enhanced ISF flux would be leakage or secretion from the capillaries. Indeed, others have reported BBB leakage and ventricular enlargement in SHR^{12,23}. In agreement with this, we found a tendency for increased water content. This was accompanied by a shift in whole brain Na⁺/K⁺ ratio. Similar changes are seen in stroke, where an increase in brain tissue sodium concentration and a concomitant decrease in brain potassium concentration are associated with vasogenic edema²⁴. Due to large concentration differences, whole brain sodium is mainly reflecting the extracellular sodium pool, whereas potassium is dominated by the intracellular pool. As we anticipate that the SHR maintains normal intra- and extracellular ion concentrations, these data point towards an expansion of the extracellular space in the brains of SHR. Although speculative, such an expansion of the extracellular space could further facilitate ISF flow due to a reduction in resistance. Taken together, the picture emerges that in SHR, BBB leakage and an increase in extracellular space are associated with enhanced flux of ISF from the capillaries into the CSF compartment.

We found that the small tracer was cleared to a larger extent than the large tracer. This was the case for both WKY and SHR. Tracers may have been eliminated across the BBB, via the ISF into the CSF, and possibly via the choroid plexus as noted previously^{15,25}.

However, in view of the enhanced spreading of tracers in SHR, the absence of a difference in clearance between WKY and SHR for both tracers appears to be a contradictory finding. One possibility is that infusion of a relatively large volume of tracers overwhelms endogenous clearance mechanisms, which obscures subtle differences in clearance rate

between SHR and WKY. This would be a situation similar to the tracer spreading results in this study. Alternatively, enhanced ISF flow may not necessarily lead to enhanced solute removal. In that case, we speculate that enhanced ISF flow relates to an increase in water and ion fluxes, but not necessarily leads to more washout of larger molecules. These molecules may be retained within the tissue at barrier sites. Indeed, we observed strong accumulation of the tracers, particularly of the high molecular weight tracer, at the borders of ISF and CSF exchange. We therefore interpret these findings as a sieving effect, resulting from relatively easy passage of water and ions, and accumulation of tracer. Whether such a mechanism is relevant for accumulation of endogenous waste products remains to be established. It is however very tempting to speculate on such a phenomenon, as tracer accumulation as observed in our experiments mirrors the pattern of amyloid β accumulation in the hippocampus of a mouse model of Alzheimer's disease²⁶.

Studies on human brain interstitial fluid flux and hypertension are scarce. Enlarged perivascular spaces are considered a marker for impaired ISF drainage²⁷ and correlate with vascular amyloid β deposition²⁸. White matter hyperintensities and enlarged perivascular spaces are also associated with dementia and may be explained by impaired drainage of ISF²⁹. Another study using MRI suggested that systolic hypertension is associated with an increase in extracellular fluid³⁰. Thus, there is only circumstantial evidence that ISF flow is altered in dementia and potentially aggravated by hypertension. Currently, treatment options therefore seem premature and await future studies that shed more light on ISF production, pathways, and impact of hypertension on clearance of waste products from the brain .

To conclude, we showed that ISF flow is greatly enhanced in the hippocampus of SHR rats as compared to normotensive WKY. In these animals, tracer distribution is consistent with bulk flow, rather than diffusion. This is based on the notion that high and low molecular weight tracers spread similarly, and strongly accumulate at border zones of ISF-CSF exchange. The retention of tracers in these areas can be explained by a sieving effect on ISF, which could be relevant for the accumulation of endogenous solutes and waste products such as amyloid β .

Acknowledgment

This project has received funding from the Internationale Stichting Alzheimer Onderzoek (ISAO) and from the European Union's Seventh Framework Programme for research technological development and demonstration under Grant agreement no 606998.

Author contributions

BB, EvB and EB designed the study and wrote the manuscript. MW, ER, RE critically reviewed the manuscript. BB, EB, JdeV, DN, MvH and RE performed the experiments.

Competing financial interests

The authors declare no competing financial interests.

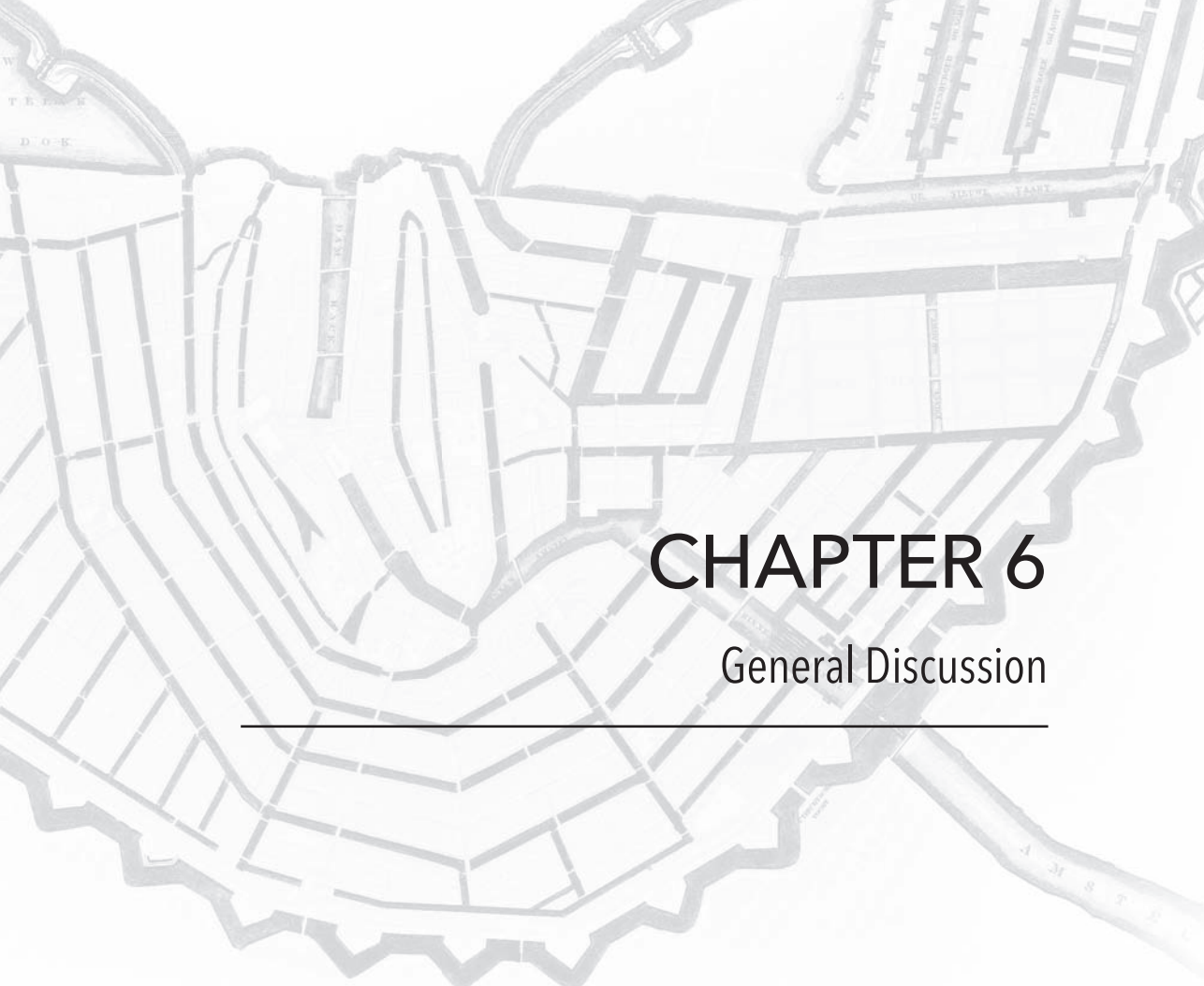
5

REFERENCES

1. Zlokovic, B. V. Neurovascular pathways to neurodegeneration in Alzheimer's disease and other disorders. *Nat Rev Neurosci* 12, 723-738, doi:10.1038/nrn3114 (2011).
2. Iadecola, C. & Davisson, R. L. Hypertension and cerebrovascular dysfunction. *Cell Metab* 7, 476-484, doi:10.1016/j.cmet.2008.03.010 (2008).
3. Feldstein, C. A. Association between chronic blood pressure changes and development of Alzheimer's disease. *J Alzheimers Dis* 32, 753-763, doi:10.3233/JAD-2012-120613 (2012).
4. Peters, R. et al. Incident dementia and blood pressure lowering in the Hypertension in the Very Elderly Trial cognitive function assessment (HYVET-COG): a double-blind, placebo controlled trial. *Lancet Neurol* 7, 683-689, doi:10.1016/S1474-4422(08)70143-1 (2008).
5. Anderson, C. et al. Renin-angiotensin system blockade and cognitive function in patients at high risk of cardiovascular disease: analysis of data from the ONTARGET and TRANSCEND studies. *Lancet Neurol* 10, 43-53, doi:10.1016/S1474-4422(10)70250-7 (2011).
6. Carnevale, D. et al. Role of neuroinflammation in hypertension-induced brain amyloid pathology. *Neurobiol Aging* 33, 205 e219-229, doi:10.1016/j.neurobiolaging.2010.08.013 (2012).
7. Faraco, G. et al. Hypertension enhances A β -induced neurovascular dysfunction, promotes beta-secretase activity, and leads to amyloidogenic processing of APP. *J Cereb Blood Flow Metab* 36, 241-252, doi:10.1038/jcbfm.2015.79 (2016).
8. Wiesmann, M. et al. Angiotensin II, hypertension, and angiotensin II receptor antagonism: Roles in the behavioural and brain pathology of a mouse model of Alzheimer's disease. *J Cereb Blood Flow Metab*, doi:10.1177/0271678X16667364 (2016).
9. Kruyer, A., Soplop, N., Strickland, S. & Norris, E. H. Chronic Hypertension Leads to Neurodegeneration in the TgSwDI Mouse Model of Alzheimer's Disease. *Hypertension* 66, 175-182, doi:10.1161/HYPERTENSIONAHA.115.05524 (2015).
10. Cifuentes, D. et al. Hypertension accelerates the progression of Alzheimer-like pathology in a mouse model of the disease. *Hypertension* 65, 218-224, doi:10.1161/HYPERTENSIONAHA.114.04139 (2015).
11. Carnevale, D. et al. Hypertension induces brain beta-amyloid accumulation, cognitive impairment, and memory deterioration through activation of receptor for advanced glycation end products in brain vasculature. *Hypertension* 60, 188-197, doi:10.1161/HYPERTENSIONAHA.112.195511 (2012).
12. Kaiser, D. et al. Spontaneous white matter damage, cognitive decline and neuroinflammation in middle-aged hypertensive rats: an animal model of early-stage cerebral small vessel disease. *Acta Neuropathol Commun* 2, 169, doi:10.1186/s40478-014-0169-8 (2014).
13. Schreiber, S. et al. Interplay between age, cerebral small vessel disease, parenchymal amyloid-beta, and tau pathology: longitudinal studies in hypertensive stroke-prone rats. *J Alzheimers Dis* 42 Suppl 3, S205-215, doi:10.3233/JAD-132618 (2014).
14. Shibata, M. et al. Clearance of Alzheimer's amyloid-ss(1-40) peptide from brain by LDL receptor-related protein-1 at the blood-brain barrier. *J Clin Invest* 106, 1489-1499, doi:10.1172/JCI10498 (2000).
15. Bedussi, B. et al. Clearance from the mouse brain by convection of interstitial fluid towards the ventricular system. *Fluids Barriers CNS* 12, 23, doi:10.1186/s12987-015-0019-5 (2015).
16. Carare, R. O. et al. Solutes, but not cells, drain from the brain parenchyma along basement membranes of capillaries and arteries: significance for cerebral amyloid angiopathy and neuroimmunology. *Neuropathol Appl Neurobiol* 34, 131-144, doi:10.1111/j.1365-2990.2007.00926.x (2008).

17. Iliff, J. J. et al. A paravascular pathway facilitates CSF flow through the brain parenchyma and the clearance of interstitial solutes, including amyloid beta. *Sci Transl Med* 4, 147ra111, doi:10.1126/scitranslmed.3003748 (2012).
18. Hladky, S. B. & Barrand, M. A. Mechanisms of fluid movement into, through and out of the brain: evaluation of the evidence. *Fluids Barriers CNS* 11, 26, doi:10.1186/2045-8118-11-26 (2014).
19. Abbott, N. J. Evidence for bulk flow of brain interstitial fluid: significance for physiology and pathology. *Neurochem Int* 45, 545-552, doi:10.1016/j.neuint.2003.11.006 (2004).
20. Papadopoulos, M. C. & Verkman, A. S. Aquaporin water channels in the nervous system. *Nat Rev Neurosci* 14, 265-277, doi:10.1038/nrn3468 (2013).
21. Bakker, E. N. et al. Lymphatic Clearance of the Brain: Perivascular, Paravascular and Significance for Neurodegenerative Diseases. *Cell Mol Neurobiol* 36, 181-194, doi:10.1007/s10571-015-0273-8 (2016).
22. Bedussi, B. et al. Paravascular channels, cisterns, and the subarachnoid space in the rat brain: A single compartment with preferential pathways. *J Cereb Blood Flow Metab*, doi:10.1177/0271678X16655550 (2016).
23. Ritter, S. & Dinh, T. T. Progressive postnatal dilation of brain ventricles in spontaneously hypertensive rats. *Brain Res* 370, 327-332 (1986).
24. Yang, G. Y., Chen, S. F., Kinouchi, H., Chan, P. H. & Weinstein, P. R. Edema, cation content, and ATPase activity after middle cerebral artery occlusion in rats. *Stroke* 23, 1331-1336 (1992).
25. de Lange, E. C. Potential role of ABC transporters as a detoxification system at the blood-CSF barrier. *Adv Drug Deliv Rev* 56, 1793-1809, doi:10.1016/j.addr.2004.07.009 (2004).
26. Ye, L. et al. Persistence of Abeta seeds in APP null mouse brain. *Nat Neurosci* 18, 1559-1561, doi:10.1038/nn.4117 (2015).
27. Charidimou, A. et al. White matter perivascular spaces on magnetic resonance imaging: marker of cerebrovascular amyloid burden? *Stroke* 46, 1707-1709, doi:10.1161/STROKEAHA.115.009090 (2015).
28. van Veluw, S. J. et al. Cerebral amyloid angiopathy severity is linked to dilation of juxtacortical perivascular spaces. *J Cereb Blood Flow Metab* 36, 576-580, doi:10.1177/0271678X15620434 (2016).
29. Weller, R. O., Hawkes, C. A., Kalaria, R. N., Werring, D. J. & Carare, R. O. White matter changes in dementia: role of impaired drainage of interstitial fluid. *Brain Pathol* 25, 63-78, doi:10.1111/bpa.12218 (2015).
30. MacLulich, A. M. et al. Higher systolic blood pressure is associated with increased water diffusivity in normal-appearing white matter. *Stroke* 40, 3869-3871, doi:10.1161/STROKEAHA.109.547877 (2009).





CHAPTER 6

General Discussion

Regulation of extracellular volume and fluid composition provides a robust microenvironment for brain cells. In peripheral tissue, fluid surplus and solutes are removed from the interstitium via drainage into lymphatic channels. Since the central nervous system lacks a proper lymphatic vasculature, a substantial part of this drainage may occur along paravascular spaces. Carare *et al.* described a perivascular outflow route for interstitial fluid and solutes along the vessel wall of cerebral capillaries and arteries¹. In contrast, the recently described 'glymphatic pathway' suggests an influx route for cerebrospinal fluid along penetrating arteries. In this view, cerebrospinal fluid would then move to the brain parenchyma where it mixes with the interstitial fluid and eventually exits the brain along the paravascular space of veins². These diverging data have prompted an extensive debate, which raised fundamental questions, such as: Is there a bulk flow in the interstitium or is movement of solutes dominated by diffusion? What is the direction and the driving force of fluid bulk flow along blood vessels? – Does hypertension affect fluid homeostasis?

The objective of my PhD was to address these questions. Below, I discuss the major findings of my research.

Interstitial fluid transport in the brain parenchyma

Movement of solutes in the brain may occur by two mechanisms, diffusion down the concentration gradient and/or convection by bulk flow. Removal of tracers from the parenchyma via interstitial bulk flow has been described in several studies³⁻⁸. However, Sykova and Nicholson showed that solutes within the interstitial fluid mainly disperse via diffusion and speculated that bulk flow is mainly restricted to the perivascular space^{9,10}. The study presented in **chapter 2** seemed to support the presence of interstitial bulk flow. Fluorescent tracers (500 kD and 3 kD) infused in the striatum moved along the extracellular spaces towards the lateral ventricles at the same speed, despite the large difference in tracer size. Similarly, in **chapter 5**, tracers (500 kD and 3 kD) infused in the hippocampus of normotensive (WKY) and hypertensive (SHR) rats moved because of convection towards the third ventricle, and distributed over the same area. The infusion rate we used was low: 0.34 μ L/min as compared to theoretical¹¹ and experimental studies¹. However, since we wanted to rule out any impact of pumping, we decided to investigate the fate of tracers that were released passively from the needle tip. Also in this case, tracers of different molecular size spread similarly. However, to our surprise, this approach uncovered a significantly larger distribution area of tracers in the hippocampus of SHR as compared to WKY. Our interpretation is that active injection of dyes from the pipettes, even at a very low rate, easily overwhelms endogenous distribution mechanisms. We still believe that those data from **chapters 2 and 5** that were based on injection are of value. Notably, these data identify pathways of lowest resistance through the interstitium. Such pathways indicate watersheds, where excess interstitial

fluid, depending on the source location, reaches the subarachnoid space, paravascular space or ventricles. The passive release experiments still do suggest the existence of an interstitial bulk flow, but this flow seems very slow in normotensive animals. To the best of our knowledge, the passive diffusion approach has never been used before and we believe that the impact of infusion in experimental approaches is an issue that has been underestimated so far.

Preferential drainage paths for cerebrospinal fluid in the brain

The continuous cerebrospinal fluid production by the choroid plexus generates a bulk flow in the subarachnoid space. In agreement with this, we observed that tracers moved in the subarachnoid space after infusion into the cisterna magna (**chapters 2 and 3**). After 30 min, the signal was prominent along the ventral side of the brain up to the olfactory bulb. Examination of tracer distribution using confocal microscopy in **chapters 2 and 3** showed that tracers moved preferentially along the arteries from the circle of Willis, and paravascular space of leptomeningeal vessels and feeding arteries of large caliber. To explain this finding, we speculate that the rounded and rigid shape of arteries, unlike the flattened veins, may create a relatively large, low resistance path for fluids (see sketched cross-section of fig. 7, **chapter 3**). This could also explain the appearance pattern of tracer observed in vivo by other groups²: first in the arterial paravascular space and subsequently in the subarachnoid space and in the space around veins. Thus, differences in resistance may create a functional compartment where fluid and solutes run, without necessarily being physically separated from the subarachnoid space as was suggested by *liff et al.*². Finally, from the subarachnoid space, drainage of cerebrospinal fluid occurs via several outflow paths. These paths include arachnoid granulations that empty into the venous sinus; the cribriform plate; and the newly discovered dural lymphatics^{12,13}. In several species, the cribriform plate seems to be a major exit route for fluid in the brain^{14,15}. Indeed, using 3D reconstruction of data obtained by the imaging cryomicrotome, in the rat we observed very high concentrations of dye in the cribriform plate after injection in the cisterna magna. At the cribriform plate there might be connection between cerebrospinal fluid, the nasal lymphatics and the lymph nodes.

Tracer distribution along penetrating vessels

Following injection into the cisterna magna, tracer distribution along the paravascular space of penetrating vessels was very limited, and was mainly found along arteries at the base of the brain. Whenever dye was found along these vessels, the concentration profile steeply dropped from the SAS towards deeper layers. We believe that these data strongly argue against the inflow of cerebrospinal fluid along the penetrating arteries that forms the base of the glymphatic pathway: if this would have been the case, water flow would drag the dye towards deeper layers, and the dye would even increase in

concentration in deeper layers as water would pass the AQP4 channels towards the interstitium. Therefore, we speculate that the movement of tracer along the para-arterial compartment from the subarachnoid space is the result of an equilibration system generated by a strong mixing movement due to arterial pulsation in the subarachnoid space. The strong mixing is thus facilitating a bidirectional interstitial fluid – cerebrospinal fluid exchange that facilitates solute removal. This view is in accordance with results obtained in recent computational models¹⁶. Whether net flow is absent or if there still is a small retrograde flow, towards the SAS, needs further experiments.

Oscillating cerebrospinal bulk flow along paravascular spaces of leptomeningeal vessels

Although the results from different groups seem to diverge on the direction of fluid drainage, there is an agreement on the relevance of arterial pulsations as driving force for paravascular flow. **Chapter 4** provides insight into paravascular fluid dynamics in relation to blood flow and blood vessel pulsatility. Microspheres infused in the cisterna magna unmasked the to and fro movement of cerebrospinal fluid along the paravascular space of leptomeningeal vessels, which is induced by the heartbeat. In these vessels, unlike the penetrating vessels, microspheres did move with a net component in the same direction as the blood flow. The to and fro movement correlates with an oscillatory blood velocity pattern and with diameter changes. However, in some cases the diameter oscillations were very small, suggesting that upstream or downstream diameter oscillations may contribute to fluid displacement. Despite the suggested role of arterial pulsation^{17,18}, it is difficult to understand how a pulsating diameter can create net flow without the presence of valves. In our view, it is more plausible that the net cerebrospinal fluid bulk flow is the result of its continuous production and elimination. The role of the space around leptomeningeal arteries as ‘highway’ and the pulsating nature of cerebrospinal fluid flow here may however be of relevance for clearance. As pointed out in the previous section, a combination of flow at the brain surface with mixing along the penetrating vessels may be an efficient mechanism removing waste products from the brain.

Ventricular system, subarachnoid space and cerebral cisterns: a connected network

After infusion in the cisterna magna we observed tracer signal in a connected network of cisterns that contains the major vessels supplying the brain (**chapter 3**). This network runs in between different anatomical regions and connects the subarachnoid space with the ventricular system. Previous data obtained in an animal model of hydrocephalus showed that the obstruction of the fourth ventricle causes a “leakage” of cerebrospinal fluid from the third and the lateral ventricles into the cerebral cisterns^{19,20}. Ghersi-Egea

described another alternative path²¹, in which the sucrose infused in the lateral ventricle spread towards the cisterns via the subarachnoid velae. Altogether, these observations extend the current knowledge on cerebrospinal fluid connections, with an alternative route from the lateral ventricles to the subarachnoid space that may become relevant when the normal outflow is obstructed.

What is the structure of the paravascular spaces along penetrating vessels?

The exact location of fluid drainage along vessels, observed after the infusion of tracers, is a subject of discussion. In **chapter 3**, we combined fluorescent microscopy with electron microscopy to investigate tracer location after cisterna magna infusion. From the cisterna magna, the tracer moved along the space just outside the layer of smooth muscle cells and further downstream along the basement membrane of capillaries. In agreement with recent work from Morris et al.²², the basement membranes of endothelial cells and smooth muscle cells were continuous with the extracellular matrix and space surrounding the vessels. We did not find a physical separation between the paravascular space and the basement membrane or evidence for the existence of pial sheets along arteries that were previously described²³.

The presence of two different pathways described in the literature, namely within the vessel wall (i.e. perivascular) or between the vessel and the parenchyma (i.e. paravascular), could have two explanations. Firstly, the two paths might exist along arteries, being separated by meningeal sheets and carrying flow in opposite direction. However, as pointed out above, we found no evidence supporting this scenario. The second and more plausible explanation is that the same pathway is described but experimental differences led to different interpretations. Thus, *in vivo* analysis may show a large paravascular space with tracer, while *ex vivo* analysis may be obscured by collapse of the paravascular space and a subsequent more close association of tracer with the basement membranes of the blood vessels. Optical coherent tomography (OCT) in human brain may shed light on the *in vivo* shape of the paravascular space. The OCT technique is noninvasive, but imaging is limited to a depth of approximately 1.5 mm. In a preliminary study in patients, we have used OCT to visualize the paravascular space of leptomeningeal vessels, across the brain surface. Data showed the presence of paravascular spaces across a range of vessel sizes, which appeared as widening of the subarachnoid space. The size of the paravascular space was linearly related with the vessel size. However, this technique would not allow discrimination between arteries and veins. The same profile was observed for the paravascular space around leptomeningeal vessels in mice. Characterization of flow dynamics is also possible by OCT, but this would have required the presence of light-reflecting particles in the paravascular space.

How does hypertension modify all this?

In **chapter 5** we provided evidence that hypertension changes the interstitial fluid homeostasis. After passive release from a pipet in the hippocampus of normotensive (WKY) and hypertensive rats (SHR), tracer distributed over a much larger area in SHR as compared to WKY. This result suggests that interstitial bulk flow in the hippocampus of SHR is markedly enhanced. Enhanced interstitial bulk flow together with a tendency for increased water content observed in hypertensive animals, raised a question: Is there more production of interstitial fluid at the brain capillary level? Since movement of fluid at the blood-brain barrier level is strictly controlled, increased production of interstitial fluid may be caused by leaky capillaries²⁴ or increased salt transport across endothelial cells into the parenchyma, followed by water. In order to investigate blood-brain leakage, we examined IgG extravasation from the blood into the parenchyma. However, we did not find a significant difference between the two strains. However, we found an increased Na^+/K^+ ratio in the SHR brain. Due to the large concentration differences between interstitium and cytoplasm, the brain sodium level mainly reflects the extracellular sodium pool, whereas potassium is dominated by the intracellular pool. Since intra- and extracellular ion concentrations are expected to be maintained, the shift in brain Na^+/K^+ ratio may reflect an expansion of the extracellular space in the brains of SHR, with consequent changes in brain architecture. Surprisingly, despite the increased interstitial fluid flow in hypertensive rats, we did not observe any differences in clearance of tracers between the two strains. Therefore, we suggest that the enhanced fluid flow specifically involves an increase in water and ion flux, while larger molecules are retained. The interstitial fluid together with solutes would move along the enlarged extracellular space towards the borders of interstitial fluid with the cerebrospinal fluid, which are rich in astrocytes and strongly expressing AQP4. Thus, these areas may filter the large molecules present in interstitial fluid. Data obtained in a mouse model of Alzheimer's disease on amyloid β deposition in the hippocampus mirrored the pattern observed in our experiments²⁵. Therefore, we speculate that in these areas there might be a relatively easy passage of water and ions with sieving of large molecules. This may be relevant for the accumulation of amyloid β . However, this hypothesis needs further investigation.

Is there a glymphatic pathway?

The glymphatic pathway depicts a drainage path for extracellular fluids in the brain. Iliff *et al.*² suggested that cerebrospinal fluid, flowing in the subarachnoid space, moves along the paravascular space of penetrating arteries. The presence of AQP4 allows cerebrospinal fluid movement into the parenchyma, where it mixes with the interstitial fluid. In the parenchyma, the interstitial fluid, together with solutes and waste, is transported towards the para-venous space, and from there drains out of the brain.

Our data suggest that paravascular space around parenchymal veins is not involved in the drainage of tracers. Fluorescent tracers infused or passively released in brain regions move towards the closest cerebrospinal fluid compartments, (i.e. ventricles as well as para-arterial space), to some extent in accordance with data from Carare *et al*¹. In addition, as indicated above, dyes injected into the cisterna magna were not transported along the paravascular space of penetrating arteries around most of the brain. This is at variance with work from Iliff *et al.*, who found labelled amyloid β along capillaries and veins, 1 hour after the injection. We speculate that this could be due to differences in experimental approach, or specific uptake of amyloid β by perivenous immune cells, as shown by Michaud *et al*²⁶. Altogether, concerns about the existence of the glymphatic pathways as described by Iliff *et al.* remain, and further studies are needed to identify the complete and exact route of extracellular fluids clearance.

Clinical implications and outlook

Knowledge of brain fluid physiology and dynamics is of great importance not only to unravel the removal mechanisms of toxic waste such as amyloid β , but also to help finding more optimal delivery strategies of therapeutic drugs to the brain as well as to support the development of diagnostic tools that are based on biomarkers from the cerebrospinal fluid. These issues clearly concern Alzheimer's disease, but are also relevant for other neurological disorders, brain cancer and multiple sclerosis.

Our data on increased interstitial flow in hypertension clearly needs to be followed up by other models and, if at all feasible, by human studies. Enhanced interstitial fluid flow in human hypertension might reduce the efficacy of clearing systems, such as blood-brain barrier transport or proteolytic degradation. The observation that in hypertension tracers were dragged towards specific 'sieving areas' may be relevant for amyloid β accumulation, providing a novel hypothesis for the link between hypertension and Alzheimer's disease. An important question that needs to be addressed is whether the increased production of interstitial fluid from capillaries is 'leakage' of a 'damaged' blood-brain barrier or active upregulation of transcapillary fluid transport. In the kidney, the potassium-sparing diuretics (i.e. amiloride) block the epithelial Na^+ channels (ENaC) reducing the amount of Na^+ available for exchange via the Na^+/K^+ ATPase, thereby decreasing the amount of K^+ secreted via diuresis. Since antihypertensive medications, specifically potassium-sparing diuretics, reduce the risk to develop Alzheimer's disease^{27,28}, an association between ions misbalance, disturbed interstitial fluid flow and increased risk for dementia may be suggested. This hypothesis encourages further research on ions concentration alterations in hypertensive conditions and the impact of antihypertensive treatment on interstitial fluid dynamics. Finally, vascular stiffness, associated with hypertension and aging, may affect arterial pulsatility and therefore brain clearance.

Conclusion

Diseases of the central nervous system have been linked to extracellular fluid flow. However, the exact pathological role of these fluids remains to be elucidated. With this thesis we revealed a continuous and extensive CSF compartment, in which solutes move, driven by bulk flow and mixing. Furthermore, we suggested that an increased flux of ions and water, associated with hypertension, may play a role in the filtering and accumulation of endogenous waste products in the brain. We also introduced a new and more subtle approach (i.e. passive release) in studying interstitial fluid flow. To conclude, the research presented in this thesis shed light on the physiology and dynamics of extracellular fluids in the brain and has provided directions for future investigations that could reveal the link between hypertension, extracellular fluids and Alzheimer's disease.



REFERENCES

1. Carare, R. O. et al. Solutes, but not cells, drain from the brain parenchyma along basement membranes of capillaries and arteries: significance for cerebral amyloid angiopathy and neuroimmunology. *Neuropathol Appl Neurobiol* 34, 131-144, doi:10.1111/j.1365-2990.2007.00926.x (2008).
2. Iliff, J. J. et al. A paravascular pathway facilitates CSF flow through the brain parenchyma and the clearance of interstitial solutes, including amyloid beta. *Sci Transl Med* 4, 147ra111, doi:10.1126/scitranslmed.3003748 (2012).
3. Szentistvanyi, I., Patlak, C. S., Ellis, R. A. & Cserr, H. F. Drainage of interstitial fluid from different regions of rat brain. *Am J Physiol* 246, F835-844 (1984).
4. Cserr, H. F., Depasquale, M., Patlak, C. S. & Pullen, R. G. Convection of cerebral interstitial fluid and its role in brain volume regulation. *Ann N Y Acad Sci* 481, 123-134 (1986).
5. Cserr, H. F. Role of secretion and bulk flow of brain interstitial fluid in brain volume regulation. *Ann N Y Acad Sci* 529, 9-20 (1988).
6. Rennels, M. L., Gregory, T. F., Blaumanis, O. R., Fujimoto, K. & Grady, P. A. Evidence for a 'paravascular' fluid circulation in the mammalian central nervous system, provided by the rapid distribution of tracer protein throughout the brain from the subarachnoid space. *Brain Res* 326, 47-63 (1985).
7. Ichimura, T., Fraser, P. A. & Cserr, H. F. Distribution of extracellular tracers in perivascular spaces of the rat brain. *Brain Res* 545, 103-113 (1991).
8. Abbott, N. J. Evidence for bulk flow of brain interstitial fluid: significance for physiology and pathology. *Neurochem Int* 45, 545-552, doi:10.1016/j.neuint.2003.11.006 (2004).
9. Sykova, E. & Nicholson, C. Diffusion in brain extracellular space. *Physiol Rev* 88, 1277-1340, doi:10.1152/physrev.00027.2007 (2008).
10. Nicholson, C. & Sykova, E. Extracellular space structure revealed by diffusion analysis. *Trends Neurosci* 21, 207-215 (1998).
11. Morrison, P. F., Laske, D. W., Bobo, H., Oldfield, E. H. & Dedrick, R. L. High-flow microinfusion: tissue penetration and pharmacodynamics. *Am J Physiol* 266, R292-305 (1994).
12. Aspelund, A. et al. A dural lymphatic vascular system that drains brain interstitial fluid and macromolecules. *J Exp Med* 212, 991-999, doi:10.1084/jem.20142290 (2015).
13. Louveau, A. et al. Structural and functional features of central nervous system lymphatic vessels. *Nature* 523, 337-341, doi:10.1038/nature14432 (2015).
14. Johnston, M., Zakharov, A., Papaiconomou, C., Salmasi, G. & Armstrong, D. Evidence of connections between cerebrospinal fluid and nasal lymphatic vessels in humans, non-human primates and other mammalian species. *Cerebrospinal Fluid Res* 1, 2, doi:10.1186/1743-8454-1-2 (2004).
15. Koh, L. et al. Development of cerebrospinal fluid absorption sites in the pig and rat: connections between the subarachnoid space and lymphatic vessels in the olfactory turbinates. *Anat Embryol (Berl)* 211, 335-344, doi:10.1007/s00429-006-0085-1 (2006).
16. Asgari, M., de Zelicourt, D. & Kurtcuoglu, V. Glymphatic solute transport does not require bulk flow. *Sci Rep-Uk* 6, doi:ARTN 3863510.1038/srep38635 (2016).
17. Kiviniemi, V. et al. Ultra-fast magnetic resonance encephalography of physiological brain activity - Glymphatic pulsation mechanisms? *J Cereb Blood Flow Metab* 36, 1033-1045, doi:10.1177/0271678X15622047 (2016).
18. Iliff, J. J. et al. Cerebral arterial pulsation drives paravascular CSF-interstitial fluid exchange in the murine brain. *J Neurosci* 33, 18190-18199, doi:10.1523/JNEUROSCI.1592-13.2013 (2013).
19. Park, J. H. et al. Cerebrospinal fluid pathways from cisterns to ventricles in N-butyl cyanoacrylate-induced hydrocephalic rats. *J Neurosurg Pediatr* 8, 640-646, doi:10.3171/2011.8.PEDS1190 (2011).

20. Yoon, J. S., Nam, T. K., Kwon, J. T., Park, S. W. & Park, Y. S. CSF flow pathways through the ventricle-cistern interfaces in kaolin-induced hydrocephalus rats-laboratory investigation. *Childs Nerv Syst* 31, 2277-2281, doi:10.1007/s00381-015-2901-5 (2015).
21. Ghersi-Egea, J. F., Finnegan, W., Chen, J. L. & Fenstermacher, J. D. Rapid distribution of intravenicularly administered sucrose into cerebrospinal fluid cisterns via subarachnoid velae in rat. *Neuroscience* 75, 1271-1288 (1996).
22. Morris, A. W., Carare, R. O., Schreiber, S. & Hawkes, C. A. The Cerebrovascular Basement Membrane: Role in the Clearance of beta-amyloid and Cerebral Amyloid Angiopathy. *Front Aging Neurosci* 6, 251, doi:10.3389/fnagi.2014.00251 (2014).
23. Zhang, E. T., Inman, C. B. & Weller, R. O. Interrelationships of the pia mater and the perivascular (Virchow-Robin) spaces in the human cerebrum. *J Anat* 170, 111-123 (1990).
24. Kaiser, D. et al. Spontaneous white matter damage, cognitive decline and neuroinflammation in middle-aged hypertensive rats: an animal model of early-stage cerebral small vessel disease. *Acta Neuropathol Commun* 2, 169, doi:10.1186/s40478-014-0169-8 (2014).
25. Ye, L. et al. Persistence of Aβ seeds in APP null mouse brain. *Nat Neurosci* 18, 1559-1561, doi:10.1038/nn.4117 (2015).
26. Michaud, J. P., Bellavance, M. A., Prefontaine, P. & Rivest, S. Real-time in vivo imaging reveals the ability of monocytes to clear vascular amyloid beta. *Cell Rep* 5, 646-653, doi:10.1016/j.celrep.2013.10.010 (2013).
27. Peters, R. et al. Incident dementia and blood pressure lowering in the Hypertension in the Very Elderly Trial cognitive function assessment (HYVET-COG): a double-blind, placebo controlled trial. *Lancet Neurol* 7, 683-689, doi:10.1016/S1474-4422(08)70143-1 (2008).
28. Khachaturian, A. S. et al. Antihypertensive medication use and incident Alzheimer disease: the Cache County Study. *Arch Neurol* 63, 686-692, doi:10.1001/archneur.63.5.noc60013 (2006).







CHAPTER 7

Summary and Appendix

Summary
Samenvatting
List of publications
Portfolio
Curriculum Vitae
Acknowledgments

SUMMARY

The aim of the thesis was to investigate the physiology of brain extracellular fluids and their possible role in the removal of solutes from the central nervous system, which lacks a proper lymphatic system. Despite the multitude of studies on brain fluid dynamics, the scientific community does not share a common view. **Chapter 1** introduces the physiological background of brain fluids and their implications in the maintenance of homeostasis. Furthermore, this chapter collects the most recent data available in the literature on removal of solutes from the central nervous system. This forms the basis for the experiments in the following chapters. In **chapters 2-4** we looked at the anatomy and flow patterns under physiological conditions in mice and rats. In **chapter 5** we studied the impact of hypertension in spontaneously hypertensive rats.

As introduced in **chapter 1**, interstitial fluid and cerebrospinal fluid transport in the brain is an open debate. In **chapter 2**, we evaluated the fate of fluorescent extracellular fluid tracers after injection in the mouse striatum and cisterna magna. We chose to infuse two tracers with different molecular weight to discriminate between flow and diffusion. Using confocal microscopy and a 3D imaging cryomicrotome, we described the presence of an interstitial bulk flow from the striatum towards the adjacent CSF compartments. We found the choroid plexuses to be involved in the uptake of small solutes from the ventricles. Tracers infused in the cisterna magna found their way to the subarachnoid spaces and from there they were cleared, among others, via the cribriform plate. Finally, our data suggested that tracers may enter arterial paravascular spaces from two sides, both through bulk flow from the parenchyma and through mixing of CSF from the subarachnoid space.

Chapter 3 describes a study set up to clarify the anatomical relation between cerebral blood vessels, cerebrospinal fluid compartments and paravascular spaces in the rat brain. For this purpose, we used different imaging techniques to obtain anatomical information at macroscale down to the nanometer scale. After infusion of a fluorescent tracer into the cisterna magna, we analyzed the brains using a 3D imaging cryomicrotome, confocal microscopy, and correlative light and electron microscopy. The tracer was strongly co-localized with the major arteries and veins in the subarachnoid space and in large cerebral cisterns. Coronal sections of the brain imaged with confocal microscopy showed a novel cisternal connection between the subarachnoid space and the ventricular system. Correlative light and electron microscopy images showed that tracer injected into the cisterna magna, followed the space just outside the layer of smooth muscle cells and further downstream along the basement membrane of capillaries. We also observed that the intracranial pressure was highly pulsatile and we suggested that it might generate mixing in the cerebrospinal fluid compartments. Taken together, our data suggested the existence of an extensive CSF compartment that encompasses the subarachnoid space, paravascular channels, cerebral cisterns and ventricular system.

In the previous chapter we suggested that pulsatility might create a mixing movement in the cerebrospinal fluid compartments. To further investigate this hypothesis we measured velocity of cerebrospinal fluid flow in the paravascular space of leptomeningeal vessels and vessel pulsatility (**Chapter 4**). For this purpose, we developed an *in vivo* approach to determine the velocity of cerebrospinal fluid flow in mice along leptomeningeal vessels. Fluorescent microspheres were used to trace the cerebrospinal fluid after infusion in the cisterna magna. The leptomeningeal vasculature was imaged through a thinned cranial window, and videos were acquired with a high speed camera. In mice, microspheres moved preferentially in the close vicinity of the blood vessels. This observation supported the hypothesis of low resistance paths for cerebrospinal fluid flow along leptomeningeal vessels. We found that flow in these channels was pulsatile, attributable to the cardiac cycle, with a net antegrade component. Pulsations have repeatedly been suggested to induce flow. However, it is hard to see how pulsatile diameter variations of leptomeningeal vessels itself could generate a net flow. We believe that the *vis a tergo* of cerebrospinal fluid production in the choroid plexuses, is a more likely source of net flow. However, we do speculate that pulsatility in the paravascular space may be important, as it can create mixing of cerebrospinal fluid in the paravascular space of penetrating arteries. Such mixing could facilitate the removal of waste products from otherwise possibly stagnant parts of the paravascular system.

Then, we investigated the relation between vascular pathology and changes in brain extracellular fluids. As midlife hypertension increases the risk to develop Alzheimer's disease, and removal of amyloid β might be partially dependent on interstitial fluid flow, we decided to investigate the impact of hypertension on interstitial fluid flow in the hippocampus of rats (**chapter 5**). Fluorescent tracers were either infused or passively released into the hippocampus of normotensive and hypertensive rats. As in **chapter 2**, we used tracers with different molecular weights to discriminate between bulk flow and diffusion. After passive release, confocal images showed a drastically enhanced spreading of tracers in the hypertensive rats, while no difference was observed after infusion. After passive release, tracers spread inhomogeneously and accumulated at the interstitial-cerebrospinal fluid borders, around arteries, and towards the stratum lacunosum moleculare. This stratum is an area rich in aquaporin-4, a specialized water channel. We also found a tendency for increased water content in hypertensive rats, accompanied by a shift in the whole brain Na^+/K^+ ratio. Altogether, our data suggest a strongly enhanced interstitial fluid flow in the hippocampus of hypertensive rats. This flow drains towards cerebrospinal fluid compartments, including paravascular spaces around arteries. Here, we speculate that interstitial fluid crosses the boundaries set up by astrocytes, while large solutes are filtered and eventually accumulate.

Finally, the major findings of this thesis and the proposed directions for future research in brain fluids dynamics and their role in pathophysiology are discussed in **chapter 6**.

SAMENVATTING

Het doel van dit promotieonderzoek was om de fysiologie van cerebrale extracellulaire vloeistoffen en hun mogelijke rol in het verwijderen van opgeloste stoffen uit de hersenen beter te begrijpen. Deze vloeistoffen zijn het bloed, de cerebrospinale vloeistof, en de interstitiële vloeistof, waarbij opvallend genoeg een lymfestelsel in de hersenen ontbreekt. Ondanks de vele studies op het gebied van hersenvloeistof dynamica, ontbreekt consensus binnen de wetenschappelijke gemeenschap over de stroomrichting, de drijvende krachten, en de precieze anatomie van de structuren waarbinnen deze vloeistoffen zich bevinden. **Hoofdstuk 1** introduceert de fysiologische achtergrond van de verschillende hersenvloeistoffen en hun noodzaak voor het behouden van homeostase. In dit hoofdstuk wordt ook de meest recente literatuur op een rij gezet over het afvoeren van opgeloste stoffen uit het centrale zenuwstelsel. Deze achtergrond vormt de basis voor de experimenten in de volgende hoofdstukken. **Hoofdstukken 2-4** beschrijven studies aan de anatomie en stromingspatronen onder fysiologische condities in muizen en ratten. **Hoofdstuk 5** behandelt de invloed hierop van hoge bloeddruk (hypertensie) in spontaan hypertensieve ratten.

Zoals beschreven in **hoofdstuk 1**, is er een debat gaande over interstitiële vloeistof en de interactie met cerebrospinale vloeistof. In **hoofdstuk 2** hebben we het lot van fluorescente tracers onderzocht na injectie in het striatum en de cisterna magna van de muis. We hebben ervoor gekozen om twee tracers te injecteren, met verschillende moleculaire massa's, om onderscheid te kunnen maken tussen stroming en diffusie. Gebruikmakend van confocaal microscopie en een '3D imaging cryomicrotome', vonden we aanwijzingen voor de aanwezigheid van stroming van interstitiële vloeistof van het striatum naar aangrenzende cerebrospinale vloeistof compartimenten. We vonden ook dat de plexus choroïdeus een rol speelt in de opname van sommige opgeloste stoffen vanuit de ventrikels. Tracers geïnjecteerd in de cisterna magna vonden hun weg naar de subarachnoïdale ruimtes, waar vanaf ze werden geklaard, o.a. via de cribriforme plaat. Onze data lieten verder zien dat tracers arteriële paravasculaire ruimtes kunnen bereiken via twee wegen; zowel door stroming vanuit het parenchym als vanuit de subarachnoïdale ruimte, waarschijnlijk door menging.

Hoofdstuk 3 beschrijft een studie naar de anatomische relatie tussen cerebrale bloedvaten, cerebrospinale vloeistof compartimenten en paravasculaire ruimtes in het rattenbrein. We hebben hierin verschillende afbeeldingstechnieken gebruikt om anatomische informatie te verkrijgen van macro- tot nanometerschaal. Na infusie van een fluorescente tracer in de cisterna magna, hebben we de breinen geanalyseerd met behulp van een '3D imaging cryomicrotome', confocaal microscopie, en 'correlative light and electron microscopy'. De resultaten lieten zien dat de tracer sterk gelokaliseerd was rondom de grote arteriën en venen in de subarachnoïdale ruimte en in de grote

cisternae. Afbeeldingen van coronale secties van het brein lieten een niet eerder onderkende verbinding zien tussen de subarachnoïdale ruimte en het ventriculair systeem. Afbeeldingen gemaakt met 'correlative light and electron microscopy' lieten zien dat de tracer de ruimte net buiten de laag glad spierweefsel volgt en verder stroomafwaarts langs de basaal membraan van haarvaten loopt. We vonden ook een zeer pulsatiele intracraniale druk en veronderstellen dat dit kan leiden tot menging in de compartimenten met cerebrospinale vloeistof. De resultaten van dit hoofdstuk laten zien dat er een uitgebreid en continu cerebrospinaal vloeistofcompartiment bestaat, dat gevormd wordt door de subarachnoïdale ruimte, paravasculaire kanalen, cerebrale cisternae en het ventriculaire systeem.

Hoofdstuk 4. In het voorgaande hoofdstuk stelden we voor dat pulsatiliteit zou kunnen leiden tot menging in de cerebrospinale vloeistof compartimenten. Om deze hypothese verder te onderzoeken hebben we het stromingsprofiel gemeten van cerebrospinale vloeistof in de paravasculaire ruimte van leptomeningeale vaten, evenals de pulsatiliteit van de vaten zelf. Daartoe hebben we een methode ontwikkeld om de stroomsnelheid van cerebrospinale vloeistof rondom leptomeningeale vaten *in vivo* te bepalen in muizen. Hiervoor werden fluorescente microsferen gebruikt, die met behulp van een hoge snelheidscamera werden gevolgd na injectie in de cisterna magna. Om de microsferen en leptomeningeale vaten te kunnen zien werd een stukje schedel dunner gemaakt door deze af te schrapen. De microsferen verplaatsten zich bij voorkeur in de nabijheid van de bloedvaten. Deze observatie ondersteunt de gedachte dat er paden bestaan met een lagere weerstand rondom de leptomeningeale vaten. Stroming in deze kanalen was pulsatieel, toe te schrijven aan de hartcyclus, met een netto voorwaartse component. Het is vaker gesuggereerd dat pulsaties stroming induceren. Echter, het is moeilijk om in te zien hoe pulsatiele variaties in de diameter van leptomeningeale vaten een netto stroming kunnen genereren. We denken dat de productie van cerebrospinale vloeistof in de plexus choroïdeus een meer waarschijnlijke oorzaak is voor de voorwaartse component van de stroming. Echter, we speculeren dat pulsatiliteit in de paravasculaire ruimte toch van groot belang zou kunnen zijn, omdat het kan leiden tot menging van cerebrospinale vloeistof in de paravasculaire ruimte rondom penetrerende arteriën. Dit soort vermenging zou verwijdering van afvalstoffen kunnen faciliteren uit anderszins mogelijk stilstaande delen van het paravasculaire systeem.

Hoofdstuk 5. Vervolgens hebben we de relatie onderzocht tussen vasculaire pathologie en veranderingen in de extracellulaire vloeistoffen in het brein. Hypertensie, met name op middelbare leeftijd, vergroot het risico op het ontwikkelen van de ziekte van Alzheimer. Omdat verwijdering van amyloid β deels afhankelijk zou kunnen zijn van de stroming van interstitiële vloeistoffen, onderzochten we de invloed van hypertensie op interstitiële vloeistofstromingen. Fluorescente tracers werden geïnjecteerd of passief afgegeven (diffusie vanuit de naald) in de hippocampus van normotensieve en hyper-

tensieve ratten. Net als in **hoofdstuk 2**, gebruikten we tracers met verschillende moleculaire massa's om onderscheid te maken tussen bulk stroming en diffusie. Na passieve afgifte was een drastisch versterkte verspreiding van tracers te zien in de hypertensieve ratten, terwijl er geen verschil zichtbaar was na injectie. Dit laat zien dat injectie, ook van kleine volumina, endogene mechanismen van verspreiding al snel overstemt. Na passieve afgifte verspreidden tracers zich inhomogeen en hoopten ze op bij de grenzen van interstitiële en cerebrospinale vloeistof, rond arteriën, en richting het stratum lacunosum moleculare. Dit stratum is rijk aan aquaporin-4, een gespecialiseerd waterkanaal. We vonden ook een tendens tot toename in de hoeveelheid water in de hersenen van hypertensieve ratten, samen met een duidelijke verandering in de Na^+/K^+ ratio. Deze resultaten suggereren een disbalans in de homeostase van water en zouten, gepaard gaande met een sterk verhoogde interstitiële vloeistofstroming in de hippocampus van hypertensieve ratten. Deze stroming wordt afgevoerd richting cerebrospinale vloeistof compartimenten, waaronder paravasculaire ruimtes rond arteriën. We denken dat interstitiële vloeistoffen relatief makkelijk deze grenzen kunnen passeren, die grotendeels gevormd worden door astrocyten, terwijl grotere moleculen op deze plaatsen gefilterd worden en uiteindelijk accumuleren.

Tot slot worden in **hoofdstuk 6** de belangrijkste bevindingen uit dit promotieonderzoek besproken en suggesties gedaan voor toekomstig onderzoek.



LIST OF PUBLICATIONS

1. Do TM, **Bedussi B**, Chasseigneaux S, Dodacki A, Yapo C, Chacun H, Scherrmann JM, Farinotti R, Bourasset F (2013) Oatp1a4 and an L-thyroxine-sensitive transporter mediate the mouse blood-brain barrier transport of amyloid-beta peptide. *J Alzheimers Dis* 36: 555-561
2. **Bedussi B**, van Lier MG, Bartstra JW, de Vos J, Siebes M, VanBavel E, Bakker EN (2015) Clearance from the mouse brain by convection of interstitial fluid towards the ventricular system. *Fluids Barriers CNS* 12: 23
3. Bakker EN, Bacskai BJ, Arbel-Ornath M, Aldea R, **Bedussi B**, Morris AW, Weller RO, Carare RO (2016) Lymphatic Clearance of the Brain: Perivascular, Paravascular and Significance for Neurodegenerative Diseases. *Cell Mol Neurobiol* 36: 181-194
4. **Bedussi B**, van der Wel NN, de Vos J, van Veen H, Siebes M, VanBavel E, Bakker EN (2016) Paravascular channels, cisterns, and the subarachnoid space in the rat brain: A single compartment with preferential pathways. *J Cereb Blood Flow Metab.* 2017 Apr;37(4):1374-1385.
5. **Bedussi B**, Naessens DMP, de Vos J, Olde Engberink R, Wilhelmus MMM, Richard E, ten Hove M, vanBavel E, and Bakker EN (2017) Enhanced interstitial fluid drainage in the hippocampus of spontaneously hypertensive rats. *Sci Rep.* 2017 Apr 7;7(1):744
6. **Bedussi B**, de Vos J, vanBavel E, and Bakker EN (2017) Paravascular spaces in mice and man: low resistance pathways for cerebrospinal fluid flow (*Accepted JCBFM* (2017))

PORTFOLIO

PhD period: 2014-2017
 Name PhD supervisor: Prof. Dr. E.T. van Bavel
 Name PhD Co-supervisor: Dr. N.T.P. Bakker

PhD TRAINING – SmArteR Fellowship

Courses	Year	ECTS
Laboratory animals, Article 9	04/2014	1.4
Basic Microscopy	10/2014	1.6
Cardiovascular Diseases	10/2014	1.5
The AMC World of Science	11/2014	0.7
Scientific writing in English for publication	02/2015	1.5
Project Management	02/2016	0.6
Oral presentation in English	02-03/2016	0.8
SMARTER summer school, workshop dedicated to small artery research		
Garda, Italy	10/2014	6
Munster/Amsterdam	03/2015	10
London, UK	11/2015	6
Munich, Germany	06/2016	6
Freiburg, Switzerland	11/2016	2
SMARTER summer school, workshop for complementary skills (entrepreneurship...)		
Munich, Germany	05/2016	4
Seminars and Workshops		
Department seminars	2014-2017	3
Journal club	2014-2017	3
Ruysch Lectures	2014-2017	1
(Inter)national conferences		
DEBS, Biezenmortel, NL (Poster)	2014	0.5
Brain 2015, Vancouver, CA (Poster)	2015	0.5
CVB 2015, Paris, FR (Poster)	2015	0.5
AMC/Umc Cardio research meeting, Amsterdam, NL (Poster)	2015	0.5
Translational Neuroscience Network, Amsterdam, NL (Poster)	2015	0.5
6 th Cardiovascular Conference, Ede, NL (Poster)	2016	0.5
5 th International CAA Conference, Boston, USA (Oral presentation)	2016	1
Virtual Human Physiology, Amsterdam, NL (Poster)	2016	0.5
Amsterdam Cardiovascular Science, Amsterdam, NL, (Poster)	2016	0.5

Courses	Year	ECTS
Teaching		
MSc project (Daan van den Oever)	2014	1
MSc Project (Daphne Naessens)	2015	1
BCs Project (Malyssa ten Hove)	2016	1
Lecture at the Cardiovascular research Master (VUMC)	2016	1
Practicum/Student Demonstrations	2014-2016	1
Parameter of esteem		
Award		
Young Investigator Award (International CAA Association, CAA Conference)	2016	

CURRICULUM VITAE

Beatrice Bedussi was born on April 7, 1985 in Brescia, Italy. After obtaining the Baccalaurate in Modern Foreign Languages in Brescia, she moved to Pavia to study Pharmacy. During her studies Beatrice was granted with an Erasmus Placement fellowship to conduct a research project abroad. She moved to Paris, and worked for her master thesis project at the laboratory of Pharmacokinetics of the Faculty of Pharmacy, Paris Descartes University. Her master thesis was supervised by Dr. Maria Laura Amadio (University of Pavia) and by Dr. Fanchon Bourasset (University Paris Descartes). She graduated at the Faculty of Pharmacy of the University of Pavia in July 2013. After graduation, she obtained the license to practice as pharmacist, and started to work in Italy. In March 2014, she joined Prof. Ed van Bavel's group at the Department of Biomedical Engineering and Physics at the Academic Medical Center, The Netherlands. Here, she worked as Ph.D. student, financially supported by a Marie Curie Fellowship, within the SmArteR consortium. Under the supervision of Prof. Ed T van Bavel and Dr. Erik NTP Bakker, she investigated the transport of cerebral extracellular fluids in the brain. In 2016, the International CAA Association awarded her with the Junior Investigator Award. The results of her research are collected in this thesis.

